UNIVERSITÉ DU QUÉBEC À MONTREAL

FROM ALKALINE INTRUSION-RELATED TO OROGENIC MINERALIZATIONS: THE WASAMAC GOLD DEPOSIT, ABITIBI GREENSTONE BELT, CANADA

THESIS
PRESENTED
AS PARTIAL REQUIREMENT
OF THE MASTERS OF EARTH SCIENCES

BY
NICOLAS MÉRIAUD

SEPTEMBRE 2015

UNIVERSITÉ DU QUÉBEC À MONTRÉAL

LE GISEMENT AURIFÈRE DE WASAMAC (ABITIBI) ; UN EXEMPLE DE MINÉRALISATION OROGÉNIQUE ASSOCIÉE AUX INTRUSIONS ALCALINES

MÉMOIRE
PRÉSENTÉ
COMME EXIGENCE PARTIELLE
DE LA MAÎTRISE EN SCIENCES DE LA TERRE

PAR
NICOLAS MÉRIAUD

SEPTEMBRE 2015

AVANT-PROPOS

Ce mémoire est rédigé sous la forme d'un article scientifique qui sera soumis à publication sous le titre: *From Alkaline Intrusion-Related to Orogenic Mineralizations : The Wasamac Gold Deposit, Abitibi Greenstone Belt, Canada*. Sa présentation est de ce fait différente des mémoires habituellement présentés à l'UQAM : la rédaction est en anglais et les tableaux et figures sont présentées à la fin de l'article. Michel Jébrak, directeur de maîtrise, sera co-auteur de cet article. Ce format de mémoire est utilisé pour l'opportunité de l'exercice de rédaction et de communication d'informations scientifiques en anglais, et d'ouvrir à l'international les résultats associés.

REMERCIEMENTS

En premier lieu je tiens à remercier Michel Jébrak pour m'avoir permis cette merveilleuse opportunité de recherche. Cela m'a permis de découvrir deux nouveaux centres d'intérets: la géologie des gites et le processus de recherche scientifique ; les nombreuses et riches conversations ont également beaucoup contribué à cela. Merci aussi pour les nombreuses opportunités de terrain (Abitibi, Utah, Colorado) et celles concernant l'apprentissage de la communication scientifique au travers des congrès : Explo Abitibi 2013 (Val d'Or, QC, Canada), Québec Mines 2013 (Québec, QC, Canada), GAC-MAC 2014 (Fredericton, NB, Canada), SEG 2014 (Keystone, CO, USA), RST (Pau, France), et Rencontre CONSOREM UQAM 2015.

Je tiens également à remercier toute l'équipe de Mines Richmont qui m'a apporté un grand soutien durant la durée de la maîtrise. Particulièrement : Daniel Adam, Raynald Vincent, Nathalie Landry, Julie St Georges, Claude Pilote, Chloé Esnault, Coralie Crozier, Maxime LeBacq et Hélène Mellier. Je tiens aussi à remercier Mines Richmont pour la riche opportunité de m'avoir fait participer à la campagne d'exploration de 2012, j'y ai énormément appris grâce à chacune des personnes précédemment citées.

Mes remerciements se tournent aussi vers tout le soutien technique et l'aide dans la réflexion apportée par les élèves et professionnels de l'UQAM. Merci à Raynald Lapointe pour l'accès à tout l'équipement de l'UQAM et l'aide pour certaines analyses. Merci à Michelle Laithier pour l'apprentissage de Coreldraw et l'aide pour la réalisation de certaines figures. Merci aussi à Sadia Mehdi de l'UQAC pour l'aide durant les analyses LA-ICPMS. Un grand merci à Jeffrey Vaillancourt puis à Denise Roy pour toute l'aide à la gestion. Merci aussi à Silvain Rafini et Stéphane Faure pour les nombreuses discussions très pertinentes dans l'aide à la compréhension et à la communication des informations associées à ce travail. Je tiens

également à remercier tous les professeurs qui m'ont permis de bénéficier des 8 postes d'auxiliaires que j'ai pris un immense plaisir à faire, et qui m'ont permis de découvrir l'enseignement ; merci, donc, pour votre confiance Michel Jébrak, Michel Gauthier, Olivier Nadeau, Pierre Lacoste, François Goulet et Claire Somers.

Merci enfin à tous mes collègues qui m'ont tant apporté durant ces deux dernières années: Sacha, Christophe, Julien, Noémie, Ludo, Christian, ainsi que Jocelyn, Yannick, Morgann, Christine, Pierre-Alain, Sam tant pour les discussions scientifiques que les à côtés. J'adresse aussi un clin d'œil à Stéphane Roudaut et Emilie Delpech qui m'ont beaucoup aidé au départ. Enfin, merci à Pauline d'avoir été si compréhensive et patiente durant les moments difficiles et durant l'éloignement des terrains, merci pour ce soutien qui m'a été essentiel et précieux. Enfin mes remerciements se tournent vers mes parents et ma famille sans qui tout cela m'aurait été impossible.

TABLE DES MATIÈRES

AVANT-PROPOS i
REMERCIEMENTS v
LISTE DES FIGURES ix
LISTE DES TABLEAUX x
RÉSUMÉ xi
INTRODUCTION GÉNÉRALE 2
CHAPITRE I
FROM ALKALINE INTRUSION-RELATED TO OROGENIC MINERALIZATIONS: THE WASAMAC GOLD DEPOSIT, ABITIBI GREENSTONE BELT, CANADA 8
Abstract 9
1.1 Introduction 10
1.2 Regional Geologic Setting 12
1.2.1 Geology and structural setting of the Rouyn-Noranda gold district 12
1.2.2 Wasamac Deposit geology 14
1.2.2.1 Lithologies 14
1.2.2.2 Structural geology 16
1.2.2.3 Metamorphic assemblage 18
1.3 Alteration footprints and paragenesis 18
1.3.1 Sampling and analytical methods 18
1.3.2 Alteration assemblages 20
1.3.2.1 Petrology and mineralogy 20
1.4 Gold mineralization 24
1.4.1 Gold mineralogy and relations with pyrite 24
1.4.2 Pyrite zonations 26
1.5 Discussion 28

1.5.1 Hydrothermal alteration signatures 28
1.5.2 Mineralization and maturation process 32
1.5.2.1 Early gold-bearing pyrite stage and pyrite overgrowths 32
1.5.2.2 Evolution of gold characteristics 34
1.5.2.3 Comparison with other deposits and implication for ore genesis 35
1.6 Conclusion 37
Aknowledgements 38
References 38
CONCLUSION GÉNÉRALE 66
APPENDICE A
ANALYSES GEOCHIMIQUES DU GISEMENT DE WASAMAC 68
APPENDICE B
ANALYSES LA-ICP-MS DES PYRITES DU GISEMENT DE WASAMAC 84
BIBLIOGRAPHIE GÉNÉRALE 105

LISTE DES FIGURES

Figure Page
Figure 1.1 Geological setting of the Blake River Group 45
Figure 1.2 Geological map of the Francoeur-Wasa shear zone 46
Figure 1. 3 Simplified typical cross-sections of Francoeur and Wasamac 47
Figure 1.4 Longitudinal section of the FWSZ in the Wasamac deposit 48
Figure 1.5 Macro- and micro-photographs of Wasamac lithologies 49
Figure 1.6 Macro- and micro-photographs of Wasamac alteration facies 50
Figure 1.7 Immobile elements diagram 51
Figure 1.8 REE diagram from unaltered and altered units 51
Figure 1.9 Alkali and silica diagram 52
Figure 1.10 Isocone diagrams of selected elements 53
Figure 1.11 Mass balance calculations from samples described in Fig.10 54
Figure 1.12 Longitudinal summary of alteration 55
Figure 1.13 Longitudinal summary of gold mineralogy 56
Figure 1.14 Micro-photographs of gold mineralizations 58
Figure 1.15 LA-ICP-MS maps of a pyrite grain 59
Figure 1.16 Schematic model of pyrite zonations and metallic anomalies 60
Figure 1.17 Schematic interpretation of hydrothermal and tectonic processes 61
Figure 1.18 Proposed geological setting of Wasamac, Francoeur, Kerr-Addison and Kirkland Lake deposits 62

LISTE DES TABLEAUX

Tableau Page

Table 1.1 Alteration and mineralization essential caracteristics described within alkaline intrusion-related deposits, orogenic gold deposits and within the Wasamac deposit..... 63

Table 1. 2 Descriptive comparison between several gold deposits situated within the CLLFZ..... 65

RÉSUMÉ

Le gisement de Wasamac est un exemple de gite d'or de ceinture de roches vertes archéennes appartenant à la Sous-province de l'Abitibi, Craton du Lac Supérieur, à 15km au sud-ouest de Rouyn-Noranda, Québec, Canada. Le gisement est situé le long de la Faille Francoeur-Wasa (FWSZ), structure pluri-kilométrique de second ordre parallèle à la Faille Cadillac-Larder Lake (CLLFZ) recoupant les unités méta-volcaniques du Groupe de Blake-River. La FWSZ est caractérisée par une déformation ductile de puissance décamétrique, de direction est-ouest et à pendage vers le Nord à 55° de moyenne. La minéralisation en or est strictement associée avec la portion mylonitisée et altérée de la faille.

Un total de 252 923 onces d'or (1 892 448 tonnes à 4,16 g/t Au) a été miné entre 1965 et 1971. Les ressources indiquées sont estimées à 1 402 263 onces d'or (15 251 529 tonnes à 2,86 g/t Au) et les ressources inférées sont estimées à 1 605 388 onces d'or (18 758 786 tonnes à 2,66 g/t Au). La minéralisation en or est spatialement associée à de la pyrite micrométrique disséminée au sein de deux faciès d'altération pervasifs affectant les méta-andésites mylonitisées. Les deux faciès d'altération aurifères présentent une forte affinité alcaline et sont reliés à deux évènements hydrothermaux distincts.

Une altération potassique précoce est caractérisée par une couleur rouge très intense causée par des micro-inclusions d'hématite « poussiéreuse ». La minéralisation aurifère est principalement incluse dans des grains de pyrite sous forme de tellurures d'or. L'association métallique associée à ce faciès d'altération est fortement enrichie en Te-Au-Ag-Mo-Pb-Bi-W.

Le deuxième faciès d'altération, plus tardif, est sodique et présente majoritairement une composition riche en albite et en pyrite. La minéralisation en or associée est distinctement en or natif, présent en grains libres et disséminés dans l'assemblage d'altération. Ce faciès présente une signature géochimique en éléments métalliques similaire à l'altération potassique précoce, mais moins concentrée.

De tels assemblages minéralogiques et métalliques sont communs aux gisements spatialement associés aux intrusions alcalines. Régionalement, plusieurs minéralisations en Ontario présentes le long de la CLLFZ appartiennent à ce type de gite et sont associés à des syénites. Malgré l'absence d'intrusion alcaline dans le gisement Wasamac, ce dernier présente de nombreuses similitudes avec les gites spatialement associés aux intrusions syénitiques tout comme avec les gites orogéniques. Il est proposé que le gisement Wasamac illustre la superposition de ces deux modèles de gites.

MOTS CLÉS : Gisement d'or archéen, remplacement, mylonite, ductile, tellurures, or natif, pyrite, hydrothermalisme alcalin.

INTRODUCTION GÉNÉRALE

Avec plus de 4 200 tonnes d'or et 72 gisements, dont 37 contenant plus de 10 tonnes d'or et 4 contenant plus de 100 tonnes d'or (Dubé et Gosselin, 2007; Rafini, 2014), la Faille Cadillac-Larder Lake (CLLFZ) est une des structures archéennes les plus fertiles au monde (Goldfarb et al., 2001, 2005). Elle comprend des gites aurifères de type orogénique, volcanogène et porphyrique. Ces dernières décennies, des travaux de recherche sur les gites orogéniques se sont concentrés sur la caractérisation des critères physico-chimiques associés à la précipitation de l'or (McCuaig et Kerrich, 1998 ; Goldfarb et al., 2001, 2005, références associées). L'étude des composantes structurales et géochimiques permettent de contraindre des caractéristiques type pour les gites d'or orogénique, très majoritairement définis à moins de 1 km de corridors tectoniques majeurs (Rabeau et al., 2013). Cependant, tant l'âge précis ou la source des minéralisations et de l'activité hydrothermale sont beaucoup moins contraints voire encore incompris (Groves et al., 2003). De récents progrès sur la source et les processus minéralisants émergent grâce à l'utilisation de nouvelles technologies permettant l'observation de nanoparticules d'or en association avec les sulfures (Cabri et al., 1989; Cook et Chryssoulis, 1990; Mumin et al., 1994; Large et al., 2007; Cook et al., 2009). Large et al., (2007, 2009) a ainsi pu démontrer une source sédimentaire de l'or pour des gisements d'âge protérozoïque et inférieur grâce à la cartographie à l'échelle microscopique de sulfures aurifères.

La forte corrélation spatiale entre les intrusions felsiques et alcalines et les minéralisations aurifères est décrite depuis longtemps au sein de ceintures de roches vertes archéennes (Colvine, 1989; Witt, 1992, Thompson et al., 1999; Lang et Baker, 2001; Robert, 2001; Hart et Goldfarb, 2005; Neumayr, 2008; Mair et al., 2011). De récentes études considèrent les gisements spatialement associés aux intrusions comme un type de gite distinct. En Abitibi, deux modèles génétiques relatifs aux minéralisations spatialement associées aux syénites ont été proposés : (1) une

circulation hydrothermale riche en or contemporaine de l'intrusion possiblement d'origine magmatique, et (2) un contrôle structural des minéralisations dans l'intrusion par contraste rhéologique avec l'encaissant (Zhang et al., 2014; Bigot et Jébrak, 2015). Cependant, malgré l'émergence de nouveaux outils analytiques, la distinction entre les gites de type orogénique et spatialement associé aux intrusions est encore sujet à controverse (Sillitoe et al., 2008; Cook et al., 2009). Mair et al. (2011) proposent une distinction génétique pour les gisements aurifères associés aux intrusions en étudiant leur situation tectonique proche de frontières crustales et au dessus de remontées mantelliques dans la lithosphère subcontinentale métasomatisée. Ils proposent également une période précise de mise en place coïncidant avec des régimes tectoniques transitionnels post-orogéniques. Plus récemment, les études sur les gisements de Young Davidson (Zhang et al., 2014), Beattie (Bigot et Jébrak 2015) et Malartic (Helt et al., 2014), apportent de nombreuses informations caractérisant les processus de minéralisation des gites d'or spatialement associés aux syénites. Cependant, les modèles génétiques associés sont encore sujets à controverse.

Entre Rouyn-Noranda et Kirkland Lake, plusieurs gisements sont situés le long de la Faille Cadillac-Larder Lake (CLLFZ) et le long de failles de second ordre ; ils présentent une affinité alcaline plus ou moins prononcée. La présence d'intrusions alcalines n'est pas été décrite dans tous les gisements. Cette région représente un environnement régional propice à l'étude des relations et des éventuelles interactions entre les gites de type orogénique et ceux associés aux syénites. La minéralisation en or la plus importante du camp minier de Rouyn-Noranda est le gisement volcanogène de l'ancienne mine Horne, avec une production de 260 t d'or (Monecke et al., 2008). Les gisements aurifères et indices d'or suivants sont décrits au sud-ouest de Rouyn-Noranda en Ontario et au Québec par différents auteurs : Kerr-Addison (332,61 t Au) (Kishida et Kerrich, 1987; Smith et al., 1993), Cheminis (9,17 t Au), Omega (20,82 t Au) (Ispolatov et al., 2008), Baie Renault (Legault et Rabeau, 2007), Francoeur (16,07 t Au) (Couture et Pilote, 1994). A l'Ouest de ces gisements, des

minéralisations aurifères spatialement associées à des syénites sont aussi décrites le long de la CLLFZ : Kirkland Lake (748,55 t Au) (Ispolatov et al., 2008) et Young Davidson (Zhang et al. 2014). Trois interprétations génétiques ont été proposées pour ces gisements : (1) orogénique à Francoeur, Kerr-Addison, Cheminis, Omega et Young Davidson (?), (2) spatialement associé à un porphyre à Cu-Mo-Au (Baie Renault) et (3) spatialement associé à des syénites pour les gisements de Kerr-Addison (?), Young Davidson (?), et Kirkland Lake.

Le gisement Wasamac (83,46 t Au) est associé à une zone de déformation de second ordre de plus de 20km : la zone de faille Francoeur-Wasa (FWSZ). Quatre zones économiques sont identifiées le long de la FWSZ au gisement Wasamac: les Zones Principale, 1, 2 et 3. Les minéralisations en or y sont associées à une forte altération hydrothermale alcaline. Cette altération est remarquable par deux faciès : potassique et albitique. Ce mémoire présente une description minéralogique et géochimique des altérations ainsi que des minéralisations du secteur de Wasamac. On établira la datation relative des évènements d'altération ainsi que l'évolution parallèle de la minéralogie de l'or. Les zonations des pyrites et la disposition de l'or associée seront caractérisées par des analyses au microscope électronique à balayage (MEB) et par spectrométrie de masse à plasma induit couplée à l'ablation laser (LA-ICP-MS). Il sera discuté ensuite la corrélation entre les processus hydrothermaux et l'activité tectonique de la FWSZ. Cette étude permettra de bien situer la gitologie du gisement de Wasamac par rapport aux gisements spatialement associés aux syénites et aux gisements orogéniques.

L'objectif de ce travail est de proposer une interprétation des processus de mise en place de la minéralisation de Wasamac. Nous caractérisons les altérations et les minéralisations du gisement, puis les comparerons avec celles décrites dans d'autres gisements le long de la CLLFZ. Une comparaison sera enfin effectuée avec les gisements aurifères associés aux syénites.

Références

Bigot, L., & Jébrak, M., 2015. Gold Mineralization at the Syenite-Hosted Beattie Gold Deposit, Duparquet, Neoarchean Abitibi Belt, Canada. Economic Geology, v.110 (2), p.315-335.

Cabri, L.J., Chryssoulis, S.L., de Villiers, J.P., Laflamme, J.G., & Buseck, P.R., 1989. The nature of "invisible" gold in arsenopyrite. The Canadian Mineralogist, v.27 (3), p.353-362.

Colvine, A.C., Fyon, J.A., Heather, K.B., Marmont, S., Smith, P.M., & Troop, D.G., 1988. Archean Lode Gold Deposits in Ontario; Ontario Geological Survey ; Miscellaneous Paper, v.139, 136p.

Cook, N.J., & Chryssoulis, S.L., 1990. Concentrations of invisible gold in the common sulfides. The Canadian Mineralogist, v.28 (1), p.1-16.

Cook, N.J., Ciobanu, C.L., & Mao, J., 2009. Textural control on gold distribution in As-free pyrite from the Dongping, Huangtuliang and Hougou gold deposits, North China craton (Hebei Province, China): Chemical Geology, v.264, p.101-121.

Couture, J.F., & Pilote, P., 1994. Gîtologie des gisements d'or du district de Rouyn-Noranda : études récentes. Ministère de l'Énergie et des Ressources, Québec ; DV 92-07, 143p.

Dube, B., & Gosselin, P., 2007. Greenstone-hosted quartz-carbonate vein deposits. Mineral Deposits of Canada: A synthesis of major deposit-types, district metallogeny, the evolution of geological provinces, and exploration methods: Geological Association of Canada, Mineral Deposits Division, Special Publication, v.5, p.49-73.

Goldfarb, R.J., Baker, T., Dube, B., Groves, D.I., Hart, C.J., & Gosselin, P., 2005. Distribution, character, and genesis of gold deposits in metamorphic terranes. Economic Geology 100th anniversary volume, v.40.

Goldfarb, R.J., Groves, D.I., & Gardoll, S., 2001. Orogenic gold and geologic time: a global synthesis. Ore geology reviews, v.18 (1), p.1-75.

Groves, D.I., Goldfarb, R.J., Robert, F., & Hart, C.J.R., 2003. Gold deposits in metamorphic belts: Overview of current understanding, outstanding problems, future research, and exploration significance: Economic Geology, v.98 (1), p.1-29.

Hart, C.J.R., & Goldfarb, R.J., 2005. Distinguishing intrusion-related from orogenic gold systems. New Zealand Minerals Conference Proceedings, p.125-133.

Helt, M.K., Williams-Jones, A.E., Clark, J.R., Boswell, A.W., & Wares, R.P., 2014. Constraints on the genesis of the Archean oxidized, intrusion-related Canadian Malartic gold deposit, Quebec, Canada. Economic Geology, v.109, p.713–735.

Ispolatov, V., Lafrance, B., Dubé, B., Creaser, R., & Hamilton, M., 2008. Geologic and structural setting of gold mineralization in the Kirkland Lake-Larder Lake gold belt, Ontario. Economic Geology, v.103 (6), p.1309-1340.

Kishida, A., & Kerrich, R., 1987. Hydrothermal alteration zoning and gold concentration at the Kerr-Addison Archean lode gold deposit, Kirkland Lake, Ontario. Economic Geology, v.82 (3), p.649-690.

Lang, J.R., & Baker, T., 2001. Intrusion-related gold systems: the present level of understanding. Mineralium Deposita, v.36 (6), p.477-489.

Large, R.R., Maslennikov, V.V., Robert, F., Danyushevsky, L.V., & Chang, Z., 2007, Multistage sedimentary and metamorphic origin of pyrite and gold in the giant Sukhoi Log deposit, Lena gold province, Russia, Economic Geology, v.102, p.1233-1267.

Large, R.R., Danyushevsky, L., Hollit, C., Maslennikov, V., Meffre, S., Gilbert, S., Bull, S., Scott, R., Emsbo, P., Thomas, H., Singh, B., & Foster, J., 2009. Gold and trace element zonation in pyrite using a laser imaging technique: implications for the timing of gold in orogenic and Carlin-style sediment-hosted deposits, Economic Geology, v.104 (5), p.635-668.

Legault, M., & Rabeau, O., 2007. Étude métallogénique et modélisation 3D de la Faille de Cadillac dans le secteur de Rouyn-Noranda (Phase 2). Ministère des Ressources Naturelles et de la Faune, Québec ; RP2007-03, 11p.

Mair, J.L., Farmer, G.L., Groves, D.I., Hart, C.J., & Goldfarb, R. J., 2011. Petrogenesis of postcollisional magmatism at Scheelite Dome, Yukon, Canada:

Evidence for a lithospheric mantle source for magmas associated with intrusion-related gold systems. Economic Geology, v.106 (3), p.451-480.

McCuaig, T.C., & Kerrich, R., 1998. P-T-t deformation fluid characteristics of lode gold deposits: evidence from alteration systematics. Ore Geology Reviews, v.12 (6), p.381-453.

Monecke, T., Gibson, H., Dubé, B., Laurin, J., Hannington, M.D., & Martin, L., 2008. Geology and Volcanic Setting of the Horne Deposit, Rouyn-Noranda, Quebec, Initial Results of a New Research Project. Geological Survey of Canada.

Mumin, A.H., Fleet, M.E., & Chryssoulis, S., 1994, Gold mineralization in As-rich mesothermal gold ores of the Bogosu-Prestea mining district of the Ashanti gold belt, Ghana; remobilization of invisible gold, Mineralium Deposita, v.29, p.445-460.

Neumayr, P., Walshe, J., Hagemann, S., Petersen, K., Roache, A., Frikken, P., Horn, L., & Halley, S., 2008. Oxidized and reduced mineral assemblages in greenstone belt rocks of the St. Ives gold camp, Western Australia: vectors to high-grade ore bodies in Archaean gold deposits ? Mineralium Deposita, v.43 (3), p.363-371.

Rabeau, O., Royer, J.J., Jébrak, M., & Cheilletz, A., 2013. Log-uniform distribution of gold deposits along major Archean fault zones. Mineralium Deposita, v.48 (7), p.817-824.

Rafini, S., 2014. Typologie des minéralisations aurifères associées à la Faille de Cadillac. Rapport du projet CONSOREM 2011-01 et 2012-01, 45p.

Robert, F., 2001. Syenite associated disseminated gold deposit in the Abitibi green-stone belt, Canada: Mineralium Deposita, v.36, p. 505-516.

Sillitoe, R.H., 2008. Special paper: major gold deposits and belts of the North and South American Cordillera: distribution, tectonomagmatic settings, and metallogenic considerations. Economic Geology, v.103 (4), p.663-687.

Smith, J.R., Spooner, E.T.C., Broughton, D.W., & Ploeger, F.R., 1993. Archean Au-Ag-(W) Quartz Vein/Disseminated mineralisation within the Larder Lake - Cadillac Break, Kerr Addison - Chesterville System, North East Ontario, Canada, Ontario Geoscience Research Grant Program, Grant No. 364; Ontario Geological Survey, Open File Report 5831, 310p.

Thompson, J.F.H., Sillitoe, R.H., Baker, T., Lang, J.R., & Mortensen, J.K., 1999. Intrusion-related gold deposits associated with tungsten-tin provinces. Mineralium Deposita, v.34 (4), p.323-334.

Witt, W.K., 1992. Porphyry intrusions and albitites in the Bardoc-Kalgoorlie area, Western Australia, and their role in Archean epigenetic gold mineralization. Canadian Journal of Earth Sciences, v.29 (8), p.1609-1622.

Zhang, J., Lin, S., Linnen, R., & Martin, R., 2014. Structural setting of the Young-Davidson syenite-hosted gold deposit in the Western Cadillac-Larder Lake Deformation Zone, Abitibi Greenstone Belt, Superior Province, Ontario. Precambrian Research, v.248, p.39-59.

CHAPITRE I

FROM ALKALINE INTRUSION-RELATED TO OROGENIC MINERALIZATIONS: THE WASAMAC GOLD DEPOSIT, ABITIBI GREENSTONE BELT, CANADA

Abstract

The Wasamac deposit is an example of an Archean greenstone-hosted gold deposit located in the Abitibi belt, 15km southwest of Rouyn-Noranda, Quebec, Canada. The deposit is localized along the Francoeur-Wasa Shear Zone (FWSZ), which is a second-order kilometric-scale fault of the Cadillac-Larder Lake Fault Zone (CLLFZ), crosscutting meta-volcanic units of the Black River Group. The FWSZ is characterized by a ductile deformation following an east-west direction parallel to the CLLFZ and dips 55° to the North. Gold mineralization is strictly associated with the altered mylonitized portion of the fault.

A total of 252 923 oz Au (1 892 448 tonnes grading 4.16 g/t Au) have been mined between 1965 and 1971. Indicated resources are estimated at 1 402 263 oz Au (15 251 529 t at 2,86 g/t Au) and inferred resources are estimated at 1 605 388 oz Au (18 758 786 t at 2,66 g/t Au). Gold mineralization occurs spatially in association with disseminated micrometric pyrite related to two pervasive alteration affecting mylonitized meta-andesites. Both gold-rich alterations display a strong alkaline character and were related to two successive hydrothermal events.

The early potassic alteration is characterized by an intense red coloration due to high dusty hematite content. Gold mineralization is predominantly trapped into pyrite as gold-telluride minerals. The metallic assemblage constituting K-feldspar hydrothermal event is strongly enriched in Te-Au-Ag-Mo-Pb-Bi-W.

The late sodic alteration is albite-rich and marked by higher pyrite content. Gold mineralization associated is mostly native. It shows similar metallic enrichments with lower intensities.

Such alteration assemblages and metallic anomalies are usually described close to and within alkaline intrusion-related gold deposits. Regionally, deposits in Ontario within the Cadillac-Larder-Lake Fault Zone display similar characteristics spatially related to syenite-hosted gold deposits. The Wasamac deposit shares similarities with both syenite-related gold deposit and orogenic gold deposits. It is proposed that the Wasamac deposit illustrates the overlapping of both deposit types.

KEYWORDS: Archean gold deposit, replacement, mylonite, ductile shear zone, telluride, native gold, pyrite, alkaline hydrothermalism.

1.1 Introduction

With more than 4 200 tons of gold and 72 gold deposits, 37 of which contain more than 10 tons of gold and 4 of which are >100 tAu deposits (Dubé & Gosselin, 2007; Rafini, 2014), the CLLFZ is one of the most fertile Archean structure in the world (Goldfarb et al., 2001, 2005). It comprises orogenic, volcanogenic and porphyry style mineralizations. In the last few decades, extensive investigations characterised gold deposition conditions and tectonic settings for orogenic deposits (McCuaig & Kerrich, 1998; Goldfarb et al., 2001, 2005 and references therein). Both structural and geochemical components characterises the orogenic deposits group, sitting along the major fault zones and within second and third order related structures (Rabeau et al., 2013). However, precise timing of mineralisations and hydrothermal fluids source remains poorly understood (Groves et al. 2003). Recent studies focused on gold nanoparticles in association with sulphides and allowed a better understanding for both source and processes (Cabri et al. 1989; Cook & Chryssoulis, 1990; Mumin et al., 1994; Large et al., 2007; Cook et al., 2009). Large et al. (2007, 2009) proposed a sedimentary source for gold within proterozic and younger examples of deposits, based on micrometric to nanometric detailed mapping of sulphides.

The strong spatial correlation between felsic/alkaline intrusive stocks and gold deposits has long been described within Archean greenstone belts (Colvine, 1989; Witt, 1992, Thompson et al., 1999; Lang & Baker, 2001; Robert, 2001; Hart & Goldfarb, 2005; Neumayr, 2008; Mair et al., 2011). Studies have recently been carried out to consider late Archean alkaline intrusion-related deposits as a distinct type of gold deposit (Robert, 2001).

In the Rouyn-Noranda area, gold mineralizations are related to the 260 t Au VMS deposit described in the Rouyn-Noranda historic mining camp (Monecke et al.,

2008). The following gold deposits and showings are known southwest of Rouyn-Noranda (Fig.1): Kerr-Addison (332.61 t Au) (Kishida & Kerrich, 1987; Smith et al. 1993), Cheminis (9.17 t Au), Omega (20.82 t Au) (Ispolatov et al., 2008), Baie Renault Syenite (Legault & Rabeau, 2007), Francoeur (16.07 t Au) (Couture & Pilote, 1994). In the Western part of the CLLFZ, deposits from Kirkland Lake mining camp (748.55 t Au total) and Young-Davidson are described along the CLLFZ and are spatially associated with syenite intrusions (Ispolatov et al., 2008; Zhang et al., 2014). Three different genetic interpretations have been proposed for these deposits: (1) orogenic in Francoeur, Kerr-Addison, Cheminis, Omega, and Young Davidson (?), (2) porphyry-related at Baie Renault Syenite and (3) syenite-hosted/related such as Kerr-Addison (?), Kirkland Lake deposits, and Young Davidson.

In the Abitibi Greenstone Belt, two genetic models are proposed for gold mineralization spatially associated with syenites: (1) a gold-rich magmatic-hydrothermal system related to the intrusion, and (2) intrusions acting as brittle hosts for gold mineralization (Zhang et al., 2014; Bigot & Jébrak, 2015). However, despite emerging analytical techniques, the distinction between orogenic and intrusion-related mineralizations remains controversial (Sillitoe et al., 2008; Cook et al., 2009). Mair et al. (2011) propose a genetic distinction for intrusion-related gold deposits focussed on the tectonic setting close to lithospheric boundaries and above previously metasomatized subcontinental lithospheric mantle. They also suggest a specific timing emplacement coincident with postcollisional and transitional tectonic regimes. Most recent studies on the alkaline intrusion-related Young-Davidson deposit (Zhang et al., 2014), Beattie deposit (Bigot & Jébrak, 2015) and Malartic deposit (Helt et al., 2014) bring several informations on mineralization processes related to gold deposits spatially associated with syenite-related and granite-related deposits. Therefore genetic implication for gold mineralization still remains contentious.

Southwest of Rouyn-Noranda, numerous gold deposits are hosted along the CLLFZ or within second order faults. They display an irregularly pronounced

alkaline hydrothermal signature. As the presence of alkaline intrusion is not described associated with all the deposits, this area may represent an interesting zone to study in order to understand the hydrothermal relations between syenite-related and orogenic deposits.

The Wasamac deposit (83.46 t Au) is sitting along a 20km-long second order fault zone: the FWSZ (Fig.2). In the vicinity of the deposit, four economic zones were recognised along the FWSZ, from west to east: Main, 1, 2 and 3 (Fig.3). Gold mineralizations are associated with strong alkaline hydrothermal alterations. These alterations are spatially associated with the FWSZ where alkaline intrusions are rare and not spatially controlled by the fault zone. The purpose of this study is to characterize the alterations and mineralizations at the Wasamac gold deposit in order to estimate the factors controlling the mineralization. Comparisons with other gold deposits in the area and in the vicinity of the CLLFZ will also be observed.

This work focuses on geochemical and mineralogical descriptions of the alkaline alterations and mineralizations from the Wasamac deposit. Gold mineralogy and its relations with pyrite zonations will be studied using SEM and LA-ICP-MS analyses. A correlation between hydrothermal processes, gold mineralization and the structural setting will be proposed. The Wasamac gold deposit could represent a transitional deposit between syenite-related and orogenic gold models.

1.2 Regional Geologic Setting

1.2.1 Geology and structural setting of the Rouyn-Noranda gold district

On its Western half, the CLLFZ crosscuts the metavolcanic units of the Blake River Group (Fig.1). This volcanic group is composed of tholeiitic to calc-alkaline

units (Mueller et al., 2012) dated from 2704 to 2695 Ma (McNicoll et al., 2014; references therein). The 2900km^2 Blake River Group is associated with a sub-marine system of three overlapping caldeiras centered on the Rouyn-Noranda aera (Pearson and Daigneault, 2009; Mueller et al., 2012). The Rouyn-Noranda portion of the Blake River Group is metamorphosed from sub-greenschist to greenschist facies, except around plutons were amphibolite grade predominates (Jolly, 1978; Gélinas et al., 1984; Mueller et al., 2012). The Blake River Group is intruded by mafic to felsic and alkaline plutons, dykes and sills (Legault and Rabeau, 2006). Plutonic activity has been subdivided into five suites with respect to their age and their petrogenetic affinities (Beakhouse, 2011). They have been dated from 2750 to 2695 Ma for the pre-tectonic plutons to circa 2680 – 2668 Ma for the late-tectonic alkalic suite. The Blake River Group is locally unconformably overlain by the metasediments of the Archean Timiskaming Group and Proterozoic Cobalt Group. These sediments were respectively dated between 2678 and 2670 Ma and at 2300 Ma (Fairbairn, 1969; Ayer, 2005). The late magmatism is thus contemporous of the Timiskaming volcanism and sedimentation (Bleekhouse, 2011).

The Abitibi Greenstone Belt is the result of far-field motions associated with an oblique-plate convergence (Daigneault et al., 2002 and 2004). Its structural evolution shows a continuum from north to south (Mueller et al., 1996; Daigneault et al., 2002) during a 60 Ma-long polyphased tectonic history. According to Daigneault et al. (2004), eight distinct tectonic phases (D1 to D8) are identified in the Abitibi Subprovince. Deformation (D1) is locally described as east-west trending folds related to a N-S horizontal shortening event. Two tectonic dynamics are recognised between 2695 and 2642 Ma: a north over south thrusting movement (D2, D4, D6) systematically followed by a dextral transpressive accomodation movement (D3, D5, D8). An exhumation event (D7) is recognised at 2660 Ma nearby the Malartic

segment. The CLLFZ is related to the D4 to D8 tectonic activity between 2685Ma and 2642 Ma.

The CLLFZ portion between Rouyn-Noranda and Kirkland Lake districts shows two metallogenic environments associated with gold deposits. Along this deformation zone, gold deposits of the Kirkland Lake area are spatially linked with syenitic intrusions (Robert, 2001; Zhang et al., 2014), whereas in the Rouyn-Noranda area the CLLFZ shows disseminated mineralization associated with diversified metasomatic footprints (Couture and Pilote, 1993; Legault and Rabeau, 2007). The Wasamac deposit is located between these two districts along the FWSZ, a second-order fault parallel and 2,5 kilometers north of the CLLFZ (Fig.2). In the Wasamac property, the shear zone crosscuts the meta-volcanic units of the Blake River Group, stratigraphically composed of intermediate tuffs, andesite, andesitic volcanic breccia and rhyolite. Two intrusive rocks crosscut these units, chronologically a gabbro and a syenite, both faulted by the FWSZ. Along this break, the units of the Blake River Group have been tilted toward the North and follow the same east-west trend. The FWSZ shows strong structural similarities with the CLLFZ, presenting a thick intense ductile shearing of the volcanic units, associated with a strong metasomatic alteration (Couture and Pilote, 1994).

1.2.2 Wasamac Deposit geology

1.2.2.1 Lithologies

In the vicinity of the Wasamac deposit, the Blake River metavolcanic units are related to a bimodal volcanic activity (Pilote and Couture, 1989). It is composed of three main lithologies, intermediate to felsic in composition. Massive andesite is the

most common unit and it is the principal host of the FWSZ from surface to depth (Fig.4). It locally displays a variety of volcanic textures including aphanitic, porphyritic, amygdaloidal, pillowed and brecciated. Andesite Volcanic breccia may be locally over 50m thick. Clasts are composed of andesite-rhyodacite and intermediate to felsic tuffs in a massive or lapilli-crystal tuff matrix (Fig.5A). These synvolcanic fragments are commonly centimetric in size but may locally reach a metric size. They generally represent less than 30% compared to the matrix. Clasts frequently show an angular shape and locally present a coronitic texture. These petrographic characteristics are indicators to a polyphased pyroclastic volcanic activity from at least one proximal volcanic source.

Rhyolitic units are mostly aphanitic and locally porphyritic with quartz and feldspar millimetric phenocrysts. A few volcanogenic textures were identified locally such as flow banding and breccia. Their coloration may vary from greyish to pinkish-beige related to local pervasive albitic and sericitic alteration, which will be detailed later in this memoir. The presence of such alteration is generally spatially associated with micrometric fractures increasing towards the shear zone. Rhyolite is located on the hanging wall of the FWSZ (Fig.4). It shows a brittle deformation instead of a ductile deformation in the andesitic units.

Two generations of intrusive units crosscutting the metavolcanic units of Wasamac were intercepted by drilling: gabbros and syenites. They are both observed locally faulted by the FWSZ. Calc-alkaline gabbros were intercepted by drilling as coarse-grained thick stocks with fine-grained contacts or as metric aphanitic to fine-grained dykes and sills. Syenite dykes, grey in color, are generally metric and more rarely decametric. As they crosscut the gabbro, they are the last intrusive event identified in the vicinity of the Wasamac deposit. Their contact with the host rock is clear and straight. Locally and most frequently close to the FWSZ, contacts may

show brecciation with a red-purple tint related to a potassic pervasive alteration with rare pyrite and very low gold values (below 25ppb).

1.2.2.2 Structural geology

In the vicinity of Wasamac and Francoeur gold deposits, lithologies follow an east-west trend and dip 55° to the North on average. Along the Wasamac property, the second-order FWSZ is an east trending (~260°) mylonitic structure dipping 55° to the North. No regional foliation is observed away from the FWSZ. Host lithology is mostly the andesite and the deformation zone mostly takes place close to the contact between andesite and rhyolite. The thickness of the shear zone varies from several meters up to over a hundred meters and usually enlarges with depth. This deformation zone is characterized by a strong mineral stretching attributed to a S1 foliation (Fig.5B, C, D). This well developped S1 fabric totally erased primary textures and appears to the macroscopic scale as a mylonitic schist (Fig.5B). According to kinematic observations such as mineral lineations and pressure shadows, S1 foliation is related to a reverse movement with dextral components. Both contacts of the FWSZ are progressive over a few meters. They are marked by an increasing concentration of barren carbonate veinlets progressively sheared towards the deformation zone.

A second foliation is recognised within the FWSZ. A S2 "shear band" crenulation cleavage is locally identified with asymmetric Z-type subvertical folds close to and within the high strain zones: in the Main Zone and Zone 3 (Fig.5C, D). S2 never shows transposition into a penetrative foliation and remains a slight structural footprint. Similar S2 crenulation cleavage is regionally identified along the CLLFZ and second-order faults zones and displays a dextral transcurrent motion

(Daigneault et al., 2004; Ispolatov, Lafrance et al., 2008; Zhang et al., 2014). This structural feature was related to the last regional ductile tectonic footprint by the previously cited authors.

S1 and S2 affect all minerals of alteration. Hence, hydrothermal activity is pretectonic to syntectonic. As alteration and mineralization are strictly restricted to the FWSZ, hydrothermal activity would have been most likely syntectonic. Therefore, mineral investigations carried out on pyrites and presented section 1.4.2 of this memoir, suggests that another tardive tectonic event may have occurred. S1 and S2 show similar deformation conditions except for their directions (Fig.5.C, D), they thus took place within the same structural level. Also, they might be the result of one continuous deformation event with a change of direction or during two distinct but close deformation events.

Host lithologies present two kinds of responds to the deformation. Andesite and gabbro show ductile structural features from low to high deformation rates. Silica-rich units such as rhyolite and K-feldspar altered units are frequently brecciated within low deformation rates. Centimetric to metric elongated slivers of less deformed and brecciated units may thus be observed within the FWSZ. This rheological contrast may be the result of structural partitioning, in which competent K-altered silica-rich rocks may not be mylonitized comparatively to surrounding albitized and chlorite-rich softer units. Brittle deformation may also be described within the contacts of felsic and alkaline dykes away from the shear zone.

The regional Horne-Creek Fault (HCF) was intercepted by drilling at the Wasamac deposit. The HCF exposes from 4 to 25 meters thick quartz stockwerks and veins in association with an intense silicification of the host rock. Distal metric gouge contacts were also systematically observed with the fault. A sinistral motion

croscutting the FWSZ was regionally interpreted (Fig.2). The crosscutting relationship between the two faults shows that quartz stockwerks from the HCF crosscuts the FWSZ (Fig.5E). No shearing evidence of the HCF was noticed in drill cores and this fault records a late brittle deformation. However, Pearson and Daigneault (2009) genetically related the HCF to a synvolcanic boundary fault of the Noranda Caldera; which would chronologically relates the HCF to an older epoch than the tectonic activity of the FWSZ.

1.2.2.3 Metamorphic assemblage

The subgreenschist to greenschist-grade metamorphic assemblage described in Wasamac is composed of chlorite, actinolite and locally disseminated magnetite, calcite and anatase for both andesite and gabbro. Epidote was locally described in gabbro as irregular veins or locally pervasive. Chlorite minerals are oriented within the schistosities in or next to the FWSZ. The metamorphism peak is thus pre-tectonic to syn-tectonic, as recognised in Kerr-Addison and other nearby deposits (Kishida and Kerrich, 1987 ; Couture and Pilote, 1994 ; Ayer et al., 2005).

1.3 Alteration footprints and paragenesis

1.3.1 Sampling and analytical methods

Two sampling methods were conduced on diamond drill cores: one composed of 28 samples for detailed specific analyses and another set of 14 samples taken at the scale of the shear zone (Appendice A). The first 28 samples were selected from Main Zone, Zone 2 and Zone 3 (Fig.3). These samples were used for mineralogic, structural

and geochemical observations. They are composed of least-altered and altered units with their proximal least-altered host rock for mass balance calculations. Polished thin sections were examined on 22 samples by optical microscopy, SEM and LA-ICP-MS analyses. SEM used a Hitachi TM-3000. Laser ablation was performed with a M50 Resolution Excimer using a 193nm UV beam. Vaporized matter was transported with He gaz and ionised by plasma-Ar at 6000°K to a 7700x Agilent ICP-MS. Imaging was carried out by a series of parallel lines made of 15µm wide successive ablation spots. 26 elements were analyzed: Fe, S, Cu, Ti, Au, Ag, Te, Pb, Bi, Mo, Ni, Co, Zn, Hg, V, Pt, Cr, Mn, As, W, Ba, Sn, Sb, U, Se, Tl. Each ablation spot represents a pixel on the final mapping imagery for each element. Gold detection limit was fixed at 30ppb. Five standards were analyzed before and after the samples to correct drift. Whole rock analytical methods for the 28 samples used four acid digestion ICP-MS analyses and $Li_2B_4O_7/LiBO_2$ fusion for XRF analyses. They were conducted by Acme Labs, Vancouver.

The set of 14 samples was collected by Mines Richmont during metallurgical tests. They were selected in order to identify the geochemical characteristics of the whole shear zone's bulk mineralogy, along the four economic zones. Gold chemical composition was analyzed using a scanning-electron miscroscope equipped with an energy dispersive spectrometer (SEM-EDS). These samples bring statistical data support thanks to plane polarized reflected light microscopy and SEM-EDS studies on polished sections from heavy minerals concentrations. X-ray fluorescence (XRF), semi-quantitative X-ray diffraction (XRD) and ICP-MS analyses were also conducted on both FWSZ units and host-rocks. XRD used a Bruker AXS D8 Advance Diffractometer, XRF and ICP-MS machines are unknown. These analyses were conduced by SGS mineral services.

1.3.2 Alteration assemblages

Hydrothermal alteration is described within the Wasamac deposit as an intense pervasive metasomatic replacement of intermediate volcanic rocks. Alteration is restricted to the mylonitic portion of the shear zone. Two alkaline alterations are described, both associated with gold mineralization: one dominated by K-feldspar and one dominated by albite and carbonates. A least altered assemblage is observed affecting less deformed andesitic units. It is marked by an increasing concentration of millimetric to centimetric sheared carbonate veinlets towards the shear zone, from 3% to over 30% in volume. The distal zone is marked by variable amounts of sericite, quartz, carbonate and progressively hematized magnetite. This assemblage does not host gold mineralization with economic values.

1.3.2.1 Petrology and mineralogy

Mineralization is strictly associated to potassic and sodic pervasive alteration assemblages, in which gold is spatially associated with disseminated pyrite. K-feldspar assemblage marks a strong potassic metasomatism whereas sodic metasomatism is recognised by an albite-dominated composition. These alteration signatures present short transition zones with fresh rocks. The crosscutting relationship between the two facies shows that K-feldspar alteration predates the albitic alteration (Fig.6A, B).

K-feldspar alteration is observed as a red brick-colored aphanitic assemblage (Fig.6A, C, D), mostly composed of microcline, quartz and pyrite with smaller amounts of sericite and carbonates. This intense colour of alteration is due to inclusions of dusty hematite trapped into K-feldspar structure. No biotite was recognised. Minerals are micrometric in size and are hardly distinguishable under

optical microscopy as their size reaches a maximum of 50μm (Fig.6E, F). This alteration usually presents sharp contacts with its andesitic host and frequently appears as dyke-like units (Fig.6C). Clast-supported brecciation is also commonly observed affecting K-feldspar altered sections, particularly within their contacts with the host rock. Matrix is mostly composed of albite, carbonate, sericite, chlorite and pyrite with rare visible gold grains. Clasts vary in size from millimetric to decametric, they display angular or rounded shapes and they are not oriented. Rounded clasts have irregular contacts in result of dissolution caused by chemical reaction between the clasts and the matrix. Such brecciation has also been observed within low deformation rates. Also, local cataclasis fabric is observed, displaying millimetric to centimetric K-feldspar altered clasts in an albite-dominated matrix (Fig.6A, B). This type of breccia is characterized by successive centimetric to decimetric bands oriented within the main schistosity of the FWSZ. Late quartz veinlets may also be observed with rare chalcopyrite, molybdenite and native gold remobilizations. Outside the shear zone, syenite dykes were intercepted in drill holes. They display a red potassic alteration, related to local fracturation. These altered dykes display limited gold enrichment <25ppb, compared to least-altered syenite dykes that contain 5ppb Au on average.

Albitization is described within the Wasamac deposit as a fine-grained beige colored unit with greyish to purplish tints. It occurs as an intense pervasive alteration affecting the meta-volcanic units. Na-feldspar alteration assemblage is composed of micrometric albite, quartz, carbonates, pyrite and sericite, usually hardly discernable by optical microscopy (Fig.6E). Sulfur content is higher than in the potassic facies of alteration, commonly about 5% abundance, locally reaching 20%. Albitization affects least-altered volcanic units and overprints the potassic alteration (Fig.6A, B).

These two alteration facies indicate significant hydrothermal changes in the oxidation state. The abundant hematite causing the intense red alteration color of K-feldspar assemblage is related to a highly oxidized hydrothermal activity. The pyrite-rich albitic assemblage displaying fewer oxides may record a more reduced environment of crystallization. Both alteration assemblages are zoned at the scale of the property, along the longitudinal axis of the shear-zone. K-feldspar alteration is dominant in the central part of the fault (Zones 1 and 2) and albitic alteration prevails on both side of the latter, in Main Zone and Zone 3. The respective zonation and timing of alteration assemblages, such as the different redox crystallisation conditions for both alteration assemblages allow to distinct two separated hydrothermal events. To better understand hydrothermal processes, geochemical characterization of both altered and least-altered host rocks are proposed in the next section.

1.3.2.2 Geochemistry

Within Archean greenstone belts, Zr, Y, Nb and REE incompatible immobile elements are used in order to define precursor lithology and to monitor fractionation of compatible elements for tholeiitic to transitional volcanic units (MacLean and Barrett, 1993). Also, the immobility of Zr, Ti and Al elements can yield precise identification of metamorphosed and altered volcanics precursors (MacLean and Kranidiotis, 1987). Within the Wasamac deposit, immobility of Zr and Ti and locally that of Al, Fe, Nb, Y and REE is observed. Lithogeochemical analyses of altered units were plotted in a binary TiO_2 vs. Zr diagram to identify their volcanic precursor rock type and alteration patterns (Fig.7). Two clusters may be distinguished containing fresh and altered samples, representing andesite and rhyolite units. Greenschist facies metamorphosed units are considered as fresh or least altered.

Lithogeochemical affiliation between altered and least-altered samples is observed, which argues that pervasive alteration overprinted mafic to intermediate and felsic volcanic units. Also, similar flat profiles between altered and fresh volcanic units is observed on a REE diagram (Fig.8). Both alkaline alteration facies do not follow syenite dykes trend but that of volcanic hosts. These observations lead to propose that alkaline alterations result of hydrothermal replacement of least altered volcanic units, originally indermediate to felsic in composition.

Alteration assemblages presented in the previous section for both hydrothermal facies support a strong alkali inprint. According to LeBas et al., 1986 diagram, computing Na_2O, K_2O and SiO_2 mobile elements, fresh volcanic samples display a tholeitic to calc-alkalic signature. Altered samples profile two alkaline trends, proportional with alteration intensity and characteristic of the alteration type (Fig.9). SiO_2 concentration may vary due to micrometric irregular veinlets locally associated with potassic-altered units. In order to calculate absolute mass gains and losses of mobile elements, Grant isocon diagram method (Grant, 1986) was undertaken with selected pairs of fresh and altered units and with respect to their immobile elements concentrations. Two isocon diagrams are proposed for each alteration facies using typical altered units with their least altered proximal precursor displaying similar immobile elements ratios. Grant isocones and mass balance calculations show close chemical associations enrichment and depletion for both alteration facies (Fig.10, Fig.11), also albitic alteration appears less enriched – or depleted – in elements concentrations.

Potassic alteration shows strong enrichments in W, Pb, Bi, Te, Mo, Ag, Au, minor As, variable Cu and depletion in Zn, Mg, V (Fig.10, Fig.11). This metal assemblage paired with the destruction of the ferro-magnesian minerals is a typical signature of alkaline intrusion-related gold deposits (Thompson et al., 1999; Lang and Baker, 2001; Robert, 2001) and will be developped in the discussion section. Albitic alteration shows similar gains, but in smaller amounts, and the enrichments in Mo,

Te, Pb, Bi are less significant (Fig.11). There is an exception for the Tungsten, which gain is stronger in the Na alteration than in the K-feldspar alteration assemblage.

At the scale of the Wasamac shear zone, potassium enrichment is stronger in its central part, within the longitudinal axis of the fault (Fig.12). This enrichment is linked with the K-feldspar crystallization, which is typical of the hydrothermal activity early stage preserved in Zones 1 and 2. These zones particularly show strong Mo addition consistent with K mass gains. K enrichment is also strong in Main Zone and Zone 3 and is related to a strong sericitization (Fig.12), associated with the albitization hydrothermal event. Sodium enrichment may strongly vary in Zones 1 and 2 as albite alteration may locally not be observed at all (Fig.6.C). Main zone and Zone 3 are typically enriched in Na and less enriched in K.

1.4 Gold mineralization

1.4.1 Gold mineralogy and relations with pyrite

Within the Wasamac deposit, gold is spatially associated with disseminated As-free pyrite, the only sulphide that composes both alteration assemblages previously described. No gold-bearing lode system is associated with the Wasamac deposit; which represents a specific characteristic of the mineralization along the FWSZ (Couture and Pilote, 1994). Pyrite grains are broadly <100μm in size and <5% in abundance within K-feldspar alteration assemblage. Within the albitic alteration assemblage, pyrite is frequently >5% in abundance and coarser grained. Textural characteristics of pyrite grains will be described later in this study.

The mineralogic assemblage of gold and the relations between pyrite and gold are characteristic for each alteration facies. Gold characteristics are thus zoned at the scale of the property (Fig.13). Gold tellurides compose 50% of the mineralization on

average within the K-feldspar alteration facies identified in Zones 1 and 2. Within the albitic alteration assemblage described in Main Zone and Zone 3, native gold compose over 98% of the mineralization largely observed as free disseminated grains (Fig.13 and Fig.14.A). Rare micrometric chalcopyrite grains were described sporadically disseminated within both alteration facies.

Over 80% of telluride minerals are described in contact with pyrite grains. This gold mineralogy is very fine grained: 3,5µm on average. Composition of telluride minerals is petzite (Ag_3AuTe) and calaverite ($AuTe_2$). Ag, Bi, Pb and Ni tellurides have also been described in trace amounts. Gold tellurides mostly occur as inclusions in pyrite and are also related to local porosities. They are also frequently described within thin pyrite fracture planes (Fig.14.B, C, D, E, F). Gold tellurides filling micrometric fractures in pyrites are locally juxtaposed with native gold. SEM mapping shows that native gold is associated with larger fractures (>5µm) than for gold tellurides, hosted within smaller micrometric to sub-micrometric fracture planes. This relation between the size of pyrite fractures and gold mineralogy is a common feature described within the Wasamac deposit mineralization. Also, pyrite fractures do not show specific directions. Hence, the erratic width of fractures does not record separate structural events. The contact between native gold and tellurides in fractures may thus be related to a single brittle event. More rarely, gold tellurides were described disseminated in the alteration minerals assemblage, and associated with K-feldspar, sphene, hematite and sericite minerals.

Native gold, mostly free, is abundant within the albitic alteration assemblage. Free gold grains average size is 5,7µm and they are frequently described up to more than 10µm in size. According to SEM observations, native gold composition includes 8% silver on average. Gold is spatially associated with pyrite-rich zones, where pyrite displays a clear texture and rarely shows gold inclusions. Also, pyrite is locally

affected by brecciation and forms micrometric cataclasis zones that display angular pyrite grains with disseminated native gold grains in a cement of carbonates, albite, sericite, quartz, chlorite (Fig.14.A). Both presence of gold telluride minerals and free native gold grains is rare but locally described (Fig.14.G). Gold mineralization may thus be genetically linked to two separated events or to one event then remobilized by hydrothermal and/or structural overprinting. This will be discussed later.

1.4.2 Pyrite zonations

Thirteen pyrites were selected from both typical alteration facies in Main Zone and in Zone 2 for LA-ICP-MS investigations (Fig.15, appendix B). All of the thirteen pyrites mapped showed local Au results over the underground noise. Although pyrite is small in size in both alteration assemblages, it frequently displays zonations with spongy cores and clear secondary overgrowths. Four crystallisation stages were determined with LA-ICP-MS technique (Fig.15 and Fig.16). Usually invisible by optical microscopy, these zonations are composed of successive specific chemical assemblages observed in pyrites from the two alteration facies.

A first core (pyrite stage 1), rarely preserved, appears as an anhedral pyrite with a clear texture. This first stage of crystallisation does not carry gold or any significant metallic anomaly. Traces of As, Pb, Se, Bi, Ba, Ti and V may be noticed.

The second crystallisation phase (pyrite stage 2) is a porous pyrite carrying gold. Generally euhedral, the cavities of this pyrite are often filled with gold tellurides, sphene, silicates, hematite and chalcopyrite (Fig.15). The lattice of this pyrite generation is enriched in Ag, Au, Te, Pb, Bi, Cu +/- Zn, Co, Ti, Ba, As. Except for LA-ICP-MS analyses, most of the gold, tellurium and silver anomalies occurs as invisible particles within the pyrite stage 2 lattice, with respect to the methods of observation used in this study. Gold grains associated with pyrite lattice may thus be

inferior to the micrometric scale in size. Cu and Ti anomalies were described sporadically with strong values because of chalcopyrite and sphene inclusions (Fig.15).

According to microscopic observations on 22 samples, the first pyrite stages 1 and 2 are more abundant in the K-feldspar assemblage than in the albitic assemblage, where pyrites display a clear texture.

The third phase of crystallisation (pyrite stage 3) is a pyrite displaying clear texture overgrowths. It is composed of euhedral pyrite, generally poor in trace elements. Pyrite stage 3 locally carries large chalcopyrite inclusions and shows scarce micrometric amygdaloidal-shaped voids. Rare micrometric gold telluride inclusions were locally observed associated with this crystallisation episode. Band of successive Ni, Co and As enrichments or losses are associated with this overgrowth stage. Ni and Co zonations are frequently observed and are anti-correlated.

The fourth stage is associated with a fracturation of pyrite overgrowths. This brittle tectonic event is mostly described within the albitic alteration zones where gold is most frequently observed native and free. Metallic anomalies related to this event display Cu, Pb, Bi, Ti, Zn, V, Ag, Au, Te enrichments in the fractures. A late metallic enrichment is locally described enclosing pyrite rims and displays Pb, Bi +/- Ni, Au, Ag, Te.

Among the two alterations facies, gold is associated with pyrite spongy core related to the second overgrowth phase (pyrite stage 2). Such observation is most consistent within the K-feldspar alteration than in the albitic alteration. The fourth stage is related to a brittle event affecting pyrites stages 1 to 3. It is mostly associated with the albitic alteration, where gold is native and free. Fracturation is also observed amongst pyrites from the K-feldspar assemblage.

Even though pyrites zonations show distinctions between the potassic and albitic assemblages, the four stages were identified in both alteration facies. Also, as

albitic alteration overprints K-feldspar alteration, only one early gold enrichment episode is suggested.

1.5 Discussion

The Wasamac deposit allows to better understand the succession of alteration within the FWSZ and their connection with the gold habitus and association.

1.5.1 Hydrothermal alteration signatures

K-feldspar alteration has been largely described close to and within several alkaline intrusions as a brick-red coloured footprint, often spatially associated with quartz veins systems (Thompson et al., 1999; Robert, 2001). This intense alteration colour reflects highly oxidized hydrothermal conditions. Such hydrothermal environment was described in numerous alkaline intrusion-associated gold deposits such as Malartic, Beattie, Kirkland Lake deposits in the Abitibi greenstone-belt (Helt et al., 2014; Robert, 2001; Ispolatov et al., 2008; Bigot and Jébrak, 2015) and among deposits from Australia, USA, Bolivia, Kazakstan, Iberian Peninsula, Czech Republic and China (Thompson et al., 1999; Lang and Baker, 2001). These conditions are also reached close to and within Cu/Mo-Au porphyry intrusions (Sillitoe, 1991; Thompson et al., 1999; Sillitoe, 2002). The mineralization in Te, Ag, Au, the metallic assemblage in W, Pb, Bi, Mo, and the absence in As, Hg, Sb, Sn are typical from proximal alteration associated with alkaline intrusion-related gold deposits, described regionally and around the world (Lang and Baker, 2001; Robert, 2001; Groves et al., 2003). West of the Wasamac deposit, such gold mineralization footprint was

regionally recognised associated with syntectonic alkaline intrusions along the CLLFZ in Ontario (Ispolatov et al., 2008).

Gold solubility is notably controlled by T, $f(O_2)$, pH factors (Mikucki, 1998; references therein). These factors are usually constrained by fluid inclusion analyses. Although such observations lead to quantitative data, gold deposition conditions can be roughly constrained by its cogenetic alteration minerals associations. Oxidized K-feldspar metasomatism is known to be concomitant to numerous deposits associated with diopside, amphibole or pyrrhotite, which are consistent with lower amphibolite metamorphic grade (Mikucki, 1998; Groves et al., 2003; Goldfarb et al., 2005). In opposition to such high temperature conditions commonly associated with K-feldspar alteration, the Wasamac deposit displays a continuous greenschist facies with the absence of previously cited minerals. Also, no sign of retrometamorphism was described. K-feldspar alteration observed within the Wasamac deposit may thus be related to hydrothermal conditions displaying low hydrothermal temperatures, characteristic greenschist metamorphic grade ones.

Gold precipitation may be controlled by several mechanisms, including the cooling of the ore fluids, interaction between fluids and the host rock, phase separation associated with pressure drops, or the mixing between several fluids (Mikucki, 1988). Within the Wasamac deposit, gold-bearing pyrite stage 2 is proposed to be related to the early K-feldspar assemblage. Within this alteration assemblage, pyrite stage 2 porous texture may be related to a dissolution/recrystallization process (Putnis, 2002). The low sulphidation environment associated with highly hematized host rock relates strong variations in the oxidation state. Redox conditions may have been a critical factor in gold precipitation within the lattice of pyrite stage 2. This early K-feldspar alteration displays similar geochemical characteristics that are typical of intrusion-related gold deposits. However, amongst Archean terranes, K-feldspar alteration associated with gold mineralizations is atypical in the absence of alkaline intrusions. The observation

of pervasive K-feldspar alteration and highly oxidized hydrothermalism without that of close gold-related syenite within the FWSZ argues for the potential presence of an alkaline intrusion buried in depth beneath the FWSZ. The Wasamac deposit may thus represent a particular hydrothermal environment for gold precipitation featuring alkaline-related metasomatism within an orogenic style gold environment deposition.

Albite-dominated alteration is generally associated with chlorite, carbonates, quartz, muscovite and pyrite as a typical alteration assemblage described among worldwide Archean gold systems (Goldfarb et al., 2005). Albitization is commonly observed as a pervasive replacement under greenschist grade conditions and as "albitite" dykes (Witt, 1992; Coutute and Pilote, 1994; McCuaig and Kerrich, 1998). Among intrusion-related gold deposits, the presence of albite is nearly ubiquitous (Robert, 2001; Lang and Baker, 2001).

Within the Wasamac deposit, albite-dominated pervasive alteration consists of replacement zones of fresh volcanic units and K-feldspar altered units with an assemblage composed of albite, carbonate, sericite, pyrite +/- chlorite. Chronologically, the albite assemblage postdates the K-feldspar assemblage. They are pre- to syn-deformation (S1). Besides, according to drill core and microscopic observations, a brittle event associated with (1) the brecciation of K-feldspar altered units (Fig.6.A, B) and (2) the pyrite phase 4 (Fig.16) is described associated with an albitic hydrothermal input. Albitization may thus be related to a local renewal of tectonic activity, with potential metallogenic consequences described later. Furthermore, the albitic alteration assemblage displays higher pyrite content and fewer oxide minerals than in the K-feldspar alteration. It might thus result from more reducing hydrothermal conditions. The intense albite alteration and its dominance over sericite alteration, as observed in the Wasamac deposit, are often spatially associated with syenite-hosted gold deposits and contrasts over the prevalence of sericite over albite in orogenic gold deposits (Robert, 2001).

Five kilometers West of the Wasamac deposit, the Francoeur deposit is also hosted by the FWSZ. It displays similar geological characteristics including host rock composition, host structure type and alkaline hydrothermal alteration footprint (Couture and Pilote, 1994). Couture and Pilote (1994) described a strong albitic alteration related to albitite dykes in this deposit. They were described as feeder dykes with repect to their implication with gold mineralization and because of their direction and dip changes as they intercept the FWSZ (Fig.4). Couture and Pilote (1994) also determined three hydrothermal assemblages: (1) a widespread pervasive pre-ore carbonate-hematite-muscovite associated with late-kinematic albitite dykes, (2) a gold-bearing albite-pyrite alteration and (3) a post-ore sulphate-bearing alteration. Albitite dykes are not described within the Wasamac deposit. Also, no gold-rich K-feldspar alteration was observed in the Francoeur deposit according to Pilote and Couture (1994). However, a red-altered syenite dyke sampled in Francoeur (WSC-000818) showed a 0,1 g/t Au anomaly. Potassic and albitic metasomatisms are thus also regognised associated with gold mineralization in the Francoeur deposit. Francoeur and Wasamac similar geological contexts and close alterations and mineralizations affinities may express analogous genesis. Albitite dykes hydrothermal implication may be suggested at deeper depths beneath the FWSZ in the Wasamac deposit. Also, twenty kilometers West of the Wasamac deposit, over 5,000 mineralized albitite dykes were documented in the Kerr-Addison area. Their emplacement is related to the replacement of mafic dykes (Kishida and Kerrich, 1987; Smith et al. 1993). An intense alteration process is thus proposed. Smith et al. (1993) associate albitite dykes with the hypothetic presence of an alkaline intrusion buried 4km at depth. Numerous authors including Kishida and Kerrich (1987), Witt (1992), Smith et al. (1993), Robert (2001), and Neumayr (2008) suggested that felsic/alkaline intrusions caused both potassic and albitic hydrothermal alterations.

According to the successive emplacement of K-feldspar and albitic alterations, albite crystallization may be controlled by the hydrolytic breakdown of alkali feldspar

to albite plus sericite (Colvine, 1988). Also, metallic assemblage of albitic and K-feldspar assemblages are alike (Fig.12). Regionally, the strong implication of albitite dykes with gold mineralizations is typical (e.g. Francoeur, Kerr-Addison). Genetically, a similar interpretation of deep alkaline intrusion stocks may be related to both alkaline hydrothermal alterations described within the FWSZ.

1.5.2 Mineralization and maturation process

The Wasamac deposit displays two distinct alteration assemblages. Each one is associated with specific gold mineralizations: an early chemical precipitation of gold in porous pyrite lattice as gold-telluride minerals, followed by a tectonic control related to pyrite fracturation. Three aspects previously described characterise gold mineralization within the Wasamac deposit: (1) As-free pyrite is the only sulphide spatially associated with the mineralization, (2) pyrites from both alteration assemblages are similarly zoned, and (3) gold mineralogical characteristics are specific to each alteration facies.

1.5.2.1 Early gold-bearing pyrite stage and pyrite overgrowths

Gold-bearing sulphides have long been noticed in numerous deposits styles and geodynamic contexts, and a significant body of data is now available. Cabri et al. (1989) and Cook & Chryssoulis (1990) observed "invisible" gold particles as lattice-bounded nanoparticles and micro-inclusions of gold precipitating with As-rich sulphides. Cook et al. (2009) observed invisible gold-rich As-free sulphides, supporting that As is not an essential component for scavenging gold within pyrite lattice, however Te may cause distortion of the lattice to allow Au to enter. They also

propose that textural criterias including telluride inclusions and brecciation of pyrites play a significant role in gold concentration.

Four generations of pyrite crystallization are described within the Wasamac deposit. Gold is proposed to be related to the pyrite stage 2 as Te-minerals micro-inclusions. Gold is also partly invisible within the lattice of pyrite stage 2. Porous texture described within this gold-rich pyrite generation, allows to evaluate hydrothermal conditions (Putnis, 2002; Large, 2007, 2009). Putnis (2002) propose that porous sulphide and rich metal content associated are common features linked with a dissolution-recrystallization process. Large (2007) suggests that strong velocity of sulphide crystallization may induce porous texture. Pyrite stage 2 porosity may thus be related to two successive hydrothermal events: (1) partial dissolution of pyrite stage 1 within oxidizing conditions, and (2) rapid recrystallisation related to a hydrothermal input. Mineral inclusions associated with pyrite stage 2 are composed of oxydes (hematite, sphene), silicates (K-feldspar, quartz), sulphides (mostly chalcopyrite) and tellurides (Ag-Au-Pb-Bi telluride minerals). Dissolution-recrystallization of pyrite stage 2 such as the presence of hematite and sphene inclusions may record oxidizing conditions during this crystallization episode. This gold-rich pyrite overgrowth generation is the only one associated with high Ag-Au-Te-Pb-Bi +/- Cu values in the lattice of the pyrite with porous texture. Pyrite stage 2 is proposed to be contemporary of the K-feldspar hydrothermal alteration event within oxidized conditions.

Pyrite stages 1 and 2 are observed within the K-feldspar alteration, but they are rarely preserved within the albitic alteration, mostly composed of clear stage 3 pyrites. The latter generation (stage 3) displays overgrowths of clear pyrites, poor in elements, except for local Ni, Co and As anomalies. Large (2007) suggests that clear pyrites poor in elements or variably enriched in Ni, Co and As are related to slow growth crystallisation rates. It may thus be proposed that clear pyrites from stage 3

may have crystallized during a break in hydrothermal input. Such hydrothermal conditions may be associated with a tectonic quiescence (Fig.17).

1.5.2.2 Evolution of gold characteristics

Stage 4 is associated with a brittle deformation event. Previous generations of pyrite are fractured and locally cataclased. This stage is proposed to be contemporary to the second alteration assemblage composed of albite, chlorite, carbonàtes, sericite and pyrite in which gold is mostly native and free. Albitic alteration assemblage displays higher pyrite content compared to the oxidized K-feldspar assemblage. Also, in contrast with the K-feldspar altered zones, albitized zones display free gold grains and rare gold tellurides grains. No evidence of second hydrothermal gold enrichment is described during albitization. Gold crystallization filling pyrite fracture planes is commonly described in Wasamac (Fig.14.B, C, D, E, F). Pyrite fracturation may thus represents a critical feature related to mineralization characteristics.

Bonnemaison and Marcoux (1990), Mumin et al. (1994), Genkin et al. (1998) and Morey et al. (2008) proposed that the superposition of structural events controls the recrystallization of pre-existing gold mineralization within orogenic gold deposits. Due to successive structural destabilization of gold-rich sulphides from early stages, gold tends to recrystallize and concentrates, resulting as an overall gold enrichment. Most recently, Bigot & Jébrak (2015) highlighted similar structural control of gold chemistry at the syenite-related Beattie deposit. Within the Wasamac deposit, the size of pyrite fracture planes seems to control gold mineralogy, as tellurides fills <5µm fractures and native gold fills >5µm fractures. Metallic anomalies described in pyrite stage 2 were possibly extracted during fracturation, as Ag, Pb, Bi, Ti high concentrations are locally observed inside fractures and enclosing fractured pyrite rims (appendix B).

According to the paragenetic setting of pyrite fracturation with respect to alteration assemblages and pyrite zonations, the brittle event affecting pyrites may have controlled gold extraction from the lattice of early porous pyrites. The increasing size of gold grains and the progressive chemical loss of Te and Ag from potassic to albitic assemblages is proposed to be associated to a maturation process of gold linked with a tectonic overprint. It is thus proposed that gold mineralization related to cataclased pyrites is structurally controlled and concentrates gold from early pyrite stage 2.

1.5.2.3 Comparison with other deposits and implication for ore genesis

Amongst orogenic gold deposits, genetic interpretation for hydrothermal fluids and mineralization source is debated. Despite similar controversies regarding intrusion-related deposits, several authors suggest a magmatic source and magmatically derived hydrothermal systems (Cook et al., 2009; Helt et al., 2014). Beyond genetic discussions, studies distinguished intrusion related deposits into two groups: oxidised and reduced types (Cameron and Hattori, 1987; Thompson et al., 1999; Robert, 2001). Syenite-related deposits are oxidized, causing an intense hematization of the host rocks in comparison to reduced alkaline intrusion-related deposits generally more concentrated in pyrite. Besides, both alterations types are often spatially and chronologically associated generating the superimposition of hydrothermal signatures (Robert, 2001; Neumayr et al., 2008). Redox conditions are thus suggested as an important factor controlling gold precipitation, mostly where fluids of contrasting redox state are mixed (Robert, 2001). Regarding the Wasamac deposit, we propose that gold precipitation was triggered by low sulphidation in association with relatively oxidized fluids, during the early K-feldspar alteration. The following reduced albitic hydrothermal circulation would have been associated with a

tectonic event causing the brecciation of previous gold rich pyrites. According to mineralogical and geochemical assemblages associated with the mineralization, the Wasamac deposit shares more similarities with alkaline intrusion-related deposits than with orogenic gold deposits (Table 1).

Table 2 proposes a comparison of alteration and mineralization descriptions for several deposits along the CLLFZ and their genetic interpretation. Both typical intrusion-related and orogenic deposit types are suggested. Despite the very limited presence of alkaline intrusion associated with the Wasamac deposit, this deposit shares numerous characteristics with alkaline-intrusion type (Tab.1.1), including: K-feldspar pervasive hydrothermal alteration within oxidized conditions, strong alkaline elements mass gains associated with gold-bearing alteration, and Au-Ag-Te enriched sulphides with Mo, Pb, Bi and Cu anomalies. Robert (2001) discussed the classification of several gold deposits within the Abitibi Belt, including the Francoeur deposit, which also displays strong similarities with alkaline intrusion-related deposits.

The Wasamac deposit is hosted within a metasomatized ductile shear zone crosscutting metavolcanic units. This metallogenic environment is characteristic of orogenic gold deposits. However, it displays similar geochemical similarities with syenite-hosted gold deposits (Table 2). It may thus be proposed that gold-bearing oxidized potassic hydrothermal fluids are genetically associated with an alkaline intrusion buried at depth (Fig.18). The nearest outcropping syenites is the aera on the Baie Renault Syenite south of Dasserat Lake, 5km West of Francoeur deposit (Legault et Rabeau, 2007). Such gold-rich hydrothermal environment represents a regional significative footprint for gold mineralizations south-west of Rouyn-Noranda.

1.6 Conclusion

The Wasamac deposit is a replacement type gold deposit along a second order ductile fault zone displaying strong potassic and sodic alterations. A reduced albitic metasomatism locally overprints an oxidized potassic alteration. Gold occurs as visible and invisible telluride minerals crystallized in the lattice of the pyrite stage 2. This early event is related to the K-feldspar hydrothermal alteration. Redox conditions seem to govern the precipitation process, as host pyrites are porous and associated with a hematized assemblage. Diluted hydrothermal activity then crystallizes element-poor pyrite stage 3, presumably related to a period of quiescence of the deformation. The second hydrothermal activity, the albitization, occurs within more reducing conditions. This assemblage is mostly composed of brecciated pyrite (stage 4) and native gold. The brittle structural overprint described on K-feldspar assemblage and pyrites may be related to two tectonic settings: (1) a structural partitioning with K-feldspar altered units during the same deformation event (S1 and S2), or (2) a renew of the FWSZ tectonic activity. The fracturation of pyrite stages 1 to 3 may have induced progressive gold extraction from early pyrite stage 2, beginning with gold-tellurides crystallization in thin fractures, and then as native gold grains in the albitic alteration minerals assemblage. This event shares numerous similarities with processes occurring in orogenic gold type deposits.

The Wasamac deposit may thus be representing the superposition of two hydrothermal events, one related to alkaline magmatism and the second to remobilization by "orogenic style" hydrothermal fluids.

Aknowledgements

The authors thank Mines Richmont Inc., FQRNT and CRSNG for funding this study, part of a M.Sc. project. We particularly thanks Richmont Mines Inc, for their technical support, for all the constructive discussions and for the acces to the informations. We also would like to thank Stephane Faure, Silvain Rafini and Ludovic Bigot from the CONSOREM for the helpful comments that greatly improved the quality of the paper. We would certainly like to express our thanks to Stephane Faure and Eric Marcoux for the review of the document. We also thank Raynald Lapointe and Sadia Mehdi for the technical support during analytical works in UQAM and UQAC, and Michelle Laithier for the artwork.

References

Ayer, J.A., Thurston, P.C., Bateman, R., Dubé, B., Gibson, H.L., Hamilton, M.A., Hathway, B., Hocker, S.M., Houlé, M.G., Hudak, G., Ispolatov, V.O., Lafrance, B., Lesher, C.M., MacDonald, P.J., Péloquin, A.S., Piercey, S.J., Reed, L.E. & Thompson, P.H., 2005. Overview of results from the Greenstone Architecture Project : Discover Abitibi Initiative. Ontario Geological Survey ; Open File Report 6154, 146p.

Beakhouse, G.P., 2011. The Abitibi Subprovince plutonic record : Tectonic and metallogenic implications. Ontario Geological Survey ; Open File Report 6268, 161p.

Bigot, L., & Jébrak, M., 2015. Gold Mineralization at the Syenite-Hosted Beattie Gold Deposit, Duparquet, Neoarchean Abitibi Belt, Canada. Economic Geology, v.110 (2), p.315-335.

Bonnemaison, M., & Marcoux, E., 1990. Auriferous mineralization in some shear-zones: A three-stage model of metallogenesis. Mineralium Deposita, v.25 (2), p.96-104.

Cabri, L.J., Chryssoulis, S.L., de Villiers, J.P., Laflamme, J.G., & Buseck, P.R., 1989. The nature of "invisible" gold in arsenopyrite. The Canadian Mineralogist, v.27 (3), p.353-362.

Cameron, E.M., & K. Hattori, (1987). Archean gold mineralization and oxidized hydrothermal fluids. Economic Geology and the Bulletin of the Society of Economic Geologists, v.82 (5), p.1177-1191.

Colvine, A.C., Fyon, J.A., Heather, K.B., Marmont, S., Smith, P.M., & Troop, D.G., 1988. Archean Lode Gold Deposits in Ontario; Ontario Geological Survey ; Miscellaneous Paper, v.139, 136p.

Cook, N.J., & Chryssoulis, S.L., 1990. Concentrations of invisible gold in the common sulfides. The Canadian Mineralogist, v.28 (1), p.1-16.

Cook, N.J., Ciobanu, C.L., & Mao, J., 2009. Textural control on gold distribution in As-free pyrite from the Dongping, Huangtuliang and Hougou gold deposits, North China craton (Hebei Province, China): Chemical Geology, v.264, p.101-121.

Corfu, F., Krogh, T.E., Kwok, Y.Y., & Jensen, L.S., 1989. U-Pb zircon geochronology in the SouthWestern Abitibi greenstone belt, Superior Province. Canadian Journal of Earth Sciences, v.26 (9), p.1747-1763.

Couture, J.F., & Pilote, P., 1993. The geology and alteration patterns of a disseminated, shear zone-hosted mesothermal gold deposit ; the Francoeur 3 Deposit, Rouyn-Noranda, Quebec. Economic Geology, v.88 (6), p.1664-1684.

Couture, J.F., & Pilote, P., 1994. Gîtologie des gisements d'or du district de Rouyn-Noranda : études récentes. Ministère de l'Énergie et des Ressources, Québec ; DV 92-07, 143p.

Daigneault, R., & Mueller, W.U., & Chown, E.H., 2002. Oblique Archean subduction: accretion and exhumation of an oceanic arc during dextral transpression, Southern Volcanic Zone, Abitibi Subprovince Canada. Precambrian Research, v.115 (1), p.261-290.

Daigneault, R., Mueller, W.U., & Chown, E.H., 2004. Abitibi greenstone belt plate tectonics: the diachronous history of arc development, accretion and collision. Developments in Precambrian Geology, The Precambrian Earth : Tempos and events, v.12, p.88-103.

Eilu, P., & Groves, D.I., 2001. Primary alteration and geochemical dispersion haloes of Archaean orogenic gold deposits in the Yilgarn Craton: the pre-weathering scenario. Geochemistry: Exploration, Environment, Analysis, v.1(3), p.183-200.

Fairbairn, H.W., Hurley, P.M., Card, K.D., & Knight, C.J., 1969. Correlation of radiometric ages of Nipissing diabase and Huronian metasediments with Proterozoic orogenic events in Ontario. Canadian Journal of Earth Sciences, v.6, p.489-497.

Gélinas, L., Trudel, P., & Hubert, C., 1984. Chemostratigraphic division of the Blake River Group, Rouyn-Noranda area, Abitibi, Quebec. Canadian Journal of Earth Sciences, v.21 (2), p.220-231.

Genkin, A.D., Bortnikov, N.S., Cabri, L.J., Wagner, F.E., Stanley, C.J., Safonov, Y.G., McMahon, G., Friedl, J., Kerzin, A.L., & Gamyanin, G.N., 1998. A multidisciplinary study of invisible gold in arsenopyrite from four mesothermal gold deposits in Siberia, Russian Federation. Economic Geology, v.93, p.463-487.

Goldfarb, R.J., Groves, D.I., & Gardoll, S., 2001. Orogenic gold and geologic time: a global synthesis. Ore Geology Reviews, v.18 (1), p.1-75.

Goldfarb, R.J., Baker, T., Dube, B., Groves, D.I., Hart, C.J., & Gosselin, P., 2005. Distribution, character, and genesis of gold deposits in metamorphic terranes. Economic Geology 100th anniversary volume, v.40, p.407-450.

Groves, D.I., Goldfarb, R.J., Robert, F., & Hart, C.J.R., 2003. Gold deposits in metamorphic belts: Overview of current understanding, outstanding problems, future research, and exploration significance: Economic Geology, v.98 (1), p.1-29.

Hart, C.J.R., & Goldfarb, R.J., 2005. Distinguishing intrusion-related from orogenic gold systems. New Zealand Minerals Conference Proceedings, p.125-133.

Helt, K.M., Williams-Jones, A.E., Clark, J.R., Wing, B.A., & Wares, R.P., 2014. Constraints on the Genesis of the Archean Oxidized, Intrusion-Related Canadian Malartic Gold Deposit, Quebec, Canada. Economic Geology, v.109 (3), p.713-735.

Ispolatov, V., Lafrance, B., Dubé, B., Creaser, R., & Hamilton, M., 2008. Geologic

and structural setting of gold mineralization in the Kirkland Lake-Larder Lake gold belt, Ontario. Economic Geology, v.103 (6), p.1309-1340.

Jolly, W.T., 1978. Metamorphic history of the Archean Abitibi belt. Metamorphism in the Canadian Shield. Geological Survey of Canada, Paper, p.78-10.

Kishida, A., & Kerrich, R., 1987. Hydrothermal alteration zoning and gold concentration at the Kerr-Addison Archean lode gold deposit, Kirkland Lake, Ontario. Economic Geology, v.82 (3), p.649-690.

Kretschmar, U., & Scott, S.D., 1976. Phase relations involving arsenopyrite in the system Fe-As-S and their application, v.14, p.364-386.

Lang, J.R., & Baker, T., 2001. Intrusion-related gold systems: the present level of understanding. Mineralium Deposita, v.36 (6), p.477-489.

Large, R.R., Maslennikov, V.V., Robert, F., Danyushevsky, L.V., & Chang, Z., 2007, Multistage sedimentary and metamorphic origin of pyrite and gold in the giant Sukhoi Log deposit, Lena gold province, Russia, Economic Geology, v.102, p.1233-1267.

Large, R.R., Danyushevsky, L., Hollit, C., Maslennikov, V., Meffre, S., Gilbert, S., Bull, S., Scott, R., Emsbo, P., Thomas, H., Singh, B., & Foster, J., 2009. Gold and trace element zonation in pyrite using a laser imaging technique: implications for the timing of gold in orogenic and Carlin-style sediment-hosted deposits, Economic Geology, v.104 (5), p.635-668.

Legault, M., & Rabeau, O., 2006. Étude métallogénique et modélisation 3D de la Faille de Cadillac dans le secteur de Rouyn-Noranda. Ministère des Ressources Naturelles et de la Faune, Québec ; RP2006-03, 8p.

Legault, M., & Rabeau, O., 2007. Étude métallogénique et modélisation 3D de la Faille de Cadillac dans le secteur de Rouyn-Noranda (Phase 2). Ministère des Ressources Naturelles et de la Faune, Québec ; RP2007-03, 11p.

MacLean, W., and Barrett, T., 1993, Lithogeochemical techniques using immobile elements: Journal of geochemical exploration, v. 48, p. 109-133.

MacLean, W., and Kranidiotis, P., 1987, Immobile elements as monitors of mass transfer in hydrothermal alteration; Phelps Dodge massive sulfide deposit, Matagami, Quebec: Economic Geology, v. 82, p. 951-962.

Mair, J.L., Farmer, G.L., Groves, D.I., Hart, C.J., & Goldfarb, R. J., 2011. Petrogenesis of postcollisional magmatism at Scheelite Dome, Yukon, Canada: Evidence for a lithospheric mantle source for magmas associated with intrusion-related gold systems. Economic Geology, v.106 (3), p.451-480.

McCuaig, T.C., & Kerrich, R., 1998. P-T-t deformation fluid characteristics of lode gold deposits: evidence from alteration systematics. Ore Geology Reviews, v.12 (6), p.381-453.

Mikucki, E.J., 1998. Hydrothermal transport and depositional processes in Archean lode-gold systems: a review. Ore Geology Reviews, v.13 (1), p.307-321.

Monecke, T., Gibson, H., Dubé, B., Laurin, J., Hannington, M.D., & Martin, L., 2008. Geology and Volcanic Setting of the Horne Deposit, Rouyn-Noranda, Quebec, Initial Results of a New Research Project. Geological Survey of Canada.

Morey, A.A., Tomkins, A.G., Bierlein, F.P., Weinberg, R.F., & Davidson, G.J., 2008. Bimodal distribution of gold in pyrite and arsenopyrite: Examples from the Archean Boorara and Bardoc shear systems, Yilgarn craton, Western Australia, Economic Geology, v.103, p.599-614.

Mueller, W. U., Daigneault, R., Mortensen, J. K., & Chown, E.H., 1996. Archean terrane docking : upper crust collision tectonics, Abitibi greenstone belt, Quebec, Canada, Tectonophysics, v.265 (1), p.127-150.

Mueller, W.U., Friedman, R., Daigneault, R., Moore, L., & Mortensen, J., 2012. Timing and characteristics of the Archean subaqueous Blake River Megacaldera Complex, Abitibi greenstone belt, Canada. Precambrian Research, v.214-215, p.1-27.

Mumin, A.H., Fleet, M.E., & Chryssoulis, S., 1994, Gold mineralization in As-rich mesothermal gold ores of the Bogosu-Prestea mining district of the Ashanti Gold Belt, Ghana: Remobilization of "invisible" gold. Mineralium Deposita, v.29 (6), p.445-460.

Neumayr, P., Walshe, J., Hagemann, S., Petersen, K., Roache, A., Frikken, P., Horn, L., & Halley, S., 2008. Oxidized and reduced mineral assemblages in greenstone belt rocks of the St. Ives gold camp, Western Australia: vectors to high-grade ore bodies in Archaean gold deposits ? Mineralium Deposita, v.43 (3), p.363-371.

Pearson, V., & Daigneault, R., 2009. An Archean megacaldera complex: the Blake River Group, Abitibi greenstone belt. Precambrian Research, v.168 (1), p.66-82.

Pilote, P., & Couture, J.F., 1989. Gisements aurifères. Rouyn-Noranda. Ministère de l'Énergie et des Ressources du Québec, DV 89-05, 95-96.

Poulsen, K.H., Robert, F., & Dubé, B., 2000. Geological classification of Canadian gold deposits, v.540. Geological Survey of Canada.

Putnis, A., 2002. Mineral replacement reactions; from macroscopic observations to microscopic mechanisms, Mineralogical Magazine, v.66, p.689-708.

Rabeau, O., Royer, J.J., Jébrak, M., & Cheilletz, A., 2013. Log-uniform distribution of gold deposits along major Archean fault zones. Mineralum Deposita, v.48, p.817-824.

Rafini, S., 2014. Typologie des minéralisations aurifères associées à la Faille de Cadillac. Rapport du projet CONSOREM 2011-01 et 2012-01, 45p.

Robert, F., 2001. Syenite-associated disseminated gold deposits in the Abitibi greenstone belt, Canada. Mineralium Deposita, v.36 (6), p.505-516.

Sharp, Z.D., Essene, E.J., & Kelly, W.C., 1985. A re-examination of the arsenopyrite geothermometer: Pressure condiserations and applications to natural assemblages. Canadian Mineralogist, v.23, p.517-534.

Simard, M., Gaboury, D., Daigneault, R., & Mercier-Langevin, P., 2013. Multistage gold mineralization at the Lapa mine, Abitibi Subprovince: insights into auriferous hydrothermal and metasomatic processes in the Cadillac-Larder Lake Fault Zone. Mineralium Deposita, v.48 (7), p.883-905.

Smith, J.R., Spooner, E.T.C., Broughton, D.W., & Ploeger, F.R., 1993. Archean Au-Ag-(W) Quartz Vein/Disseminated mineralisation within the Larder Lake - Cadillac Break, Kerr Addison - Chesterville System, North East Ontario, Canada, Ontario Geoscience Research Grant Program, Grant No. 364; Ontario Geological Survey, Open File Report 5831, 310p.

Sillitoe, R.H., 1991. Intrusion-related gold deposits. In : Gold metallogeny and exploration. Springer US, p.165-209.

Sillitoe, R.H., 2002. Some metallogenic features of gold and copper deposits related to alkaline rocks and consequences for exploration. Mineralium Deposita, v.37 (1), p.4-13.

Sillitoe, R.H., 2008. Special paper: major gold deposits and belts of the North and South American Cordillera: distribution, tectonomagmatic settings, and metallogenic considerations. Economic Geology, v.103 (4), p.663-687.

Thompson, J.F.H., Sillitoe, R.H., Baker, T., Lang, J.R., & Mortensen, J.K., 1999. Intrusion-related gold deposits associated with tungsten-tin provinces. Mineralium Deposita. v.34 (4), p.323-334.

Trépanier, S., 2013. Norme Lithomodeleur. Rapport du projet CONSOREM 2011-04, 91p.

Witt, W.K., 1992. Porphyry intrusions and albitites in the Bardoc-Kalgoorlie area, Western Australia, and their role in Archean epigenetic gold mineralization. Canadian Journal of Earth Sciences, v.29 (8), p.1609-1622.

Zhang, J., Lin, S., Linnen, R., & Martin, R., 2014. Structural setting of the Young-Davidson syenite-hosted gold deposit in the Western Cadillac-Larder Lake Deformation Zone, Abitibi Greenstone Belt, Superior Province, Ontario. Precambrian Research, v.248, p.39-59.

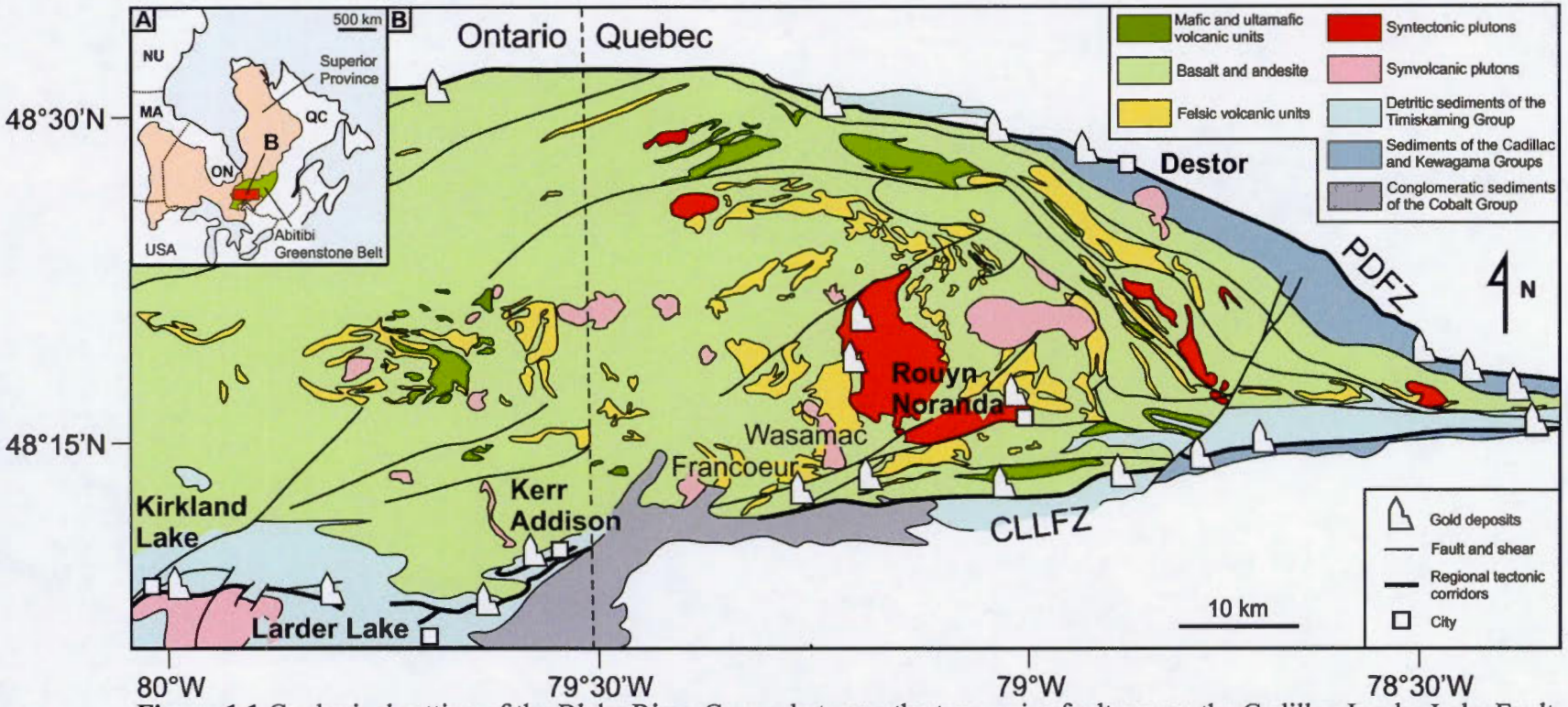

Figure 1.1 Geological setting of the Blake River Group, between the two major fault zones: the Cadillac-Larder Lake Fault Zone (CLLFZ) to the South and the Porcupine-Destor Fault Zone (PDFZ) to the North. (Modified from Rabeau et al., 2013 and McNicoll et al., 2014).

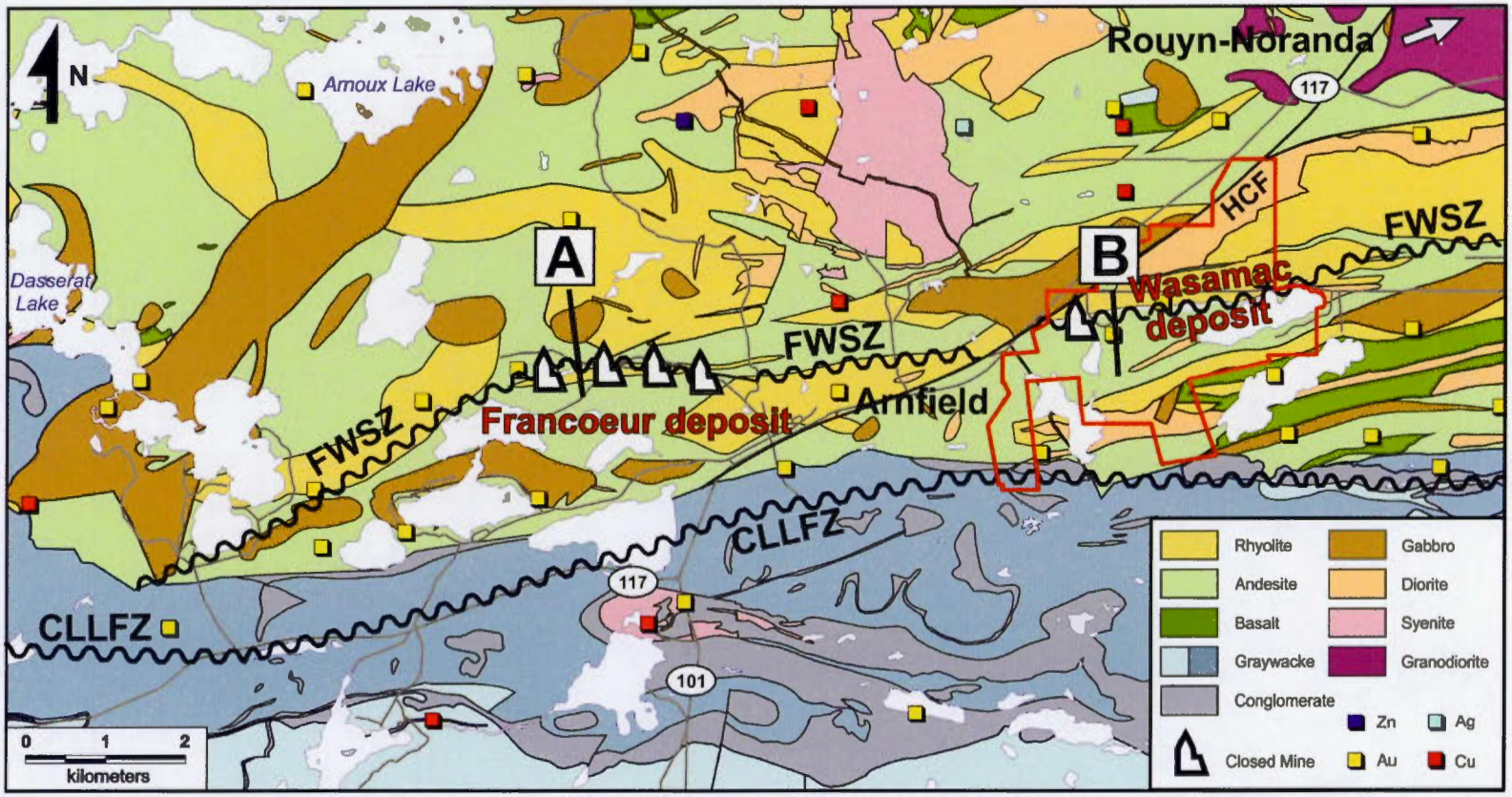

Figure 1.2 Geological map of the Francoeur-Wasa shear zone. (A) and (B) lines refers to Fig.3. cross sections of Francoeur and Wasamac deposits.

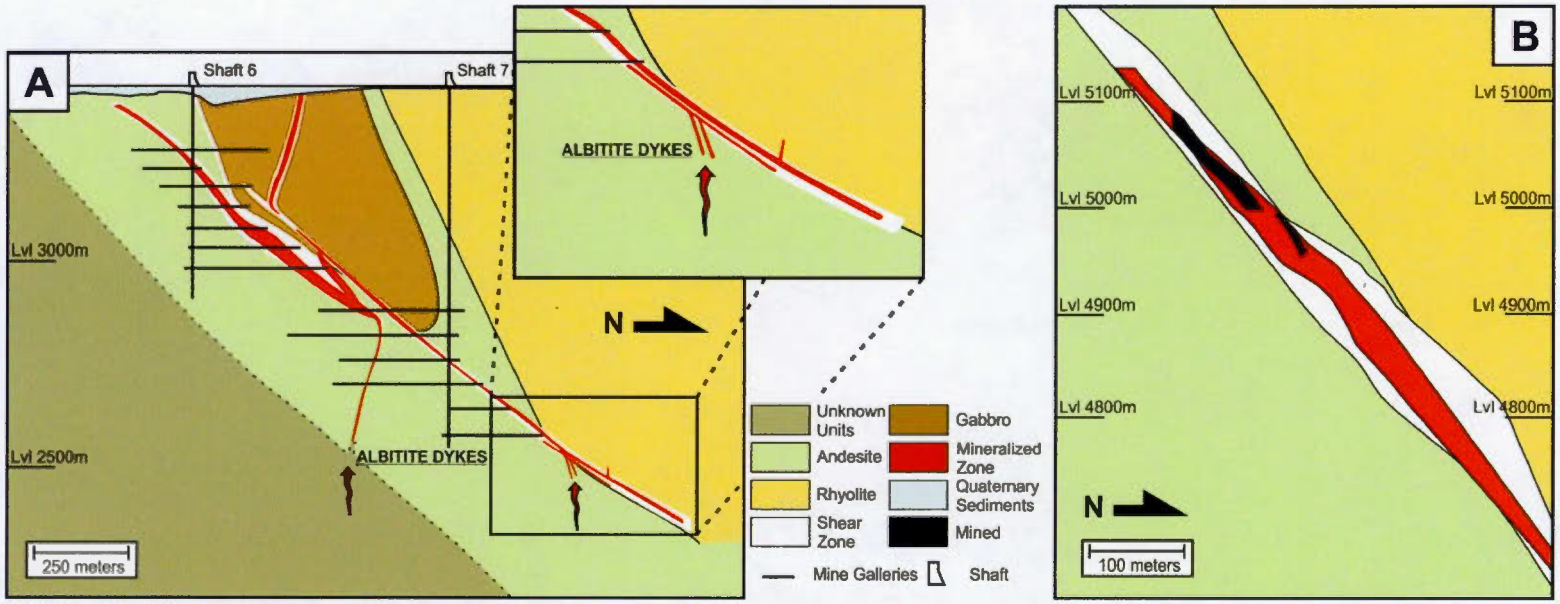

Figure 1. 3 Simplified typical geological cross-sections of Francoeur (A) and Wasamac (B) deposits. Both deposits are situated within the FWSZ and display similar geologic environments. Albitite dykes connected to the shear zone are described in Francoeur but no such dykes are observed in Wasamac.

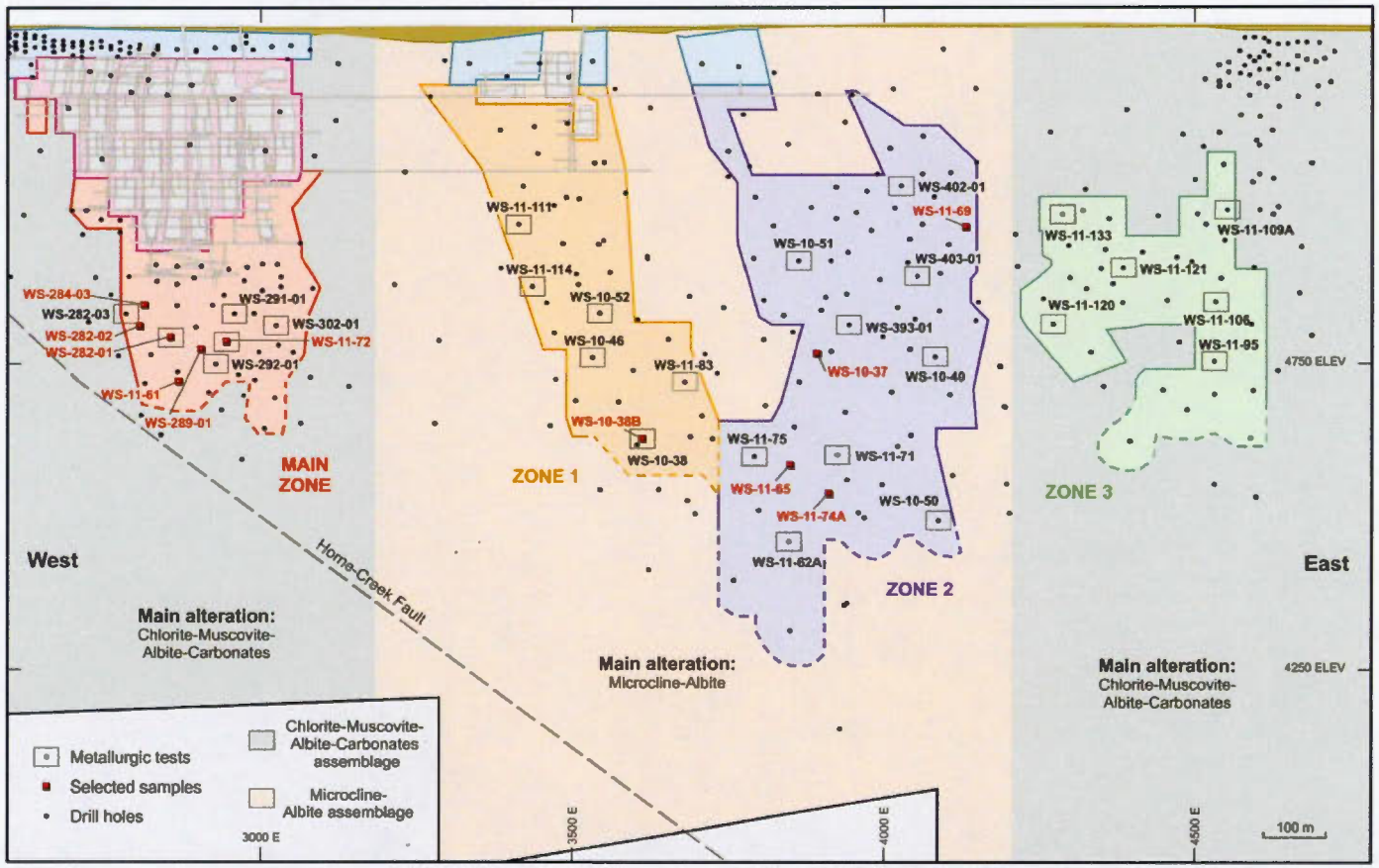

Figure 1.4 Localization of samples within a longitudinal section of the FWSZ in the Wasamac deposit. Samples written in red were selected during this master for geochemical and microscopic analyses, samples written in black were selected by Richmont Mines for metallurgical tests. Green and beige zones illustrate the particular respective zonation with the two alteration facies.

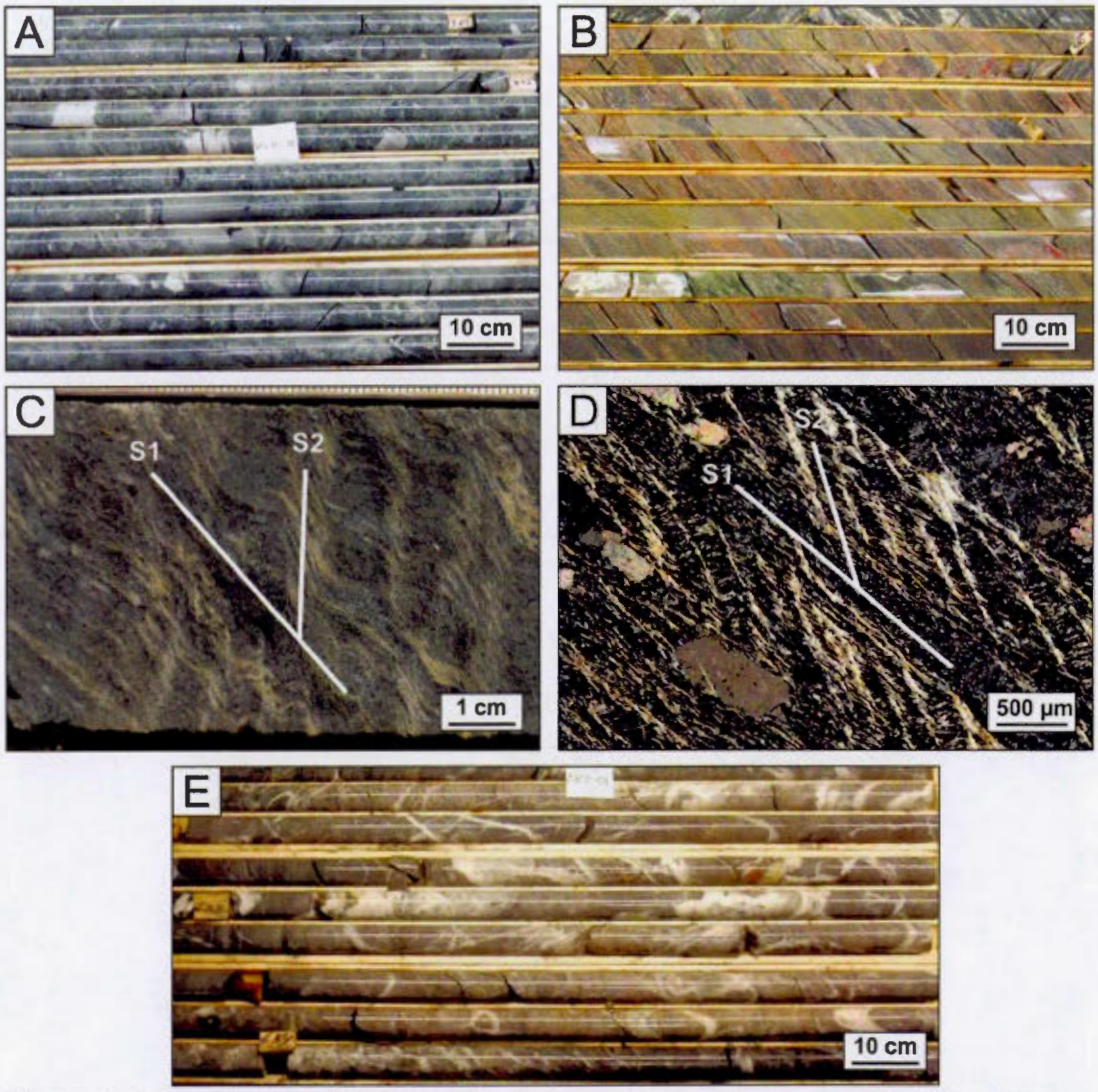

Figure 1.5 (A) Clastic tuff with centimetric rhyodacite, rhyolite and lapilli tuff blocs in an intermediate lapilli-tuff matrix. (B) Typical alteration of the FWSZ mylonite of Main Zone and Zone 3. The shear zone displays a diversity of alteration colorations related to several hydrothermal footprints. The most common alteration spatially associated with the mineralization is the albite-pyrite-sericite-carbonate assemblage. The red-coloured potassic alteration is also identified. (C) Crenulation cleavage (S2) showing centimetric asymmetric Z-shaped folds affecting a moderate altered andesite. (D) Crenulation cleavage (S2) in thin section. (E) Intersection between the Wasamac Shear Zone and the Horne-Creek Fault. Quartz veins and veinlets from the Horne-Creek Fault crosscut the FWSZ.

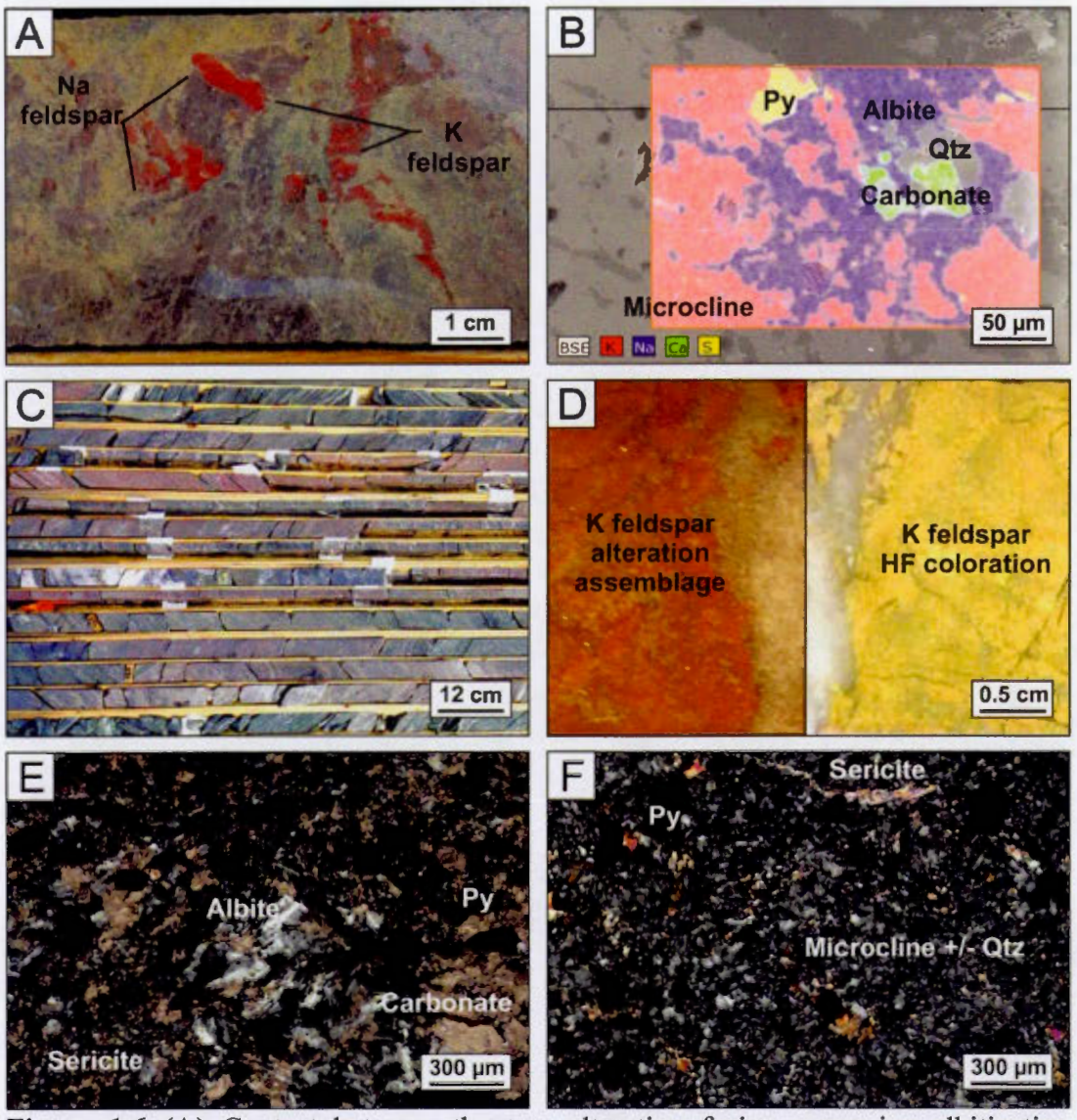

Figure 1.6 (A) Contact between the two alteration facies: pervasive albitization crosscuts potassic-altered brecciated veinlets. (B) SEM coloration of albitic and potassic alterations: albitization crosscuts the potassic alteration. (C) Typical alteration of the FWSZ Zones 1 and 2. Alteration is here restricted to intense red coloured fractured units with sharp contacts, composed of micrometric K-feldspars, sericite, carbonate and pyrite. (D) Cobaltinitrite coloration of K-feldspar pervasive alteration. (E) Microscopic photograph from transmitted polarised light of albitic alteration facies, composed of microscopic albite, sericite, carbonate and pyrite. (F) Microscopic photograph from transmitted polarised light of potassic alteration facies. Composition is micrometric hematised microcline, sericite, pyrite and carbonate.

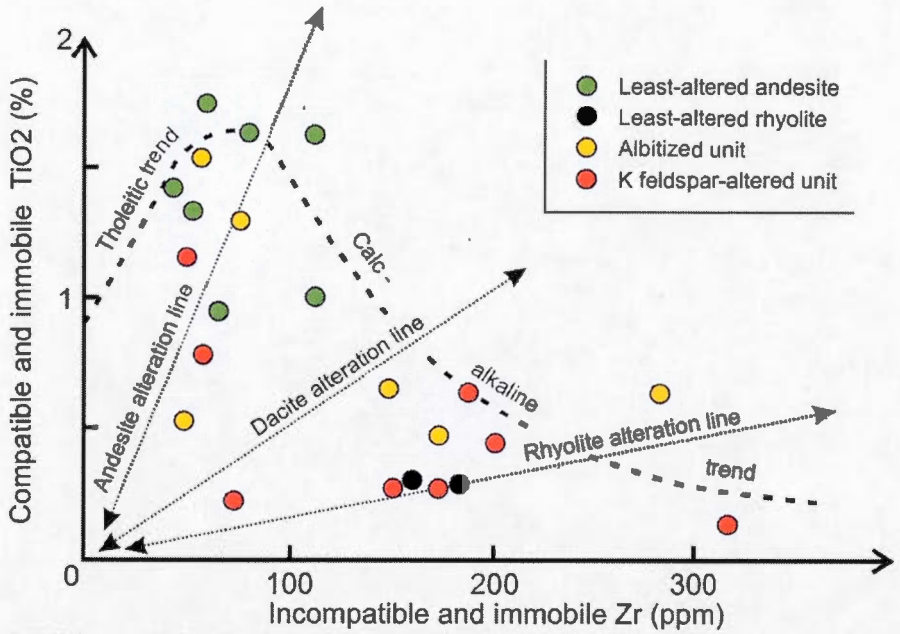

Figure 1.7 Diagram displaying altered and least-altered samples. Host rock is basaltic to andesitic and also rhyolitic in composition.

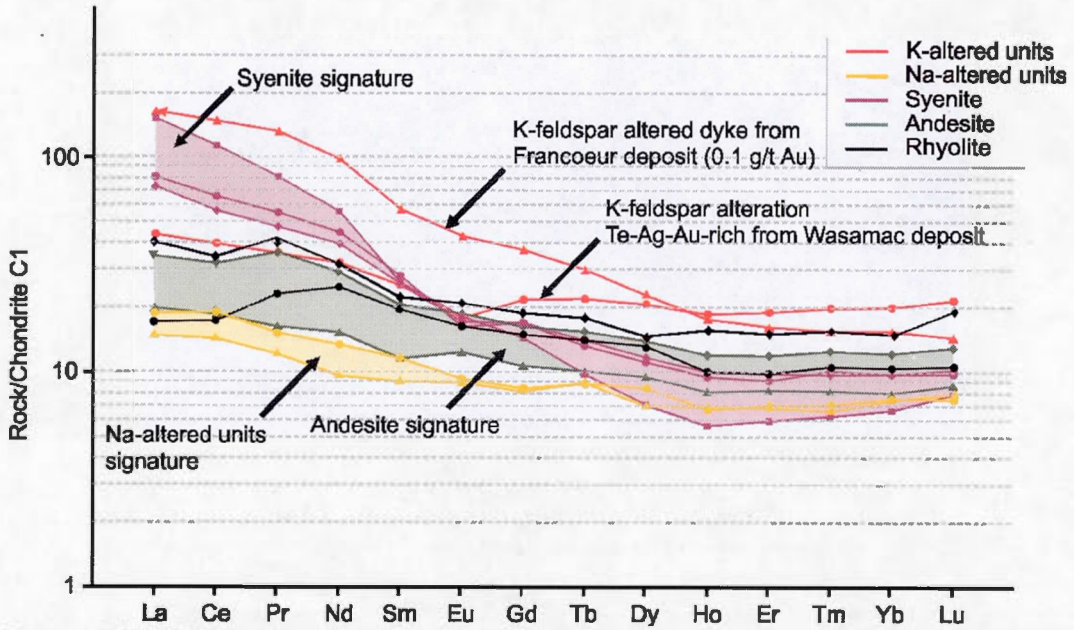

Figure 1.8 REE diagram from unaltered and altered units (from Palme and O'Neill, 2004).

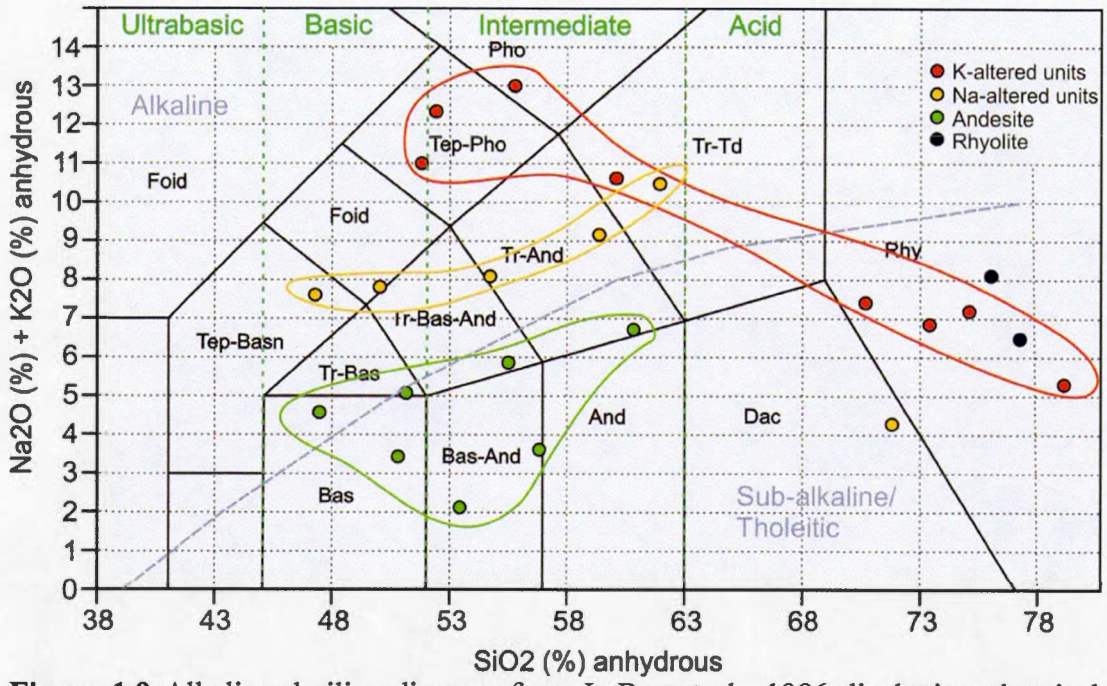

Figure 1.9 Alkali and silica diagram from LeBas et al., 1986 displaying chemical patterns of altered and unaltered volcanic units in the Wasamac deposit.

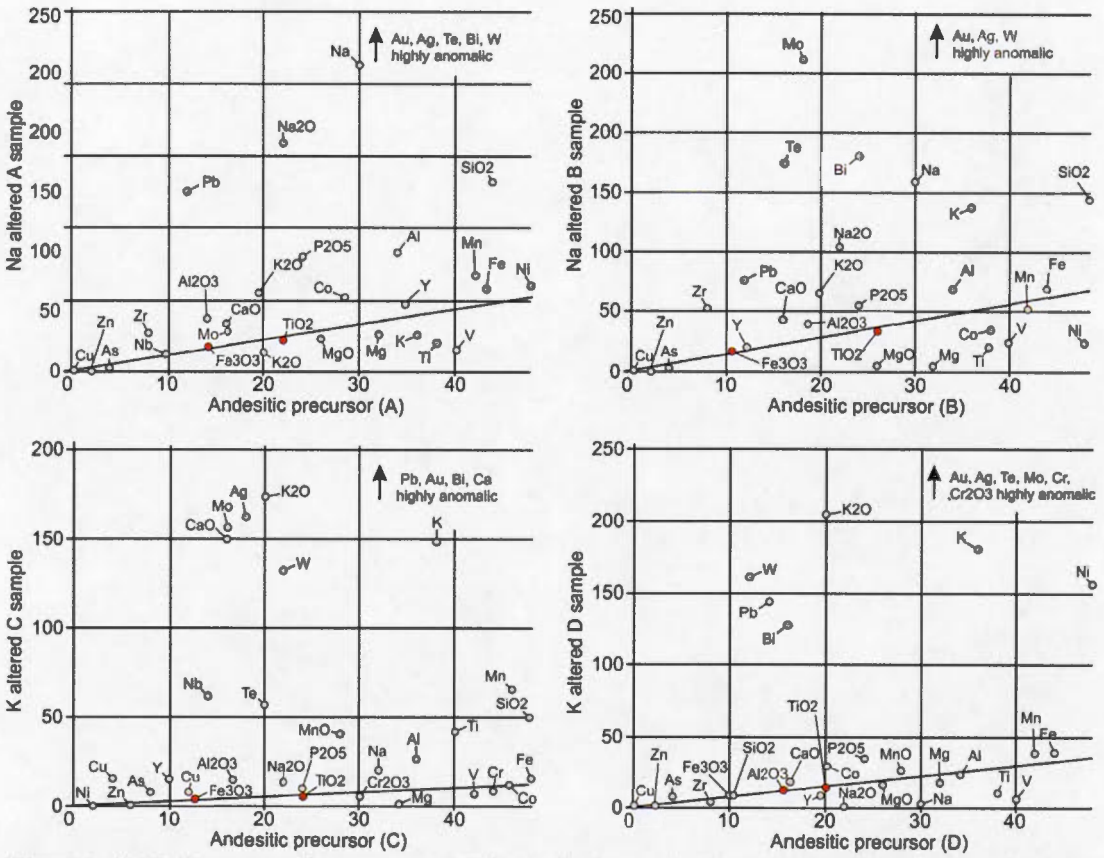

Figure 1.10 Isocone diagrams of selected elements in which altered samples are compared to their proximal unaltered host (Grant, 1986). Samples are presented with the following unaltered and altered pairs: (A) WSC-45464 and WSC-45463, (B) WSC-45454 and WSC-45467, (C) WSC-000803 and WSC-000802, (D) WSC-000820 and WSC-45469; geochemical details of which are presented in the appendix A of this memoir. Two pairs of samples are related to albitic alteration (A and B) and two pairs are related to K-feldspar alteration (C and D). The immobility isocon line has been determined by the elements spotted in red, which have been tested and considered as immobile elements and tested with Lithomodeleur software (Trépanier, 2013). Each altered sample is enriched in elements above the immobility isocon line and is depleted in elements below the line.

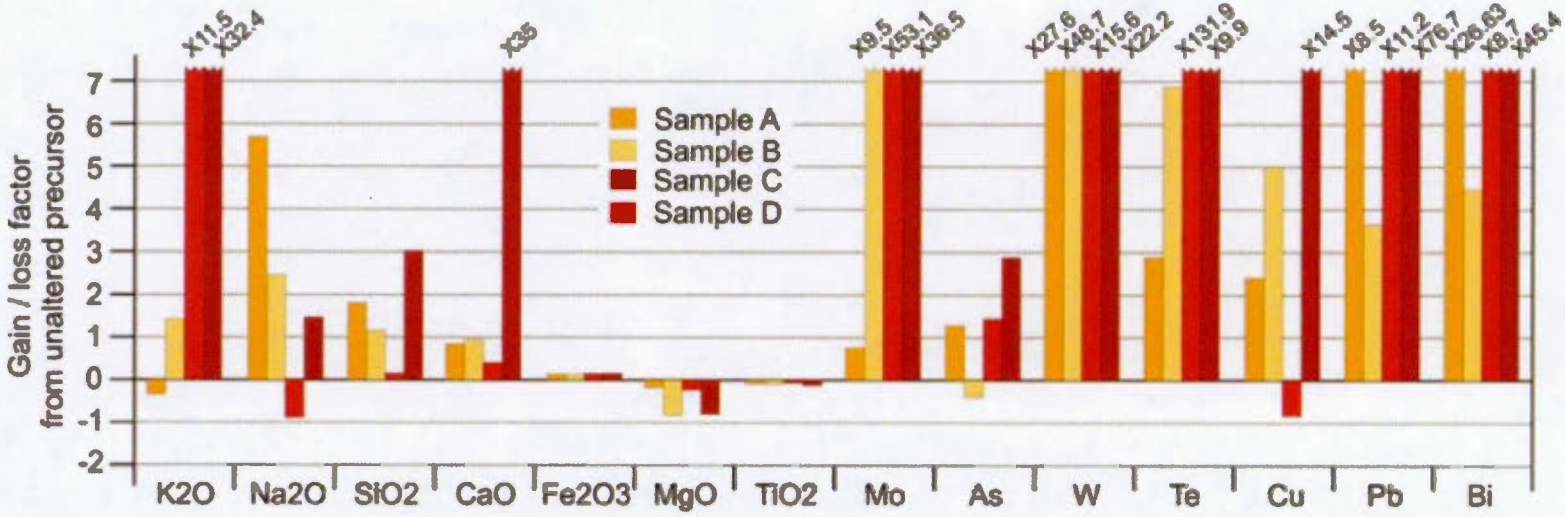

Figure 1.11 Mass balance calculations from samples described in Fig.10. Calculations were produced by the Lithomodeleur software (Trépanier, 2013). An enrichment factor of 1 means a 100% gains from the least-altered protolith, mass gain for the relative element is thus twice as the original mass.

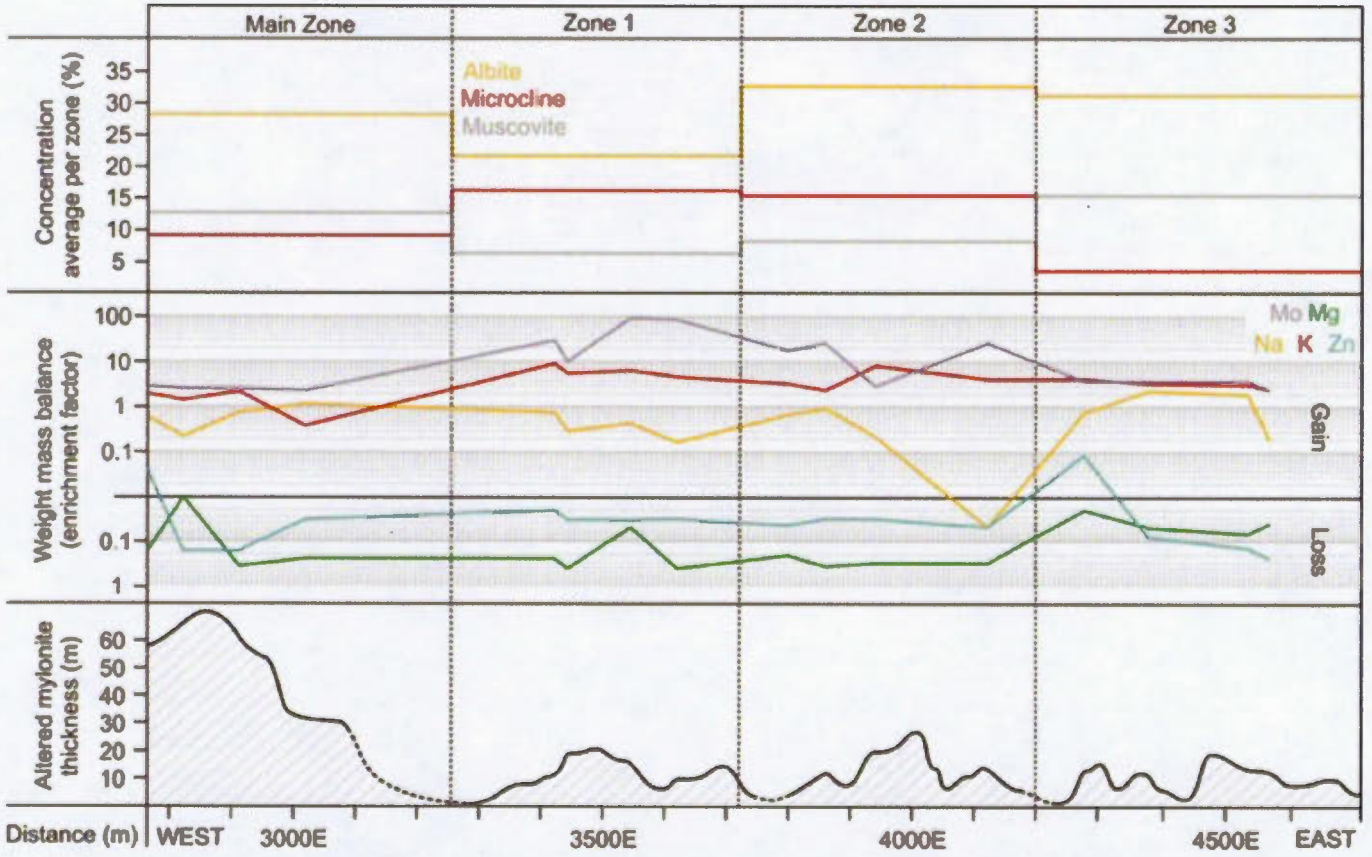

Figure 1.12 Longitudinal summary of alteration mineralogy and mass balance calculations from Wasamac deposit's four mineralized zones. The thickness of altered and mineralized faulted units is also represented. An enrichment factor of 1 means a 100% gains from the least-altered protolith, mass gain for the relative element is thus twice as the original mass.

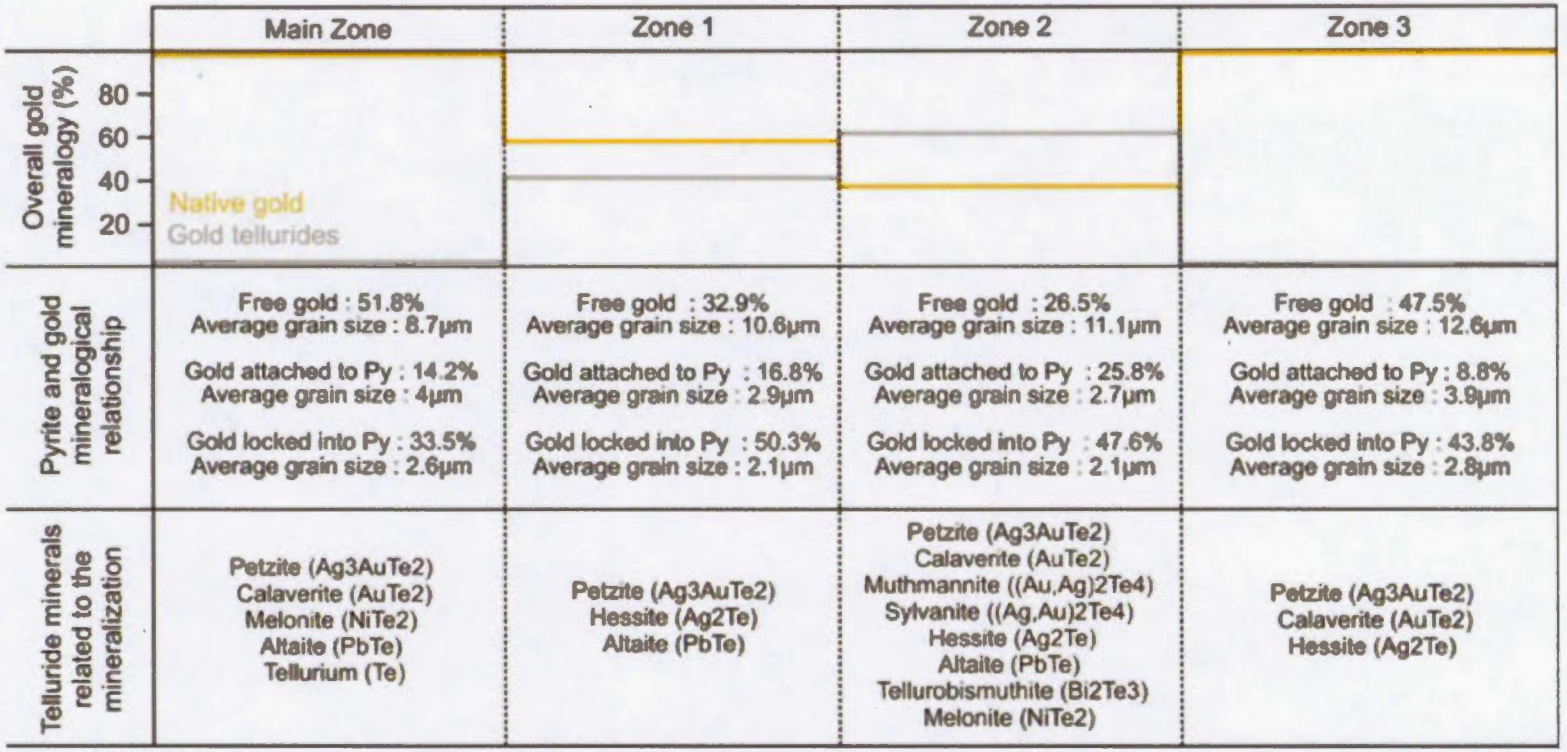

Figure 1.13 Mineralogy of gold from metallurgic tests within Wasamac deposit's economic zones along the longitudinal axis of the shear zone. Zones 1 and 2 mostly display telluride-gold minerals (calaverite and petzite) whereas Main Zone and Zone 3 display native gold. Both spatial relationships between gold and pyrite and gold grain size associated also display criteria arguing the longitudinal zonations and mineralization footprints for each alteration facies. Data collected from over 1200 gold grains by SGS.

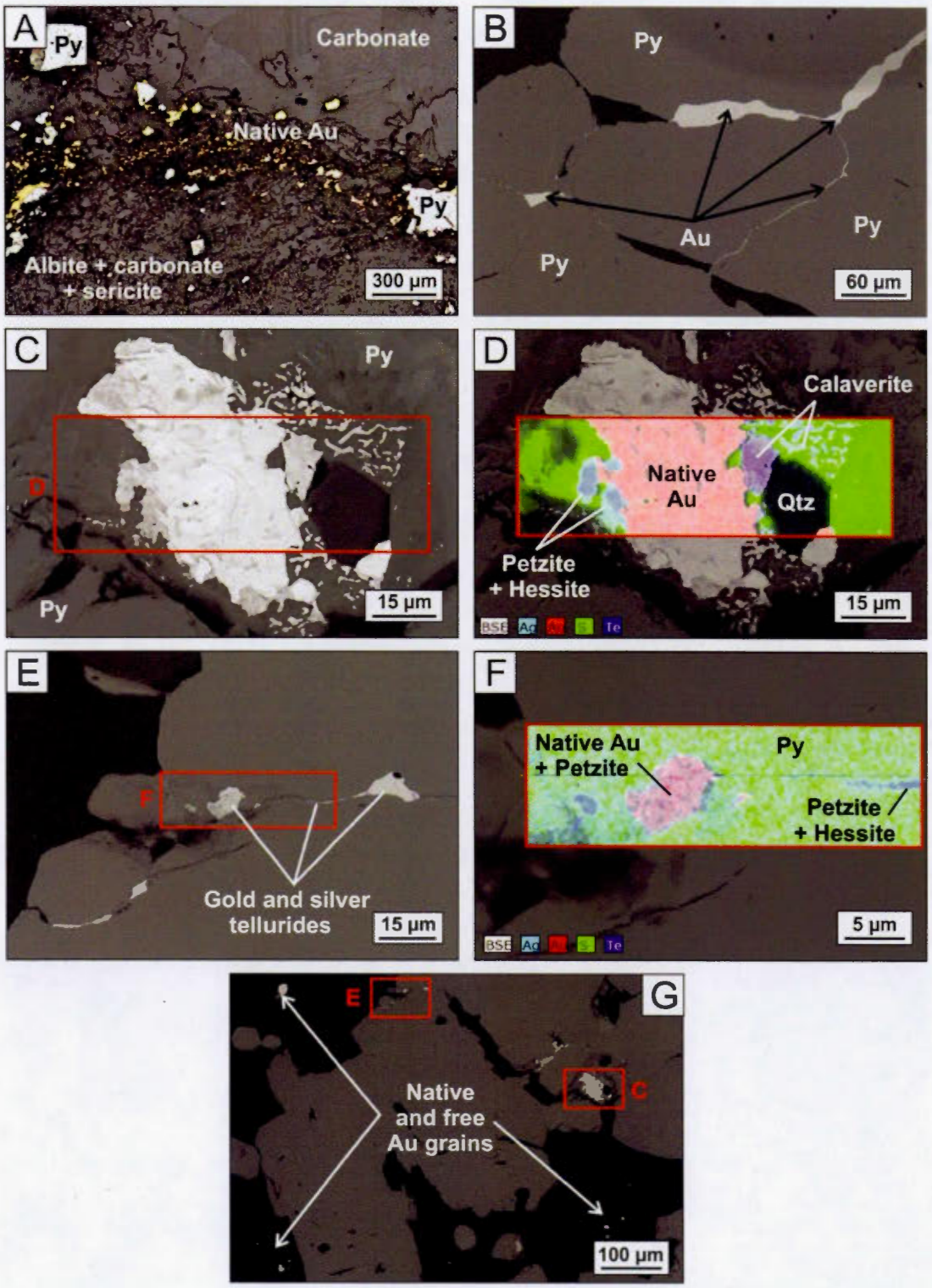
A
Py
Carbonate
Native Au
Py
Albite + carbonate
+ sericite
300 µm
B
Py
Au
Py
Py
60 µm
C
Py
D
Py
15 µm
D
Calaverite
Native
Au
Qtz
Petzite
+ Hessite
15 µm
BSE Ag Au S Te
E
F
Gold and silver
tellurides
15 µm
F
Native Au
+ Petzite
Py
Petzite
+ Hessite
5 µm
BSE Ag S Te
G
E
C
Native
and free
Au grains
100 µm

Figure 1.14 (A) Photograph of reflected light microscopy displaying free native gold associated with a cataclased zone within an albitic alteration assemblage. (B) SEM photograph of gold filling fractures in pyrite (C) SEM photograph of gold-rich fracture in pyrite. (D) SEM coloration of (C) displaying native gold and gold-silver telluride minerals filling fractures into pyrite. Thin fractures are mostly tellurium-rich, whereas wide-open fractures are native gold rich. (E) SEM image showing gold-rich fractures in pyrite. (F) Close-up of (E) showing wide-open fracture into pyrite mostly filled with native gold. Contacts with pyrite fractures show vermicular gold-silver telluride minerals. (G) Overall SEM photograph from (C) and (E) close-up photographs showing various gold mineralogy: gold-silver tellurides filling thin pyrite fractures planes, native gold filling wide fracture planes and native free gold grains.

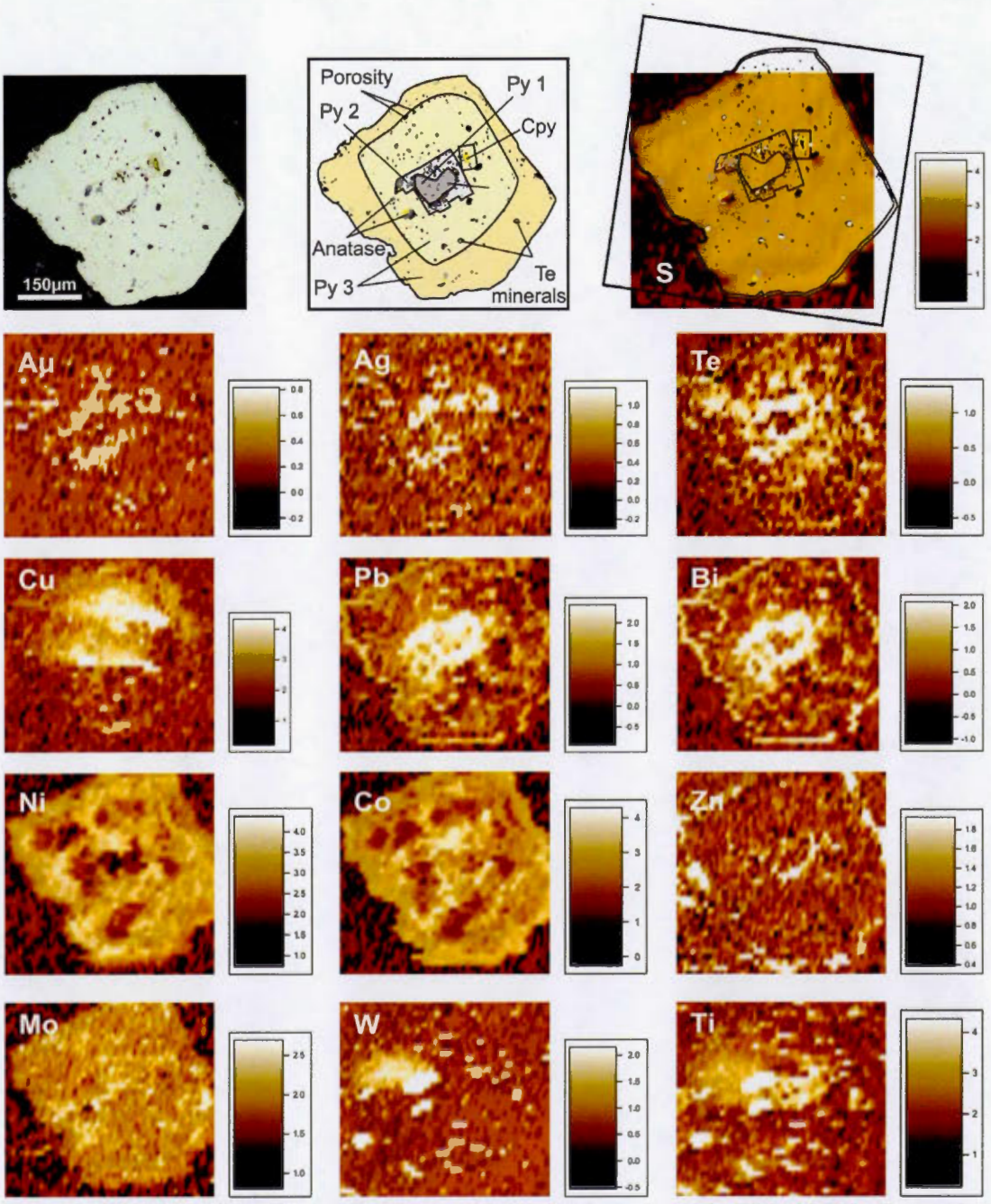

Figure 1.15 LA-ICP-MS maps of a pyrite grain from sample WS-45463. From the top left to the bottom right: photograph of target pyrite in reflected light microscopy displaying varying concentric textures, schematic interpretation of pyrite zonations, LA-ICP-MS maps of S, Au, Ag, Te, Cu, Pb, Bi, Ni, Co, Zn, Mo, W, Ti. Scale of LA-ICP-MS maps are log(10) ppm. More LA-ICPMS maps are presented in appendix B.

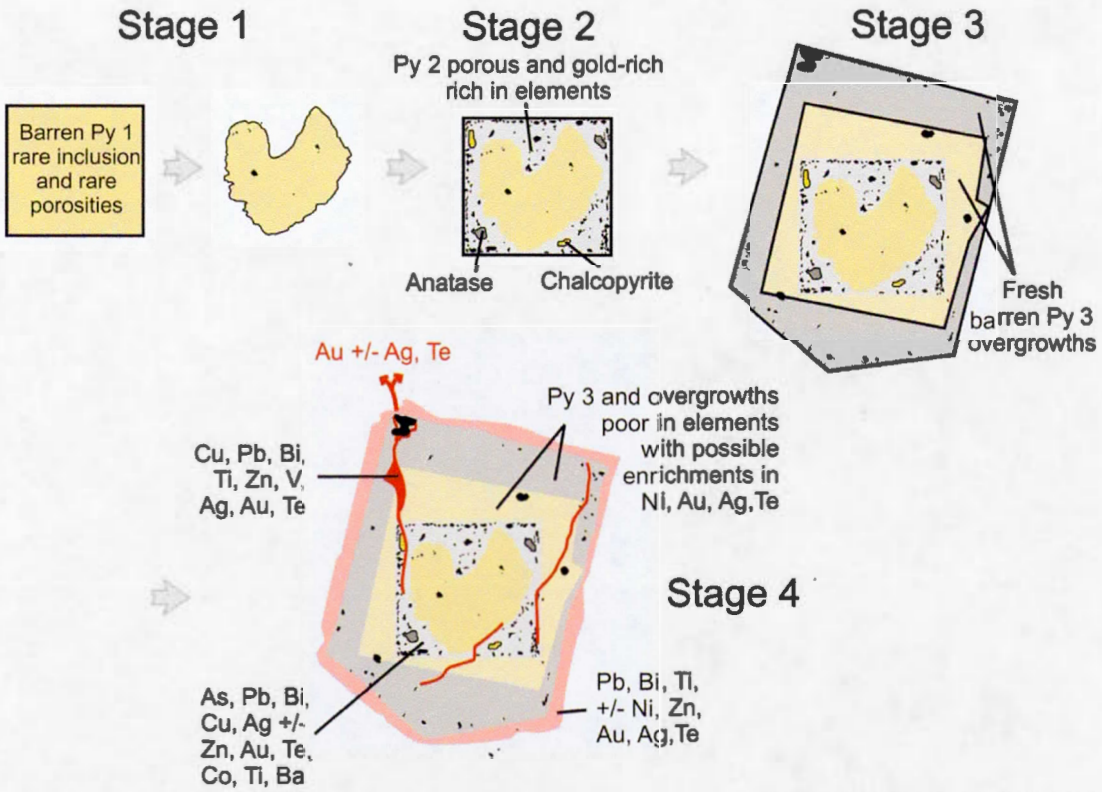

Figure 1.16 Schematic model of pyrite zonations and metallic anomalies observed with LA-ICP-MS analyses. This model represents a composite interpretation from thirteen LA-ICP-MS maps. Four events are observed: three pyrite overgrowths and a late fracturation event. Gold is related to the porous pyrite overgrowth (stage 2) and may be associated locally to the phase 3 overgrowths. The fracturation event is represented with the red irregular lines. A pink coloration represents chemical anomalies frequently observed surrounding pyrite.

Structural features	- S1 main foliation and local S2 ductile deformation - Possible structural partitioning : brecciation of K-feldspar altered units with pyrite fracturation associated and ductile deformation of albitized units.			None	- Brecciation of K-feldspar altered units - Pyrite fracturation
Alteration chemistry	- Regional metamorphic signature - Carbonate veinlets towards the strain zone	- Red potassic pervasive alteration - K2O, K, Mo, W, Pb, Bi strong anomalic values	- Greyish-beige albitic pervasive alteration as a matrix in K-altered units breccia - Na2O, Na, Cu, W, Pb, and Bi strong anomalic values	No specific alteration described	- Greyish-beige albitic pervasive alteration - Na2O, Na, Cu, W, Pb, and Bi strong anomalic values
Gold characteristics	None	- Invisible gold telluride minerals trapped in spongy pyrite structure -Few gold telluride inclusions <3µm	- Abundant gold tellurides and native gold filling fractures - Gold tellurides <5µm free native gold >5µm	- Recycling gold material from gold-rich pyrite - Rare gold telluride inclusions <3µm	- Gold tellurides and native gold filling fractures - Gold tellurides <5µm free native gold >5µm
Pyrite chemical enrichments	- Fluctuating Ni and Co anomalies - Few inclusions and porosities	- Cu, Zn, Pb, Bi, Co, Ag, Te, Au - Prevalent anatase, hematite and chalcopyrite inclusions	- Cu, Zn, Pb, Bi, Co, Ag, Te, Au - Possible gold release from pyrite lattice	- Fluctuating Ni and Co anomalies - Few inclusions and porosities - Local gold-tellurides inclusions	- Pb, Bi, Tl, Zn, Cu, Au +/- Te, Ag - Late enrichment remobilizations along fractures and around pyrite
Pyrite textural characteristics	 Slow cristallisation of barren pyrite	 Rapid cristallisation of gold-rich spongy pyrite	 Possible pyrite fracturation and gold release	 Slow pyrite cristallisation Local gold recycling	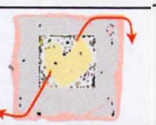 Brittle pyrite deformation Native gold release
Proposed model of tectonic and hydrothermal activity	 Initiation of reverse ductile faulting	Faulting maintenance 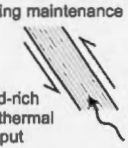 Gold-rich hydrothermal input	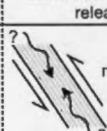 Faulting maintenance Structural partitioning between K-altered and Na-altered units	Faulting intermission 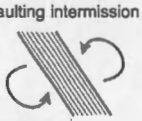 Regional fluid circulation	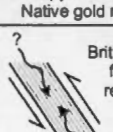 Brittle-ductile faulting recovery Barren fluid input

Figure 1.17 Schematic interpretation of Wasamac deposit's hydrothermal and tectonic processes associated with gold mineralization. Gold rich porous pyrite (stage 2) is associated with the early potassic hydrothermal event during a first tectonic event. A tectonic break is then suggested in this model, where metamorphic fluids crystallise pyrite stage 3 poor in elements. A second phase of tectonic activity is related to the late fracturation event affecting pyrites. This second tectonic activity is proposed to be associated with the albitic hydrothermal event.

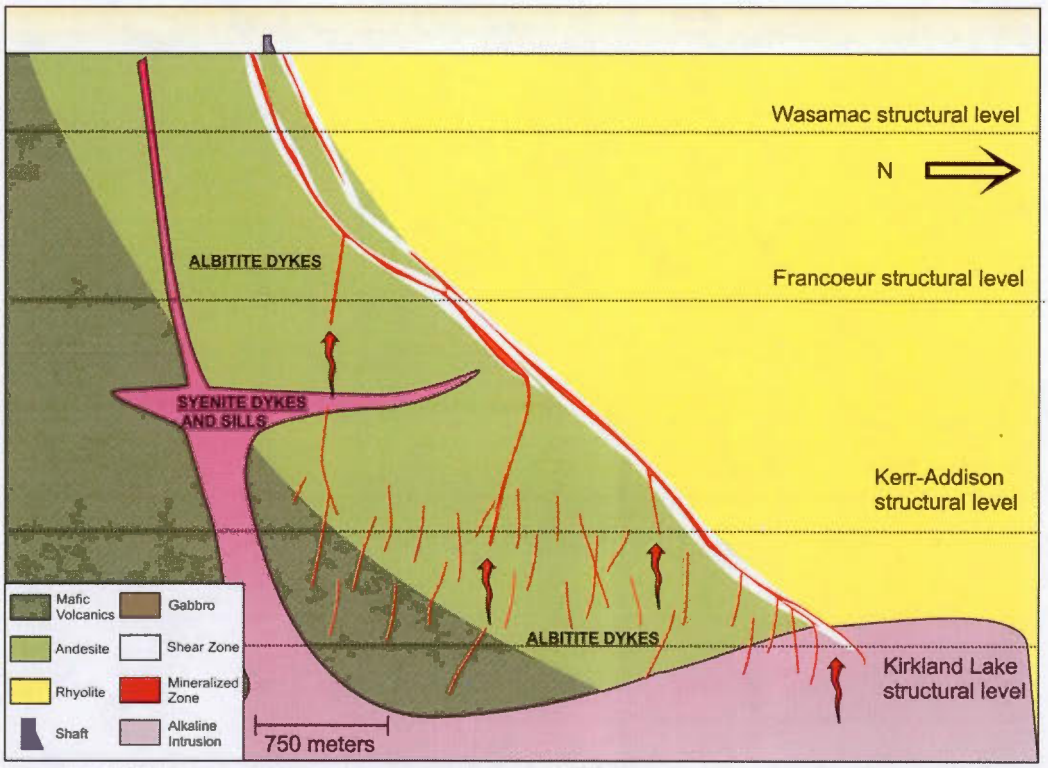

Figure 1.18 Proposed geological setting of Wasamac, Francoeur, Kerr-Addison and Kirkland Lake deposits. It is to note that the structural level setting of gold deposits seems to deepen going West, but it might be linked with variably rising heights of intrusive stocks as the metamorphic grade does not increases towards the West.

Parameter	WASAMAC	ALKALINE-RELATED	OROGENIC SHEAR ZONE
Setting of mineralization	Shear-zone in volcanites	Shear zone spatially associated with intrusions	Shear-zone in various lithologies
Nature of ore	Disseminated	Disseminated and veins/stockwerk	Disseminated and veins
Alteration mineralogy assemblage	K-feldspar, albite, carbonate, sericite, chlorite, quartz, hematite	K-feldspar, albite, carbonate, sericite, quartz, hematite +/- Biotite	Quartz, carbonate, sericite, chlorite, +/- albite, tourmaline
Ore minerals	Pyrite, gold tellurides, native gold	Pyrite, pyrrhotite, gold tellurides	Pyrite, arsenopyrite, native gold, gold tellurides
Alteration alkaline mass balance gains	Potassic then sodic	Potassic mostly	Potassic and sodic
Metallic association	Au-Ag-Te-Pb-Bi-Mo-W	Au-Ag-Te-Pb-Mo +/- Cu, Bi, F, As	Au-Ag-Te-As-W +/- Sb

Table 1.1 Alteration and mineralization essential caracteristics described within alkaline intrusion-related deposits, orogenic gold deposits and within the Wasamac deposit (Groves et al., 1998; Lang and Baker, 2001; Robert, 2001; Goldfarb et al., 2005).

	Kirkland Lake deposits	Kerr-Addison	Francoeur	Wasamac	Lapa	Matartic	Sigma-Lamaque
Host lithology	Ultramafic, tholeiitic and calc-alkaline meta-volcanic units Conglomerates and sandstones Three-phase syenitic intrusions	Ultramafic meta-volcanic units Tholeiitic mafic units Inter-bedded sediments	Meta-andesite Albitite dykes	Meta-andesite	Ultramafic and mafic volcanic units Graywacke	Porphyritic monzodiorite Metesedimentary units Mafic-ultramafic units	Andesitic flows and volcaniclastic rocks Porphyritic diorite
Host structure(s) Distance CLLFZ	CLLFZ and subsidiary second order fault zones Mostly Au-bearing veins Less Au-bearing sulphides in disseminated altered faulted units	CLLFZ and second order Kerr Fault, similarly striking Au-bearing veins Au-bearing sulphides in disseminated altered mylonite	Second order FWSZ, 2km north of the CLLFZ Disseminated Au-bearing sulphides and free native gold grains in altered mylonite	Second order FWSZ, 2,5km north of the CLLFZ Disseminated Au-bearing sulphides and free native gold grains in altered mylonite	CLLFZ Au-bearing sheared veinlets within brittle-ductile to ductile conditions	CLLFZ and proximal subsidiary fault Au-bearing veins	3,5km north of the CLLFZ along subdisiary faults Brittle vein system
Alteration mineralogical characteristics	Qtz, ser, carb, K-feldspar, alb, py Post-ore chlorite fault gouge	Four alteration assemblages: (1) Qtz, chlo, carb, ser, alb, py (2) Qtz, carb, fush (3) Alb, musc, chlo, py (4) Graph, py	Three alteration assemblages: (1) Pre-ore: Alb, carb, hem, ser, qtz (2) Alb, carb, py, ser (3) Post-ore: sulfate-bearing veinlets	Two gold-rich alteration assemblages: (1) K-feldspar, ser, carb, qtz, hem, py (2) Alb, ser, carb, chlo, py	Qtz, dol, cal, biot, musc	Pervasive potassic alteration (K-feldspar and biot), carb, py, and local qtz within host lithologies	Qtz, trm, carb, cho +/- alb, schee
Alteration geochemistry and additional informations	Strong mass gains in K and Na	Polyphased alteration events and overprinting Mass gains in K, Ca, Cu, Ag, W, Au, Ag Variable geins/losses in Na	(1) Mass gains in K2O, Rb, W, Co2, Au, S (2) Mass gains in Na2O, W, Au, S, Co2	(1) Mass gains in K, Mo, W, Pb, Bi, Te, Ag, Au (2) Mass gains in Na, Mo, W, Pb, Bi, Te, Ag, Au	Superposition of three metamorphic episodes (1) syn-ore biot. alteration (2) hornb, oligo prograde metamorphism (3) Act, alb, retrograde metamorphism	Mass gains in K, S, Ag, Te and Au, significant gains in Sb, W, Bi and Pb. Significant mass loss in Cu	Zoned alteration haloes extending up to several meters away from the veins with ser, carb, py, alb.
Mineralization mineralogical characteristics	Py + minor cpy, moly, sph Spatially associated with faulted syenitic intrusions Gold closely associated with tellurides	Gold bearing disseminated pyrite in (1) and (3) Free native gold grains in veins and veinlets in (2) Gold-rich sulphide remobilizations in (4)	Gold associated with As-free pyrite and free native gold grains	(1) Telluride gold minerals associated with As-free zoned pyrite (2) Disseminated free native gold grains	Finely disseminated auriferous apy, po +/- py Native gold disseminated in altered wall rocks	Mainly native gold and subordinate gold tellurides Spatial association with Pyrite and minor Cpy, Ga, Sph, Hm, Mo and Ag-Pb-Bi Tellurides	Py +/- po Native gold and gold tellurides in veins with crack ad seal texture
Mineralization complementary informations	High Te, Au, Mo, Pb, Ag Sporadic Cu Low As High Au/Ag	Event (3) : Gold-bearing pyrites associated with 5 000 albitite dykes High Au/Ag	Metallic signature: W, Te, Bi, Cu, Pb, Ni, Zn High Au/Ag	Chemical control of gold precipitation in (1), structural control of gold recrystallization in (2) Gold mineral maturation from (1) to (2) High Au/Ag	Characteristic Au, Sb, As and Au, As associations Early low grade mineralization (1), remobilized (2) and native gold precipitation (3)	Au concentrated in two generations of discontinous veins, and within the alteration envelopes Au deposition related to pyritization followed by oxydation events	Metallic signature: Te, B, S, Ag
Gold ressources and historic production	21,8 Moz Au produced	9,5 Moz Au produced	508 716 oz Au produced	276 536 oz Au produced 1 125 727 oz Au ressource	700 000 oz Au ressource	5,1 Moz Au produced 13,4 Moz Au ressource	Over 7 Moz Au produced
Genetic interpretation	Magmatic-hydrothermal genetic model Syenite-related overprinted by regional deformation	Orogenic gold deposit resulting of repeated cycles of hydraulic fracturing Possible genetic association for gold-bearing albitites with buried alkaline stock	Orogenic gold deposit Fluid/rock interaction between pre-ore oxidized dykes acting as a trap for gold-bearing pyrite crystallisation	Magmatic-hydrothermal genetic model Biphased alkaline hydrothermal circulation within orogenic structure possibly intrusion-related	Orogenic gold deposit associated with a polyphased metamorphic control on gold enrichment	Magmatic-hydrothermal genetic model "Oxidized" intrusion-related structurally-associated	Late brittle orogenic gold deposit within a shear-zone Possibly related to late diorite-tonalite plugs

Table 1. 2 Descriptive comparison between several gold deposits situated within the CLLFZ. Qtz: quartz, Chlo : chlorite, Ser : sericite, Carb : carbonates, Alb : albite, Dol : dolomite, Cal : calcite, Trm : tourmaline, Schee : scheelite, Biot : biotite, Fusch : fuschite, Musc : muscovite, Py : pyrite, Po : pyrrhotite, Cpy : chalcopyrite, Moly : molybdenite, Sph : sphalerite, Apy : arsenopyrite, Hm : hematite, Ga : galena. (Ispolatov et al., 2008 ; Kishida & Kerrich, 1987 ; Smith et al., 1993 ; Couture & Pilote, 1994 ; Simard et al., 2013 ; Helt et al., 2014; Poulsen et al., 2000).

CONCLUSION GÉNÉRALE

Le gisement de Wasamac est caractérisé par une minéralisation en remplacement associée à une intense altération alcaline pervasive au sein d'une faille ductile. Deux signatures hydrothermales sont décrites le long du cisaillement Francoeur-Wasa : potassique et albitique. Elles présentent des périodes de mise en place discontinues dans le temps : l'altération potassique en conditions oxydantes est localement reprise par une altération albitique sous conditions réductrices. Ces deux altérations présentent une forte signature alcaline ainsi que des assemblages métalliques similaires à ceux décrits dans les contextes aurifères associés aux intrusions alcalines. A partir de corrélations de terrain ainsi que d'observations au MEB et au LA-ICP-MS il est proposé que chaque signature hydrothermale correspond à deux évènements tectoniques de la FWSZ possiblement séparés par une période d'inactivité. La précipitation de l'or est majoritairement associée à la mise en place de l'altération potassique sous forme de tellurures d'or dans les pyrites du stade II. Les conditions redox seraient le contrôle majeur de la précipitation des sulfures piégeant l'or, d'après les textures poreuses des pyrites aurifères et l'altération hydrothermale précoce à feldspaths K et hématite. Suivant cet événement, des pyrites non poreuses et pauvres en éléments de la phase III refléteraient les circulations d'un fluide local dilué. Une seconde phase tectonique de la FWSZ engendre localement une bréchification des unités à altération potassique ainsi qu'une intense circulation hydrothermale sodique. Cet évènement hydrothermal pervasif et réducteur se superpose localement aux altérations potassiques oxydées précoces ainsi qu'aux volcanites andésitiques peu altérées (stade IV). Les pyrites des stades I à III sont localement cataclasées. Cet événement cassant des sulfures provoque une extraction de l'or de leur structure. L'or précipite dans les fractures sous forme de tellurures puis diffuse progressivement dans l'encaissant à altération albitique sous forme native.

Le gisement de Wasamac pourrait représenter la superposition de deux évènements hydrothermaux : un premier associé à une source magmatique alcaline et un second associé à une remobilisation de la minéralisation par des fluides hydrothermaux de type orogénique. Ce gisement partage les caractéristiques des gites de type orogénique et associé aux intrusions alcalines.

APPENDICE A

ANALYSES GEOCHIMIQUES DU GISEMENT DE WASAMAC

Introduction et méthodes analytiques

Deux groupes d'analyses géochimiques ont été utilisés pour décrire le gisement de Wasamac. Un premier groupe de 14 analyses entreprises par Mines Richmont utilisent des échantillons prélevés sur l'ensemble de l'épaisseur de la faille le long des quatre zones économiques (Main Zone, Zone 1, 2 et 3). Un deuxième groupe de 28 échantillons ont été sélectionnés sur forages pour l'étude précise des faciès lithologiques altérés et peu altérés du gisement de Wasamac. Le premier groupe d'échantillons permet de remarquer la signature géochimique dominante sur toute l'épaisseur de la faille le long de chaque zone, ainsi que d'identifier des possibles variations d'Est en Ouest. Le deuxième groupe d'échantillons vise à définir les caractéristiques géochimiques des deux faciès d'altérations et de les comparer à leur encaissant peu altéré. Des bilans de masse ont été entrepris avec ces deux groupes d'échantillons, mais le manque des valeurs de Zr pour le premier groupe d'échantillons restraint la qualité des résultats et sont utilisés à but qualitatif au sein de la figure 10. Le deuxième groupe d'échantillons a aussi été utilisé pour la confection de lames minces dont les observations seront détaillées au sein des annexes suivantes. Les analyses géochimiques ont été effectuées par les laboratoires AcmeLabs de Vancouver, où des mesures XRF et ICP-MS ont été conduites respectivement après dilution Li2B4O7/LiBO2 et dilution aux quatre acides. Cet appendice présente les résultats obtenus. Certains chiffres sont absents, car non demandés à l'analyse.

Résultats

Les résultats des analyses lithogéochimiques sont présentés dans les tableaux suivants. Les 28 échantillons analysés durant la maîtrise sont décris et localisés sur

une section longitudinale respectivement dans les figures 1 et 2. Les tableaux suivants présentent les résultats obtenus pour chaque échantillon. Les 4 derniers tableaux représentent les analyses du cisaillement au complet, 14 ont été utilisés dans ce mémoire (Fig.10) sur les 26 présentés.

Sample	Zone	Drill hole #	Distance FWSZ	Description
WSC-45454	Main	WS-11-72	6m (Hanging wall)	Andesite, moderate shearing, sheared Qtz-CB veinlets
WSC-45459	Main	WS-282-02	0m	Rhyolite, strong shearing, alteration in HM, AB, SE, CB, Py
WSC-45461	Main	WS-289-01	0m	Gabbro, moderate shearing
WSC-45463	Main	WS-289-01	38m (Shear zone in the Footwall)	Andesite, moderate shearing, altered in AB, SE, Py, VG
WSC-45464	Main	WS-289-01	55m (Footwall)	Andesite, no shearing, least altered
WSC-45466	Main	WS-282-01	79m (Hanging wall)	Gabbro, no shearing, least altered
WSC-45467	Main	WS-11-72	0m	Andesite (?) moderate shearing, alteration: AB, HM, SE, CL, CB, Py
WSC-45468	Main	WS-11-72	0m	Andesite (?) moderate shearing, alteration: AB, HM, SE, CL, CB, Py
WSC-45469	2	WS-11-69	45m (Hanging wall)	Andesite (?) low shearing, alteration: KF, HM, SE, CL, CB, Py
WSC-45470	2	WS-10-37	0m	Andesite (?) strong shearing, alteration: AB, SE, CB, Qtz, Py
WSC-45471	Main	WS-11-61	120m (Hanging wall)	Rhyolite, slight fracturation, alteration: Qtz, HM
WSC-45472	Main	WS-11-61	105m (Hanging wall)	Rhyolite, moderate shearing, strong fracturation, alteration: Qtz, HM, Py
WSC-45473	3	WS-11-132	0m	Andesite (?), moderate shearing, altered in AB, CB, SE, Py
ECHMAX1	Main	WS-284-03	7,5m (Hanging wall)	Rhyolite, moderate shearing and fracturation, alteration: Qtz, CL, Py
ECHMAX2	Main	WS-284-03	0m	Rhyolite, strong shearing and fracturation, alteration: Qtz, HM, CB, SE, CL, Py
WSC-000801	Main	WS-289-01	43m (Footwall)	Andesite, no shearing, least altered
WSC-000802	2	WS-10-38B	0m	Andesite (?) low shearing, alteration: KF, HM, SE, CL, CB, Py
WSC-000803	2	WS-10-38B	5m (Footwall)	Andesite, no shearing, least altered
WSC-000804	2	WS-11-74A	0m	Andesite, low shearing, least altered
WSC-000807	2	WS-11-65	0m	Andesite (?) low shearing, alteration: KF, AB, HM, SE, CL, CB, Py
WSC-000811	2	WS-11-74A	0m	Andesite (?), moderate shearing, altered in AB, CB, SE, Py
WSC-000813	West Francoeur	AS-09-95	0m	Andesite (?) low shearing, alteration: KF, HM, SE, CL, CB, Py
WSC-000814	Main	WS-11-72	396m (Hanging wall)	Syenite dyke, no shearing, moderate KF and HM alteration
WSC-000815	Main	WS-11-66	170m (Hanging wall)	Syenite dyke, no shearing, low KF and HM alteration
WSC-000816	Main	WS-11-66	173m (Hanging wall)	Syenite dyke, no shearing, strong KF and HM alteration
WSC-000818	Francoeur	R-899	364m (Hanging wall)	Syenite dyke, no shearing, strong KF, HM, Py alteration
WSC-000819	Francoeur	R-899	364m (Hanging wall)	Andesite-basalt, no shearing, least altered
WSC-000820	2	WS-11-69	50m (Hanging wall)	Andesite, no shearing, least altered

Figure 1. Tableau des échantillons sélectionnés sur forage pour analyses lithogéochimiques. Les alterations sont décrites par les codes suivants: HM: hematite, AB: albite, SE: séricite, CB: carbonates, Py: Pyrite, CL: chlorite, Qtz: quartz, KF: feldspaths potassiques.

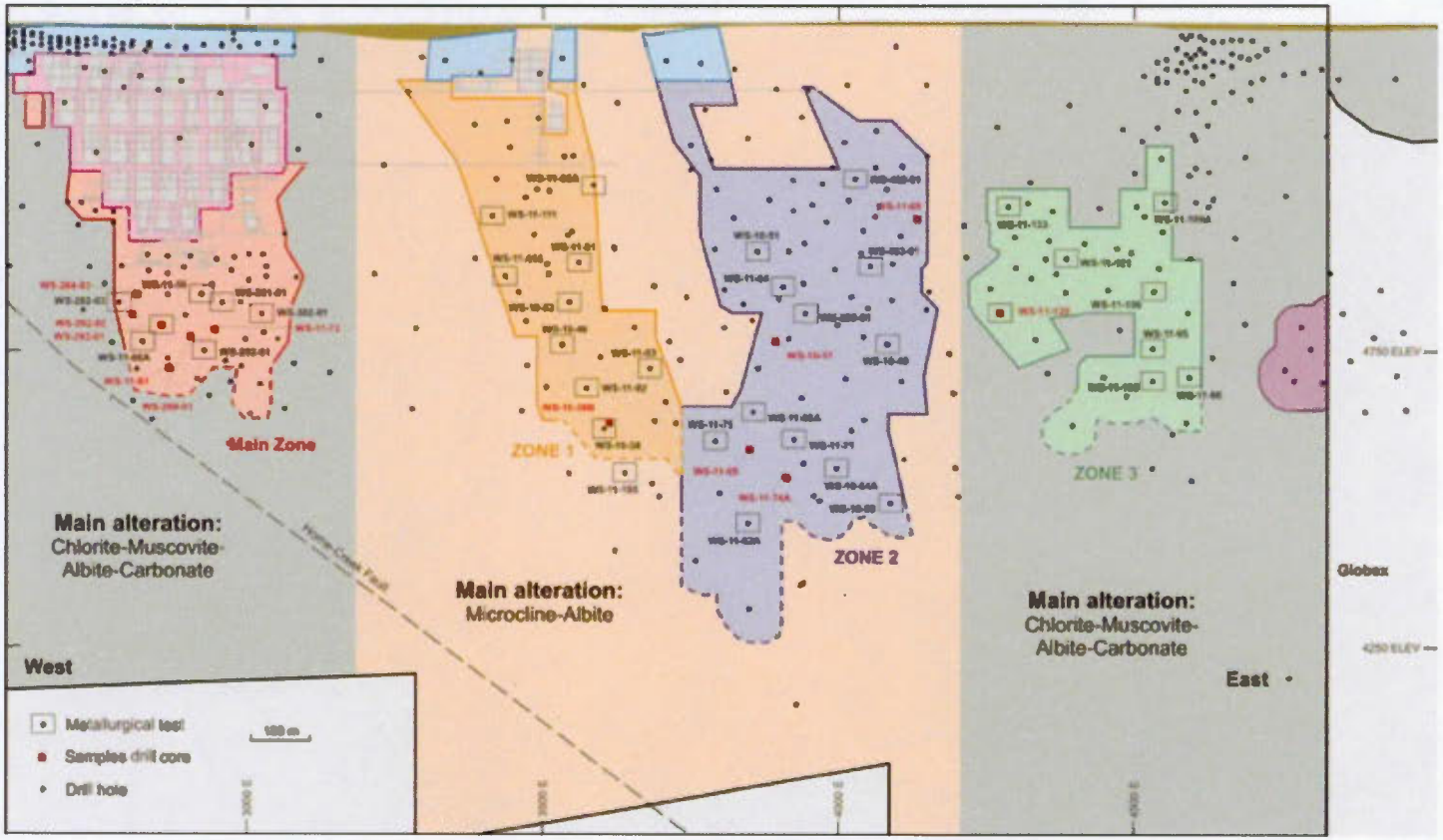

Figure 2. Localisation des échantillons sur la longitudinale E-W de la propriété Wasamac. Noter les Zones Principales et 2 associées à deux couleurs: le vert correspond au faciès d'altération albitique et le rosé correspond au faciès d'altération potassique. Les échantillons en rouge sont ceux sélectionnés pour analyses lithogéochimiques présentés Fig.1.

Sample	WSC-45454	WSC-45459	WSC-45461	WSC-45463	WSC-45464	WSC-45466	WSC-45467	WSC-45468
SiO2 (%)	48,49	68,26	40,10	52,70	43,83	45,50	57,41	57,68
Al2O3	18,59	11,28	13,22	14,55	14,04	15,39	15,48	15,77
Fe2O3	10,66	4,79	9,88	6,66	14,18	13,33	6,44	5,17
CaO	3,87	2,77	13,81	6,90	8,70	10,84	4,10	3,22
MgO	6,83	0,41	3,37	1,59	4,72	7,95	0,45	1,12
Na2O	4,42	4,26	0,11	7,29	2,52	2,47	8,36	7,43
K2O	0,38	2,92	3,00	0,46	1,70	0,20	0,50	2,78
MnO	0,11	0,02	0,17	0,10	0,15	0,21	0,05	0,07
TiO2	0,95	0,45	0,76	0,65	1,63	1,17	0,48	0,64
P2O5	0,13	0,10	0,24	0,21	0,16	0,09	0,12	0,14
Cr2O3	0,019	0,023	0,023	0,002	0,005	0,029	0,021	0,003
TOT/C	0,28	0,53	3,21	1,41	1,58	0,11	0,87	1,03
TOT/S	-0,02	2,99	0,16	3,42	-0,02	-0,02	4,27	2,87
LOI	5,33	3,44	13,57	3,52	8,2	2,86	3,29	3,99
Cu (ppm)	9,4	541,1	20,2	6,7	4,6	143,2	31,4	32,0
Pb	2,7	6,0	5,5	2,5	0,6	3,4	6,8	5,0
Zn	88	11	97	29	80	80	14	14
Ag	-0,1	2,0	0,1	9,9	-0,1	-0,1	4,4	1,8
Ni	84,4	18,2	60,9	28,8	58,1	116,2	17,0	11,4
Co	38,0	13,5	49,6	20,6	28,6	49,2	13,0	9,7
Mn	680	164	1289	736		1553	330	466
Mo	1,0	6,5	0,8	2,3	3,1	2,4	5,8	10,1
Fe	68400	34000	66300	44100		87000	42600	34500
As	3	-1	2	-1	-1,0	3	1	-1
U	0,2	0,6	0,6	0,5	0,3	-0,1	0,3	0,4
Au (ppb)	-100	15000	-100	167600	2,9	-100	34600	15500
Th (ppm)	1,0	1,7	1,9	1,7	0,7	0,2	1,1	1,4
Sr	121,0	27,0	154,0	129,0	83,7	249,0	71,0	74,0
Cd	0,1	0,3	-0,1	-0,1	-0,1	0,1	-0,1	-0,1
Sb	0,2	0,4	0,5	0,2	0,1	0,4	0,3	0,7
Bi	0,2	2,1	-0,1	0,6	-0,1	-0,1	0,6	0,3
V	210	33	195	70	458	288	49	53
Ca	25800	19800	96600	48700		73000	28700	22000
P	480	420	1150	1000		400	510	600
La	8,5	4,1	19,8	9,9	7,1	4,6	6,0	7,0

Sample	WSC-45454	WSC-45459	WSC-45461	WSC-45463	WSC-45464	WSC-45466	WSC-45467	WSC-45468
Cr	86	123	86	11		143	77	8
Mg	35300	2300	19500	9000		46600	2300	5800
Ba	38	150	622	44	292	28	63	165
Ti	5430	1690	1630	2070		6420	1140	2540
Al	82100	55000	71800	72900		82400	65600	69000
Na	31000	33550	800	53170		17840	65270	55700
K	2700	24700	25700	4000		1500	4100	20900
W	0,5	11,8	1,4	38,5	3,1	1,0	13,8	35,3
Zr	64,6	198,1	77,2	146,7	111,1	23,3	172,2	185,8
Ce	20	11	40	22	16,7	10	16	19
Sn	0,6	0,8	0,8	0,6	-1	0,5	0,6	0,9
Y	12,2	15,7	11,6	18,9	34,7	13,5	7,9	9,1
Nb	3,9	4,6	1,3	2,4	5,5	2,7	2,6	5,7
Ta	0,3	0,4	-0,1	0,2	0,3	0,2	0,2	0,4
Be	-1	-1	2	1	1	-1	2	-1
Sc	26	6	26	11	47	39	9	11
Li	46,4	7,3	27,2	6,2		19,0	4,1	2,2
S	-1000	30000	2000	35000		-1000	42000	28000
Rb	3,4	27,7	93,1	9,4	44,0	2,8	4,3	17,1
Hf	1,6	5,5	2,1	4,0	3,0	0,7	4,4	4,6
In	0,08	0,05	0,06	0,05		-0,05	-0,05	-0,05
Se	-1	2	-1	3	-1,0	-1	3	1
Te	0,8	0,9	1,3	2,9		2,9	3,5	1,5
Cs	0,2			1,2	0,5	0,3		
Ga	14,9			22,6	16,8	15,6		
Pr	3,54			3,84	2,40	1,50		
Nd	13,5			15,1	12,1	7,1		
Sm	3,08			3,44	3,89	2,19		
Eu	0,96			1,22	1,10	0,83		
Gd	3,07			3,85	5,09	2,48		
Tb	0,48			0,67	0,93	0,41		
Dy	2,89			3,73	6,12	2,41		
Ho	0,55			0,89	1,38	0,45		
Er	1,66			2,51	3,76	1,37		
Tm	0,22			0,40	0,56	0,18		
Yb	1,49			2,47	4,00	1,17		
Lu	0,25			0,49	0,63	0,21		

Sample	WSC-45469	WSC-45470	WSC-45471	WSC-45472	WSC-45473	ECH-MAX1	ECH-MAX2
SiO2 (%)	48,68	46,58	75,30	73,70	66,25	75,91	59,70
Al2O3	11,90	12,37	11,64	10,62	8,02	11,28	16,66
Fe2O3	9,24	8,08	1,42	3,94	5,68	2,09	5,90
CaO	4,87	6,97	1,47	0,80	4,75	1,64	1,68
MgO	2,57	3,67	0,09	0,41	2,25	0,41	0,70
Na2O	0,47	6,68	4,19	3,96	2,89	6,10	9,80
K2O	9,89	0,60	3,82	3,12	1,06	0,26	0,24
MnO	0,16	0,21	0,02	0,03	0,09	0,02	0,04
TiO2	1,16	1,30	0,31	0,27	0,53	0,29	0,64
P2O5	0,27	0,22	0,05	0,06	0,09	0,07	0,20
Cr2O3	0,018	0,001	-0,001	0,001	0,008	0,015	0,002
TOT/C	1,79	2,80	0,26	0,14	2,05	0,30	0,55
TOT/S	5,48	5,22	0,04	2,15	2,40	0,14	3,51
LOI	6,29	7,33	0,82	1,77	8,3	1,64	3,78
Cu (ppm)	9,3	11,0	76,2	40,6	40,5	10,7	24,2
Pb	7,2	11,2	4,8	6,5	4,2	3,7	4,5
Zn	46	41	13	20	27	16	13
Ag	9,9	5,1	-0,1	2,2	0,8	-0,1	1,4
Ni	23,1	18,9	1,3	4,1	29,6	5,6	9,8
Co	28,4	26,9	1,2	3,8	19,3	3,4	7,0
Mn	1221	1579	215	225		150	318
Mo	13,2	12,0	1,2	1,9	4,7	1,2	3,0
Fe	62000	54600	9600	29300		15200	41300
As	-1	2	1	-1	0,9	-1	-1
U	0,1	0,3	0,5	0,5	0,2	0,6	1,1
Au (ppb)	9900	4900	-100	1800	7989,3	-100	10200
Th (ppm)	0,4	0,6	1,8	1,6	0,4	1,8	3,2
Sr	100,0	148,0	53,0	84,0	73,8	53,0	111,0
Cd	0,2	0,1	-0,1	0,2	-0,1	-0,1	-0,1
Sb	0,5	0,1	0,2	0,4	-0,1	0,1	0,3
Bi	0,4	2,5	-0,1	0,5	0,5	-0,1	0,3
V	58	60	2	14	34	16	41
Ca	34600	49700	9800	4700		11600	12000
P	1110	980	220	300		310	1030
La	4,1	3,5	7,7	11,6	4,6	11,0	21,0

Sample	WSC-45469	WSC-45470	WSC-45471	WSC-45472	WSC-45473	ECH-MAX1	ECH-MAX2
Cr	81	12	4	7		95	8
Mg	14300	20300	700	3200		2400	4200
Ba	69	46	493	67	95	81	69
Ti	2630	2680	1380	1100		1050	1670
Al	56200	60900	53800	50500		56500	84400
Na	3290	49950	30060	28910		47770	76090
K	40400	4800	3300	26600		2300	2100
W	10,8	9,0	1,1	2,9	14,6	1,7	20,1
Zr	49,4	74,7	157,9	171,4	47,4	180,8	278,1
Ce	11	9	19	26	12,3	28	45
Sn	0,5	0,4	2,0	0,7	-1	0,7	0,9
Y	7,1	6,1	20,5	20,5	9,9	13,2	20,7
Nb	1,7	1,4	5,4	4,2	3,2	4,2	4,3
Ta	-0,1	-0,1	0,3	0,3	-0,1	0,3	0,3
Be	-1	-1	-1	-1	-1	-1	1
Sc	21	23	10	7	15	13	7
Li	2,4	1,4	1,4	2,5		5,0	1,2
S	58000	50000	-1000	24000		1000	36000
Rb	54,3	9,1	38,9	34,9	21,5	5,0	3,2
Hf	1,1	2,1	4,6	5,0	1,0	4,9	7,9
In	-0,05	-0,05	0,05	-0,05		-0,05	-0,05
Se	2	3	-1	2	0,9	-1	4
Te	10,8	10,0	-0,5	2,7		-0,5	1,7
Cs					0,7		
Ga					9,6		
Pr					1,46		
Nd					6,4		
Sm					1,80		
Eu					0,54		
Gd					1,71		
Tb					0,33		
Dy					2,13		
Ho					0,38		
Er					1,16		
Tm					0,18		
Yb					1,25		
Lu					0,19		

Sample	WSC-000801	WSC-000802	WSC-000803	WSC-000804	WSC-000807	WSC-000811	WSC-000813
SiO2 (%)	50,41	49,78	47,87	59,27	52,55	45,43	69,22
Al2O3	12,44	14,17	16,73	15,47	13,83	13,61	9,80
Fe2O3	15,08	3,74	12,56	9,75	8,78	9,76	4,82
CaO	5,73	9,72	1,04	1,00	4,48	8,32	2,67
MgO	5,82	0,43	10,85	2,98	1,14	2,06	0,50
Na2O	0,61	1,28	2,04	3,28	0,26	6,11	2,88
K2O	1,38	10,38	1,20	3,24	11,91	1,20	3,60
MnO	0,15	0,13	0,09	0,05	0,08	0,16	0,14
TiO2	1,42	0,22	1,00	1,74	0,77	1,54	0,28
P2O5	0,14	0,15	0,38	0,24	0,14	0,29	0,06
Cr2O3	0,011	0,009	0,047	0,009	-0,001	0,003	-0,002
TOT/C	0,76	2,17	0,11	0,13	1,22	1,82	0,45
TOT/S	0,20	2,19	-0,02	0,06	5,72	6,13	1,72
LOI	5,90	5,12	5,98	2,56	5,9	3,92	5,9
Cu (ppm)	129,3	6,0	1,5	29,1	40,0	76,6	45,9
Pb	1,7	18,1	0,9	2,1	4,1	14,1	1,0
Zn	114	18	122	101	27	53	46,0
Ag	-0,1	0,9	0,1	-0,1	14,7	10,9	0,2
Ni	58,9	5,8	370,4	4,5	9,0	4,0	2,0
Co	52,9	12,4	45,7	11,0	11,1	24,3	1,5
Mn	1190	990	692	311		1245	
Mo	0,7	6,8	0,7	0,6	2,5	0,7	1,4
Fe	88900	25000	75200	62200		62300	
As	2	-1	-1	1	-1,0	-1	-0,5
U	0,2	0,3	0,3	0,1	0,5	0,3	0,5
Au (ppb)	-100	500	-100	-100	7437,5	4700	902,8
Th (ppm)	0,6	1,9	1,4	0,6	0,6	0,6	1,5
Sr	75,0	139,0	40,0	76,0	105,1	118,0	162,8
Cd	0,1	0,3	0,1	0,1	-0,1	-0,1	-0,1
Sb	0,6	-0,1	-0,1	0,2	-0,1	0,4	-0,1
Bi	-0,1	0,6	-0,1	-0,1	0,3	0,5	-0,1
V	392	33	194	395	75	86	19
Ca	43900	69900	7300	6100		59700	
P	560	670	1600	950		1170	
La	6,0	6,7	7,5	5,5	3,7	4,2	10,8

Sample	WSC-000801	WSC-000802	WSC-000803	WSC-000804	WSC-000807	WSC-000811	WSC-000813
Cr	30	43	213	37		8	
Mg	34700	1900	59500	17500		11500	
Ba	205	342	154	286	503	78	760
Ti	9310	940	890	2240		3480	
Al	65800	58900	78000	65900		67700	
Na	4430	9110	14160	25240		46010	
K	11400	35400	9100	28400		9500	
W	1,4	1,8	0,3	1,0	20,7	14,6	8,9
Zr	42,3	71,6	111,2	58,5	57,5	55,8	150,4
Ce	16	18	19	15	9,2	11	25,5
Sn	0,9	0,3	0,3	1,2	-1	0,5	1
Y	28,6	7,2	4,7	5,0	9,8	9,5	28,9
Nb	5,2	2,2	0,5	0,7	2,8	1,6	7,6
Ta	0,3	0,1	-0,1	-0,1	0,1	0,1	0,6
Be	-1	-1	-1	-1	3	2	-1
Sc	39	5	20	34	17	31	13
Li	26,8	2,2	41,8	18,4		6,0	
S	2000	22000	-1000	-1000		60000	
Rb	31,2	38,5	23,7	63,2	153,6	23,3	33,0
Hf	1,5	2,0	2,8	1,5	1,5	1,5	4,2
In	0,09	-0,05	0,05	0,09		-0,05	
Se	-1	2	-1	-1	3,2	4	-0,5
Te	1,1	3,4	1,2	-0,5		12,0	-0,2
Cs		0,6	0,6	0,9	1,1	0,5	1,0
Ga		11,1	15,9	16,6	16,2	18,9	9,6
Pr		2,40	2,25	2,64	1,18	2,23	3,48
Nd		10,4	9,1	11,6	4,6	11,8	15,4
Sm		2,51	1,83	2,81	1,41	3,02	3,94
Eu		0,95	0,66	0,98	0,52	0,95	1,04
Gd		2,80	2,28	3,14	1,68	3,03	4,48
Tb		0,45	0,40	0,54	0,34	0,53	0,83
Dy		2,94	2,32	3,51	1,77	3,31	5,30
Ho		0,67	0,52	0,69	0,39	0,57	1,06
Er		1,75	1,35	2,07	1,13	1,63	3,17
Tm		0,27	0,20	0,30	0,17	0,27	0,51
Yb		1,79	1,25	1,87	1,23	1,71	3,31
Lu		0,27	0,19	0,31	0,20	0,27	0,55

Sample	WSC-000814	WSC-000815	WSC-000816	WSC-000818	WSC-000819	WSC-000820
SiO2 (%)	70,01	65,70	64,17	75,93	53,38	52,76
Al2O3	15,15	16,07	17,63	8,70	12,93	15,55
Fe2O3	1,90	4,53	4,12	3,73	12,32	10,11
CaO	0,84	0,96	1,02	1,63	4,70	4,38
MgO	0,29	1,60	1,64	0,05	4,93	4,32
Na2O	5,36	5,71	6,09	5,05	2,80	4,61
K2O	5,16	3,36	2,36	0,03	0,61	0,97
MnO	0,02	0,06	0,04	-0,01	0,14	0,17
TiO2	0,19	0,31	0,32	0,14	1,34	1,63
P2O5	0,05	0,15	0,18	0,01	0,16	0,19
Cr2O3	-0,002	0,003	0,003	-0,002	-0,002	-0,002
TOT/C	0,12	0,04	-0,02	0,06	1,07	0,62
TOT/S	0,03	0,13	0,18	3,37	0,07	0,03
LOI	0,9	1,3	2,2	4,1	6,5	5,1
Cu (ppm)	30,7	27,5	5,3	6,5	29,8	110,8
Pb	13,3	2,5	1,4	4,2	1,0	0,7
Zn	12,0	57,0	58,0	3,0	91,0	141,0
Ag	0,3	-0,1	-0,1	0,2	-0,1	-0,1
Ni	7,8	7,3	6,2	2,5	5,9	7,1
Co	1,2	8,4	7,9	5,0	21,8	20,2
Mn						
Mo	0,2	0,6	-0,1	4,0	0,3	0,3
Fe						
As	0,8	0,6	0,5	1,0	0,5	-0,5
U	3,5	1,4	1,3	20,5	0,2	0,1
Au (ppb)	24,3	3,5	6,7	105,1	-100,0	5,1
Th (ppm)	9,9	3,3	3,7	31,9	0,5	0,7
Sr	113,2	280,3	300,5	621,3	138,4	101,7
Cd	-0,1	-0,1	-0,1	-0,1	-0,1	-0,1
Sb	0,1	0,1	-0,1	-0,1	-0,1	-0,1
Bi	0,6	-0,1	-0,1	1,9	-0,1	-0,1
V	25	79	91	11	325	378
Ca						
P						
La	37,5	20,0	18,0	40,3	4,9	4,7

Sample	WSC-000814	WSC-000815	WSC-000816	WSC-000818	WSC-000819	WSC-000820
Cr						
Mg						
Ba	377	1150	1171	4172	164	144
Ti						
Al						
Na						
K						
W	0,7	0,9	1,7	2,1	0,6	0,8
Zr	211,0	108,6	112,4	311,5	51,5	79,1
Ce	72,7	42,2	36,2	94,7	11,9	12,4
Sn	2	-1	-1	1	-1	-1
Y	12,3	15,5	16,6	37,2	13,1	19,4
Nb	15,6	5,5	5,7	46,1	3,0	4,1
Ta	0,6	0,4	0,4	2,5	0,1	0,2
Be	4	-1	-1	6	-1	1
Sc	1	7	8	2	31	37
Li						
S						
Rb	79,9	41,7	53,9	0,3	16,1	18,7
Hf	6,8	2,7	3,1	11,5	1,5	2,1
In						
Se	-0,5	-0,5	-0,5	3,0	-0,5	-0,5
Te	0,2	-0,2	-0,2	0,4	-0,2	-0,2
Cs	0,4	0,6	0,8	-0,1	0,6	0,6
Ga	20,0	12,3	15,6	16,3	14,2	16,6
Pr	7,88	5,36	4,60	12,78	1,58	1,92
Nd	26,6	21,3	18,8	46,5	7,3	9,4
Sm	4,04	4,34	3,99	8,85	1,79	2,85
Eu	1,06	0,95	1,00	2,50	0,72	1,09
Gd	2,96	3,47	3,48	7,60	2,19	3,32
Tb	0,37	0,50	0,53	1,13	0,38	0,58
Dy	1,80	2,84	2,99	5,81	2,42	3,55
Ho	0,32	0,54	0,57	1,01	0,46	0,68
Er	0,99	1,52	1,64	2,72	1,37	1,98
Tm	0,16	0,26	0,25	0,40	0,21	0,32
Yb	1,10	1,62	1,62	2,58	1,32	2,01
Lu	0,20	0,25	0,26	0,37	0,22	0,33

Résultats géochimiques des 26 échantillons pris sur toute la zone de cisaillement, zone par zone :

Zone	ZONE PRINCIPALE					ZONE 1					
Sample	WS-282-01	WS-282-03	WS-292-01	WS-302-01	WS-291-01	WS-10-38	WS-10-52	WS-11-111	WS-10-46	WS-11-83	WS-11-114
Au	2,92	2,7	5,03	3,29	2,51	1,75	2,77	1,78	1,23	3,06	1,98
Ag	0,93	0,73	1	1,1	1	3,5	5,1	4,1	4	3,2	4,8
C(t)	2,49	1,73	2,41	1,25	1,85	1,54	2,71	2,09	1,71	2,92	2,03
S(t)	0,79	0,73	0,99	1,13	1,73	2,93	2,29	2,17	2,91	4,54	2,02
SO4	0,1	0,1	0,1	0,2	0,1	0,2	0,2	0,2	0,2	1,3	0,1
Al	66900	74600	73000	73800	75600	65200	55700	69900	69800	63200	67400
Ba	165,33	223	214	161	219	363	176	340	195	196	257
Ca	63133,33	54666,67	56400	46700	54300	51900	53400	50500	53900	57200	53600
Cr	64,67	52,67	63	39	45	45	70	68	48	53	117
Cu	75,5	78,63	89,1	61	56,5	61,9	46,3	94	47,4	43,9	67,3
Fe	66200	59866,67	58900	68200	58200	55600	48100	44700	65100	68400	52500
K	15433,33	17133,33	16900	8830	20000	31500	35000	41600	19600	16100	29900
Mg	30800	23166,67	28700	23700	18000	15100	22000	24800	21700	19700	31000
Mn	1070	923,67	952	1050	868	1020	1080	985	1160	1510	865
Mo	-7	-7	-7	-7	-7	65	59	19	-7	-7	7,6
Na	19460	22733,33	23900	34500	26400	15900	15400	18000	34300	28600	14100
Ni	80,11	46,33	103	37	25	-20	48	55	32	28	77
P	560,33	640	606	644	783	595	374	313	562	892	520
Sr	134,67	107,1	141	101	99,1	136	155	160	217	241	156
Ti	6706,67	6263,33	5800	6840	6890	6060	4350	4170	5900	5790	4080
V	281	239,33	233	254	228	180	117	146	185	162	138
Y	16,57	21,42	15,2	14,6	16,4	10,7	8,5	6,9	12,6	13,1	10,8
Zn	74,67	85,66	76	90	72	60	46	52	61	51	46

Zone	ZONE 2								
Sample	WS-10-40	WS-11-75	WS-393-01	WS-10-50	WS-10-51	WS-11-62A	WS-11-71	WS-402-01	WS-403-01
Au	3,33	2,38	3,47	1,78	1,46	1,43	1,88	2,46	1,94
Ag	2,4	3,8	6	4,8	2,2	4,3	3,9	4,8	1,2
C(t)	2,57	2,61	2,69	2,1	2,14	1,42	2,46	2,55	1,5
S(t)	4,36	2,77	3,21	2,5	1,91	1,89	2,57	2,96	1,19
SO4	0,1	0,3	0,4	0,1	0,6	0,2	1	0,1	0,1
Al	67800	62200	61800	61100	67200	71000	66400	63400	71500
Ba	201	286	292	227	170	216	216	239	269
Ca	52100	54900	50200	67600	50200	53700	50500	44500	47400
Cr	26	53	38	29	24	29	34	33	38
Cu	142	87,8	71,6	88,1	78	96,8	87,3	82,2	81
Fe	63100	61600	56100	64000	60200	68900	65200	65900	64200
K	34000	23400	49900	28900	21700	17000	34100	30400	33300
Mg	21400	20400	19300	14900	18300	21400	19800	18900	22900
Mn	1300	1240	1060	1690	1160	1340	1390	1400	1090
Mo	28	15	-7	-7	25	-7	12	-7	12
Na	9370	22800	15600	16500	27700	31400	20100	23000	13700
Ni	28	34	21	-20	-20	-20	-20	-20	-20
P	735	574	669	486	623	955	664	609	656
Sr	138	212	169	121	180	199	244	110	138
Ti	7110	5220	6210	5640	6770	8220	6950	6430	6570
V	192	178	192	164	224	254	220	206	243
Y	12,1	5,3	5,8	15,4	10,8	17,3	14,3	13,7	13,1
Zn	55	48	62	56	67	71	67	69	77

Zone	ZONE 3					
Sample	WS-11-95	WS-11-120	WS-11-121	WS-11-106	WS-11-109A	WS-11-133
Au	3,17	1,97	3,09	1,75	1,6	1,9
Ag	0,5	0,6	0,7	0,6	0,7	0,7
C(t)	2,66	3,15	2,8	2,79	3,18	2,91
S(t)	1,08	1,02	1,11	0,87	0,4	1,31
SO4	0,9	1,1	0,2	0,1	0,1	0,1
Al	68000	71300	74200	73400	65800	71200
Ba	213	239	248	227	292	196
Ca	49900	59300	49400	46600	53800	50800
Cr	70	44	76	50	54	59
Cu	72	74,2	72,5	221	75	82,7
Fe	48000	51200	49600	52900	64300	58600
K	19400	23900	20200	19400	21000	20900
Mg	18300	20400	20400	20500	28300	18700
Mn	930	944	882	1100	1340	1020
Mo	-7	-7	-7	-7	-7	-7
Na	31400	18500	36400	34100	17900	25800
Ni	37	39	34	130	27	32
P	510	404	396	332	481	421
Sr	160	150	135	131	125	93,9
Ti	4360	3950	4370	4250	6250	4460
V	138	165	129	172	236	143
Y	18,9	11,9	13,6	14,2	14	17,5
Zn	50	66	58	55	107	61

APPENDICE B

ANALYSES LA-ICP-MS DES PYRITES DU GISEMENT DE WASAMAC

Introduction

L'observation récente de l'assimilation de l'or dans la structure cristallographique des sulfures a été une découverte capitale dans la compréhension des contrôles des minéralisations aurifères. L'avènement de techniques d'observation à l'échelle microscopique et nanoscopique telles que le LA-ICP-MS a permis entre-autres, de déterminer l'origine de l'or dans les contextes de minéralisations associées à des sédiments (Large et al., 2007, 2009). Bien que dans le cas des gites d'or orogéniques ou de ceux spatialement associés aux intrusions alcalines ces techniques n'apportent pas de réponse au sujet de la source de l'or, elles permettent de contraindre avec précision les caractéristiques responsables du transport et du dépôt de l'or.

A Wasamac, l'or étant toujours étroitement associé à la pyrite, unique sulfure présent, la cartographie de ce sulfure permettra de mieux caractériser les contrôles de la minéralisation.

Le but de ces analyses est de remarquer d'éventuelles zonations ou surcroissances au sein des pyrites et d'identifier quels éléments traces y sont associés. Aussi, plusieurs zones présentant des inclusions d'or natif ou de tellurures d'or ont été analysées afin de mieux les caractériser, tout comme certaines anomalies en métaux de base identifiées précédemment au MEB. Ces analyses LA-ICP-MS des sulfures sont les seules effectuées le long du corridor Francoeur-Wasa. La distinction de zonations des sulfures et la détermination de leur chimie sont capitaux dans la compréhension du gisement, ainsi que dans la compréhension régionale des minéralisations aurifères orogéniques archéennes.

Méthode

Les analyses LA-ICPMS suivantes ont été effectuées à l'Université du Québec à Chicoutimi par Sadia Mehdi, au laboratoire LabMaTer dirigé par Dany Savard. L'ablation laser fut effectuée avec un M50 Resolution Excimer utilisant un rayon UV de 193nm de longueur d'onde. La matière vaporisée fut transportée par de l'Helium à l'état gazeux puis ionisée par plasma-Ar à 6000°K afin d'être analysée par un ICP-MS 7700x Agilent. La création des cartes fut permise par l'ablation laser de séries de lignes constituées d'ablations ponctuelles successives de 15µm de diamètre. 26 éléments ont été analysés: Fe, S, Cu, Ti, Au, Ag, Te, Pb, Bi, Mo, Ni, Co, Zn, Hg, V, Pt, Cr, Mn, As, W, Ba, Sn, Sb, U, Se, Tl. Chaque ablation représente un pixel constituant la carte finale pour chaque élément. Le seuil de détéction de l'or est fixé à 30 ppb. Au total, 13 cartographies de pyrites ont été entreprises (de 100 à 300 µm de côté) parmi les deux faciès d'altération au sein des Zones Principale et 2. Les 13 pyrites cartographiées ont toutes présenté des résultats au dessus du seuil de détection. Cinq standarts ont été analysés avant et après chaque série de points afin de corriger le signal (GSD, GSE, LAFLAME, MASS1 et MSS5)

Les logiciels IgorPro et Iolite ont été utilisés pour le traitement des cartes. Ces logiciels permettent la manipulation des données voltaïques transmises par l'ICP-MS et leur traduction en données qualitatives et quantitatives pour chaque élément analysé.

Objectif

Plusieurs objectifs ont été visés par ces analyses et sont dirigés par les questions suivantes :

→ Les pyrites des deux faciès d'altération sont-elles aussi riches en or ?

→ A quelle(s) composition(s) chimique(s) anomalique(s) de la pyrite s'associe l'or ?

→ Existe t'il des similitudes de chimie des pyrites entre les deux faciès d'altération ?

→ Quelles conclusions pouvons nous tirer quant à la cristallisation de l'or pour chacun des faciès : dans quelles conditions chimiques l'or a t'il précipité ?

→ Quelle est la chimie des inclusions d'or ? Quelle est celle du remplissage minéralisé des fractures ? Existe t'il une proportion d'or invisible et si oui quels éléments y sont associés ? L'or natif libre est-il associé à d'autres éléments chimiques ?

→ Quels liens peut-on faire avec les observations MEB et optique ?

→ Cette/ces phase(s) concorde t'elle avec celles identifiées proche des syénites aurifères ?

→ Qu'est ce que cette étude permet d'apporter au modèle géodynamique final ?

Résultats

Au total, 13 cartographies de pyrites ont été entreprises: 8 dans des pyrites de la Zone Principale (faciès de minéralisation associé à l'altération albitique) et 5 dans des pyrites de la Zone 2 (faciès de minéralisation associé à l'altération potassique). Sur les 8 cartes effectuées de la Zone Principale, quatre ont été retenues pour leur qualité et leur taille (cartes 1, 8, 12 et 13). Sur les cinq cartes de la Zone 2, deux ont été retenues (cartes 2 et 10). Les cartes non conservées traitent des pyrites de trop

petite taille pour remarquer des zonations claires ou présentent des informations redondantes à d'autres cartes. Tous les cartes sont disponibles sur demande à l'auteur : meriaud.nicolas@gmail.com.

Echantillon	Forage	Zone	Carte LA-ICPMS	Prof. Inf.	Prof. Sup.	Détail lithologique et des altérations	teneur	Proximité avec la faille
WSC 45455*	WS-10-37	2	2	541,2	541,44	CWS dans rhyolite à bonne teneur en or, forte présence de pyrite disséminée (10%), mais altération uniquement en albite,sericite et silice pervasifs.	3,74 g/t	CWS
WSC 45463*	WS-289-01	Principale	12 et 13	563,39	563,95	Dyke felsique altéré en albite et chlorite, minéralisé en pyrite fine 5 à 7 % et en VG, et fracturé au sein d'une andésite; sous le CWS ; mais passe décrite comme une reprise du CWS dans Gems Log	39	Reprise de CWS supposé (38m sous vrai CWS)
WSC 45467*	WS-11-72	Principale	8	504,35	504,75	Unité gris-vert-violacé, structure bréchique clastes aux contours corrodés. Pyrite disséminée et en amas parfois lités (présence à 3 - 4%). Très riche en Au. Veine de qtz-carbonates mm tardives. Altération en microcline, albite, chlorite, carbonates.	28,32	CWS
WSC 45469*	WS-11-69	2	10	328,4	329	Coeur d'un dyke rouge-violacé assez vif encaissé dans une andésite peu/pas cisaillée. Forte altération potassique, alération en carbonates et chlorite dans les fractures avec pyrite + concentrée également. Py micro-mm disséminée dans les clastes/unité rouge vif. La structure bréchique du "dyke" passe à fracturée puis massive vers le coeur du supposé dyke.	3 à 6	45m au dessus de CWS
WSC 45476	WS-284-02	Principale	1	634	634,33	Brèche tecto comportant des clastes beige-rouge mm à cm étirés dans la déformation, matrice chloriteuse, minéralisée en py amassée préférentiellement au contact des clastes.	N.A.	26m sous le CWS

Figure 1. Tableau des descriptions lithologiques de forage des échantillons choisis pour la cartographie LA-ICP-MS. La profondeur inf et sup est en m. CWS = cisaillement Wasamac (Zone minéralisée).

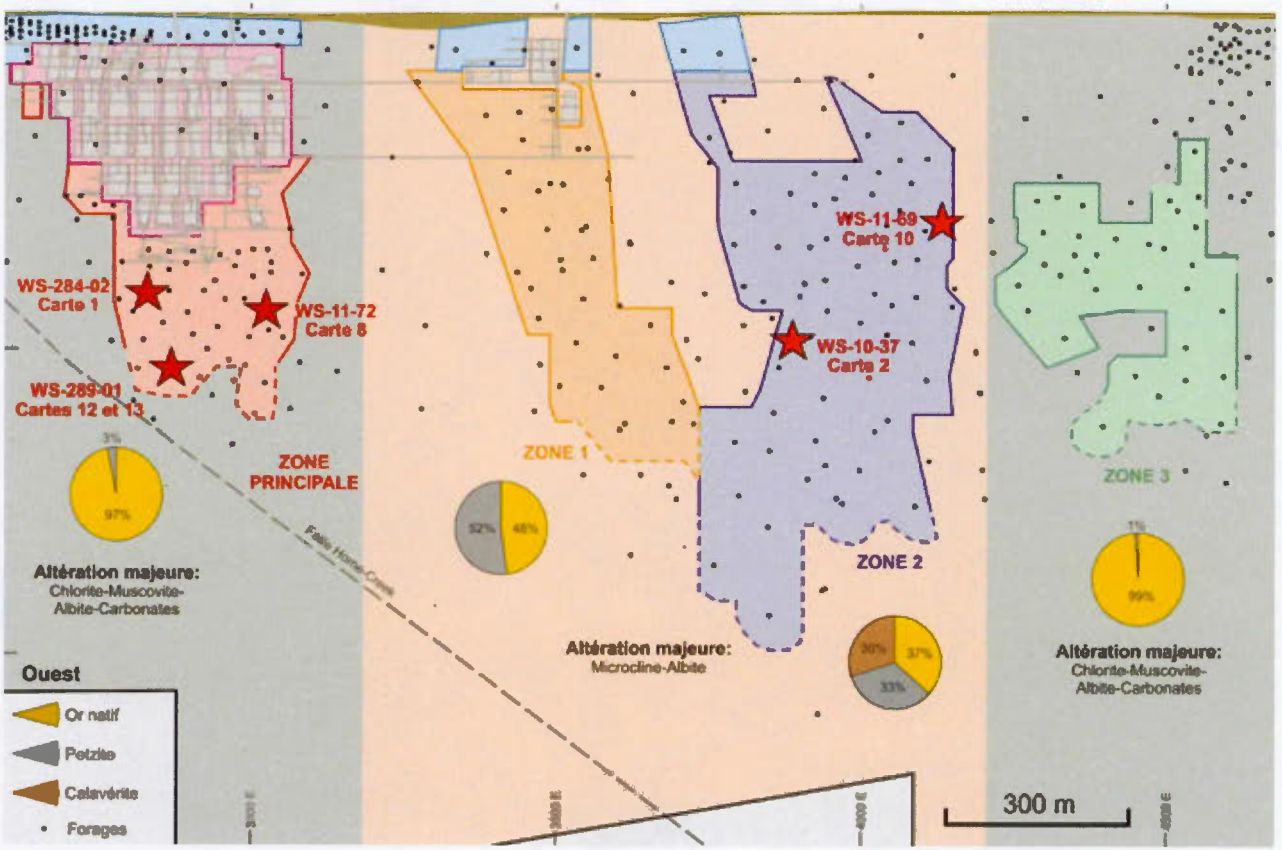

Figure 2. Localisation des pyrites cartographiées au LA-ICP-MS sur la longitudinale E-W de la propriété Wasamac. Noter les Zones Principales et 2 associées à deux couleurs: le vert correspond au faciès d'altération albitique et le rosé correspond au faciès d'altération potassique.

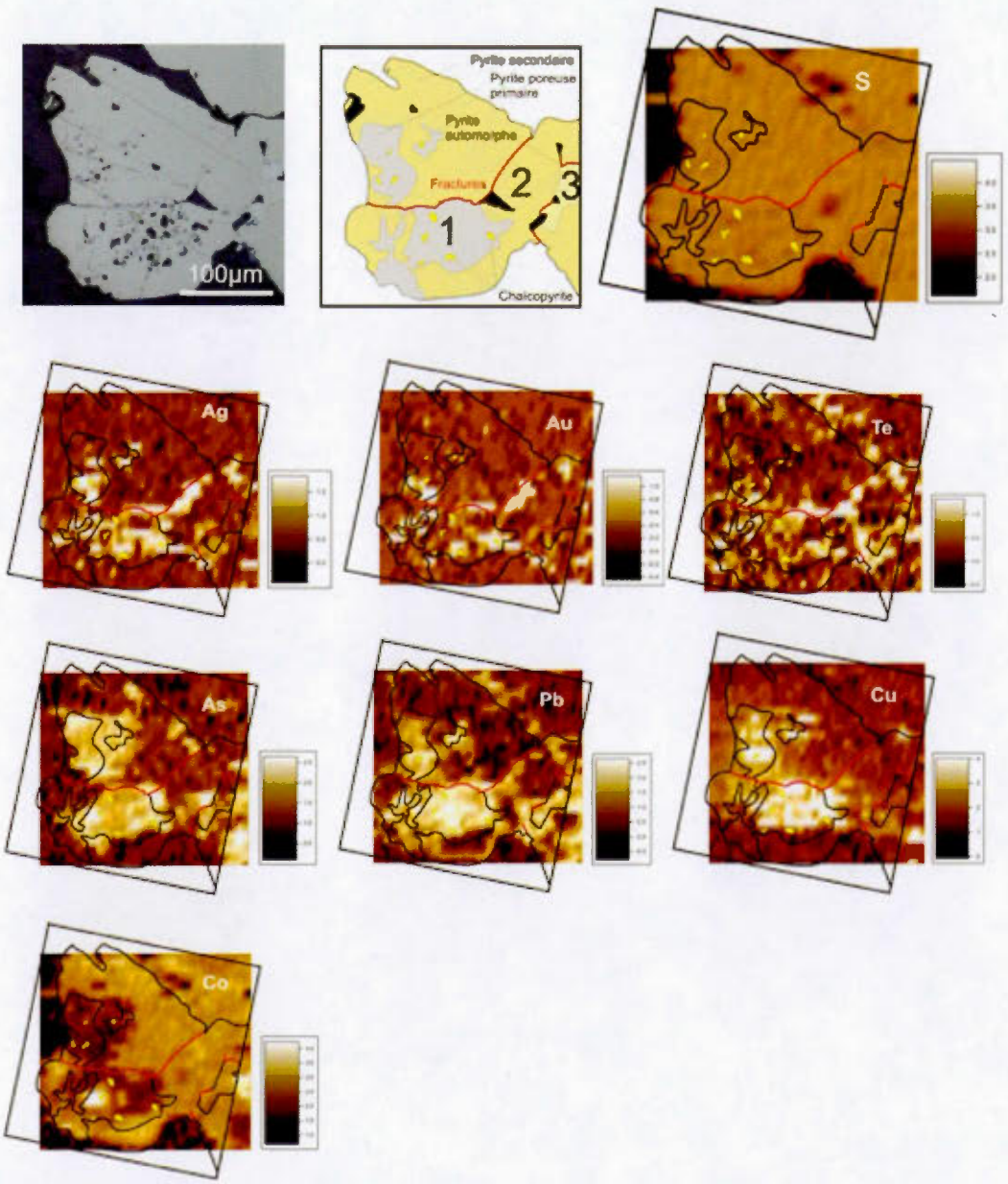

Figure 3. Carte 1, échantillon WSC-45476, forage WS-284-02, Zone Principale. Présentation d'une photographie en microscopie optique en lumière réfléchie, puis d'une représentation schématique des caractéristiques principales puis les cartographies de plusieurs éléments. Echelles en log(10) ppm.

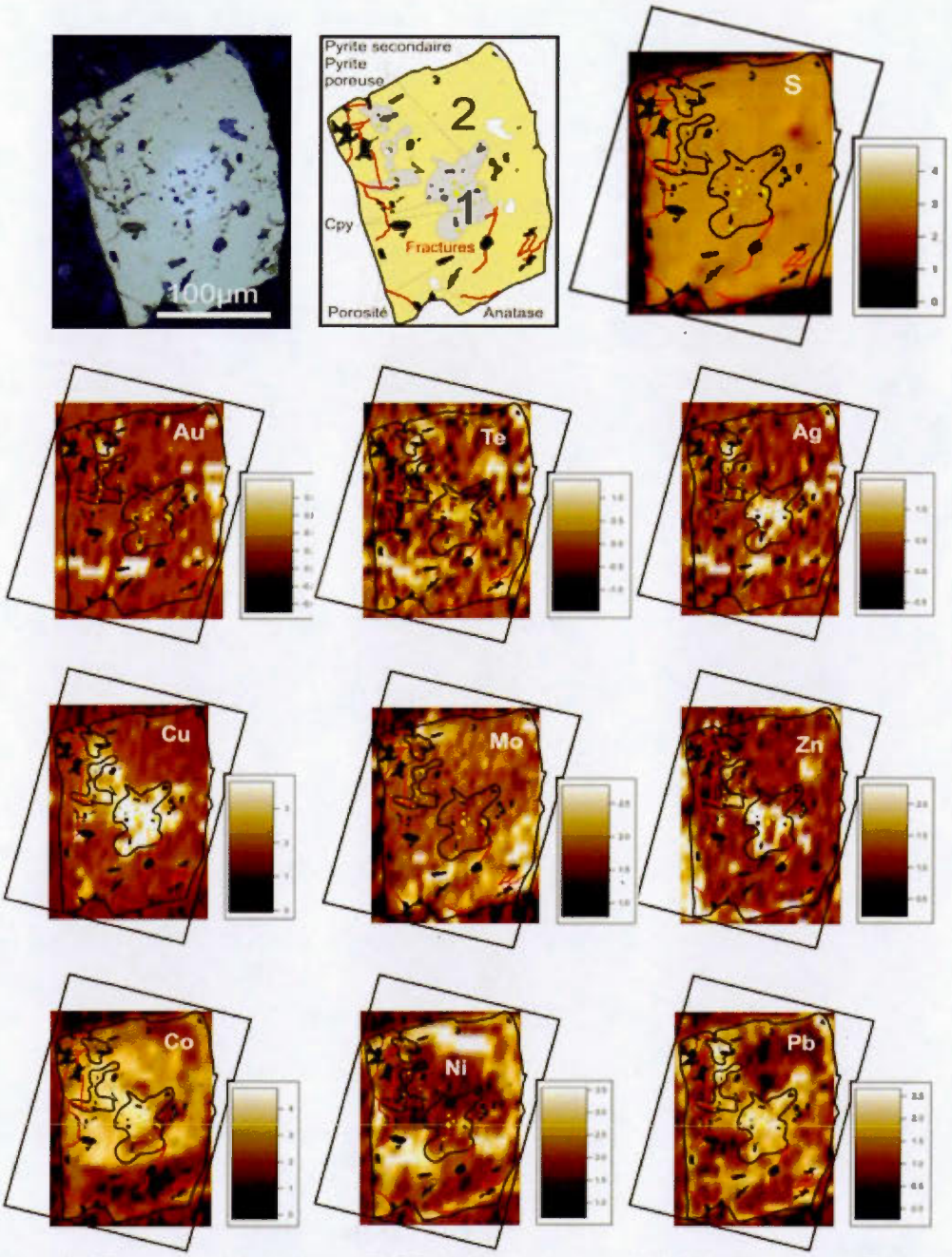

Figure 4. Carte 8, échantillon WSC-45467, forage WS-11-72, Zone Principale. Présentation d'une photographie en microscopie optique en lumière réfléchie, puis d'une représentation schématique des caractéristiques principales puis les cartographies de plusieurs éléments. Echelles en log(10) ppm.

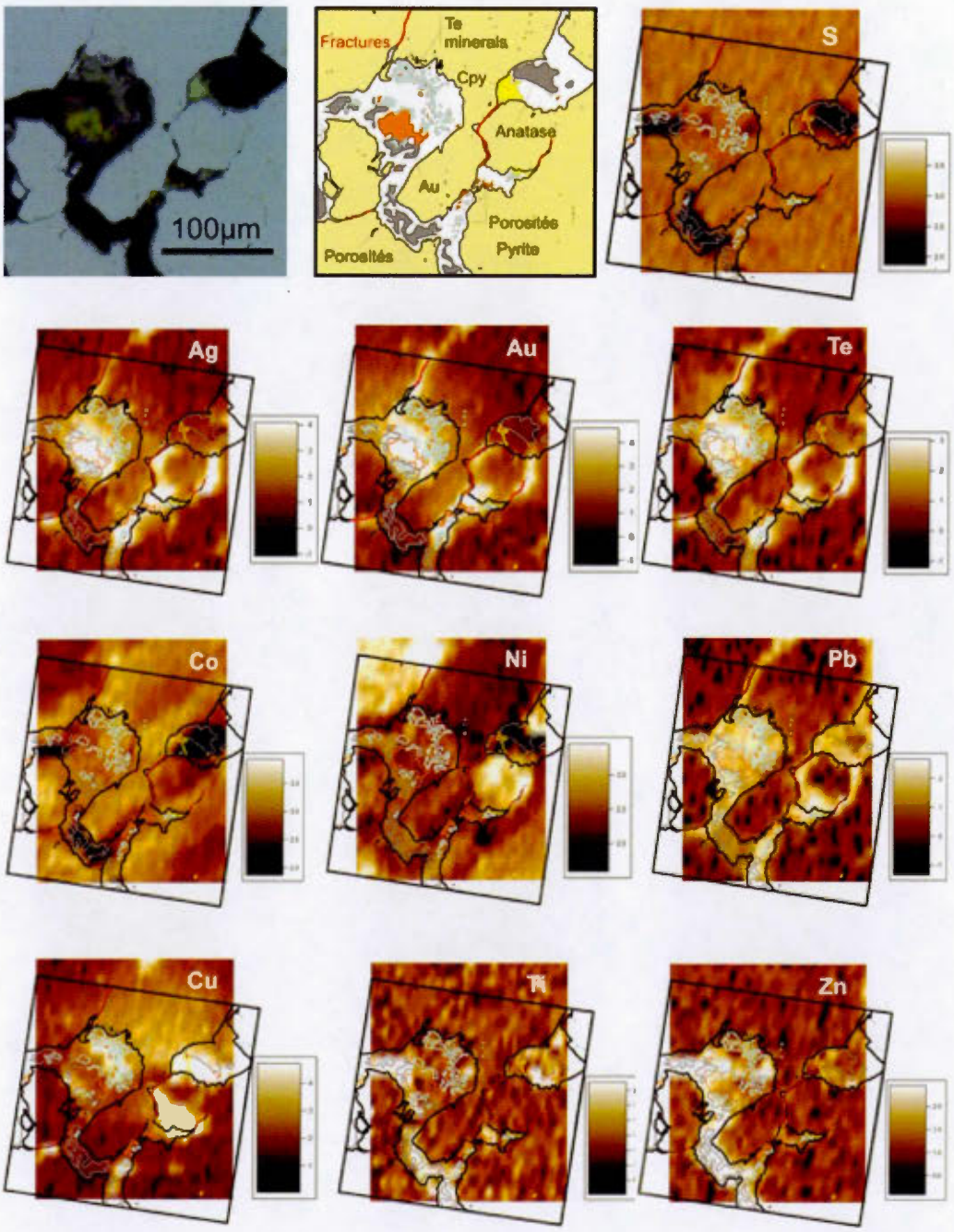

Figure 5. Carte 12, échantillon WS-45463, forage WS-289-01, Zone Principale. Présentation d'une photographie en microscopie optique en lumière réfléchie, puis d'une représentation schématique des caractéristiques principales puis les cartographies de plusieurs éléments. Echelles en log(10) ppm.

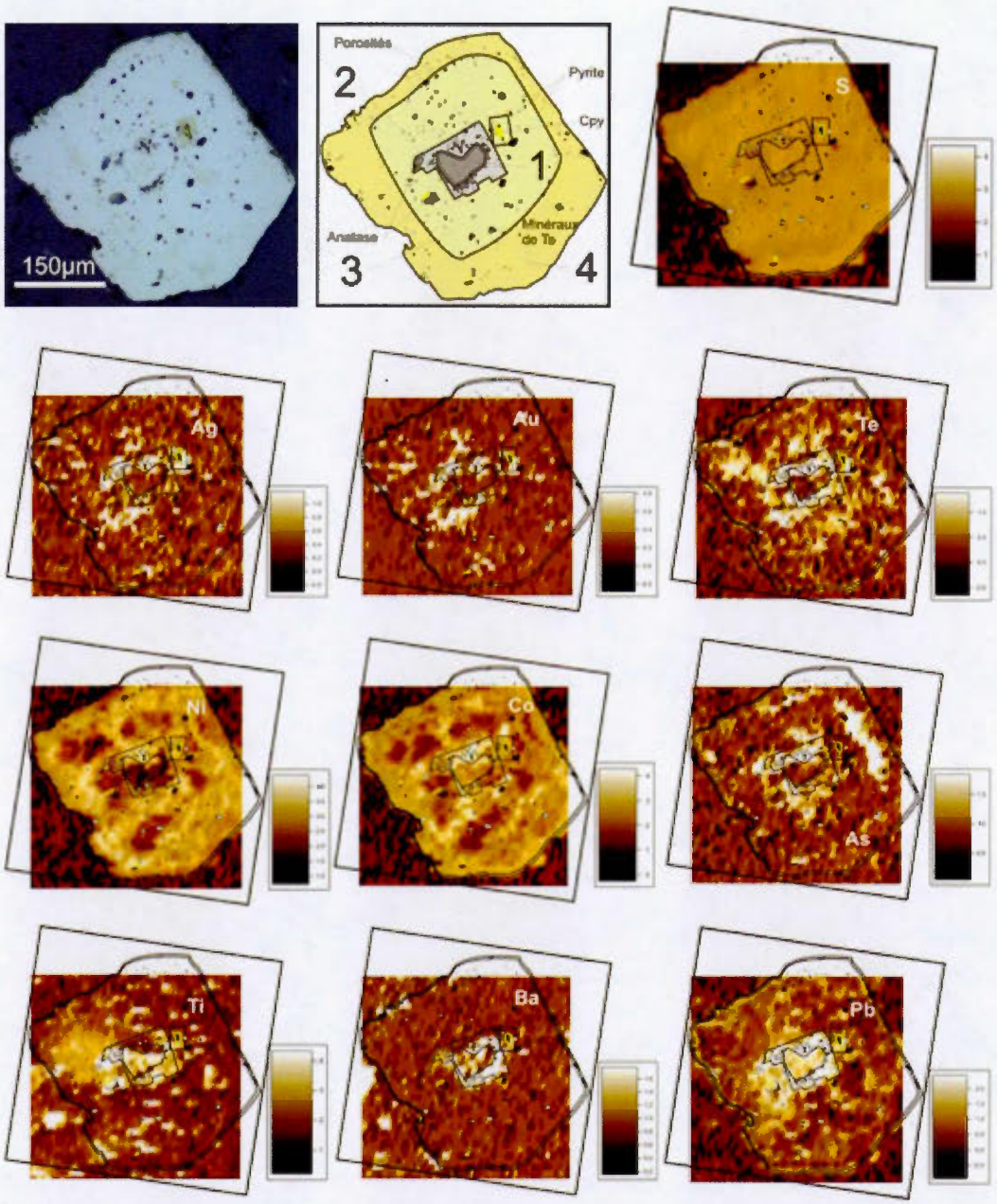

Figure 6. Carte 13, échantillon WS-45463, Forage, WS-289-01, Zone Principale. Présentation d'une photographie en microscopie optique en lumière réfléchie, puis d'une représentation schématique des caractéristiques principales puis les cartographies de plusieurs éléments. Echelles en log(10) ppm.

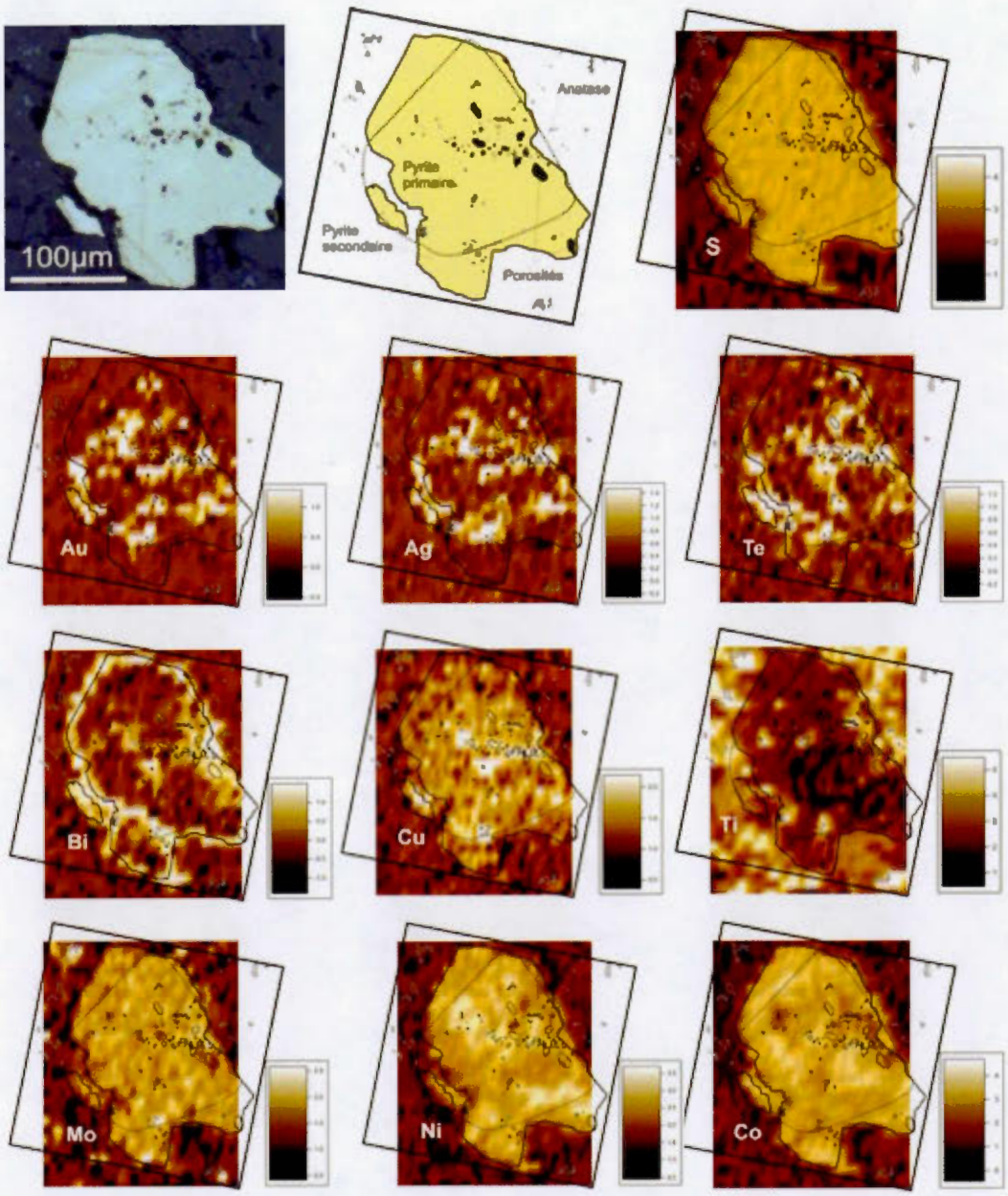

Figure 7. Carte 2, échantillon WS-45470, forage WS-10-37, Zone 2. Présentation d'une photographie en microscopie optique en lumière réfléchie, puis d'une représentation schématique des caractéristiques principales puis les cartographies de plusieurs éléments. Echelles en log(10) ppm.

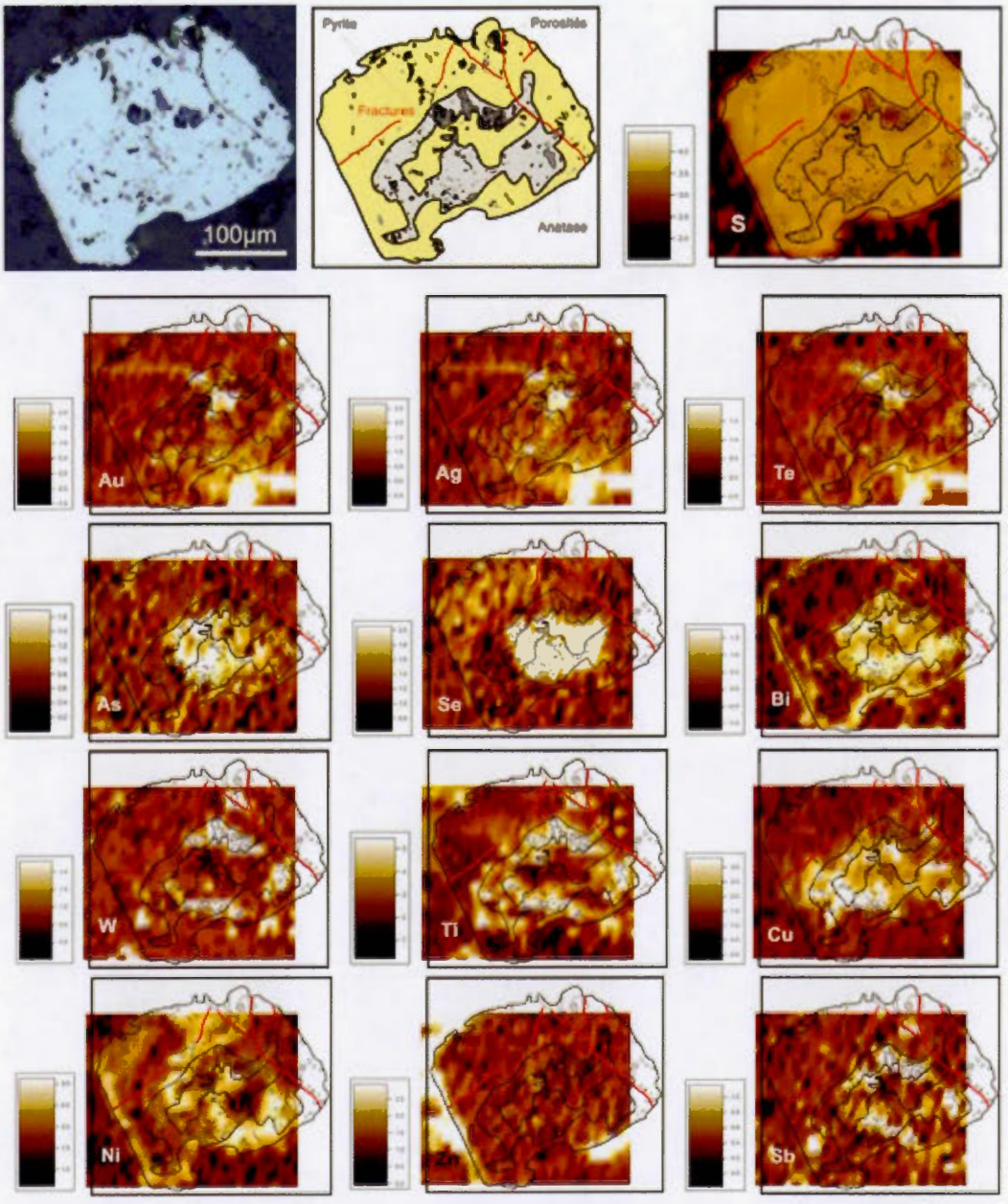

Figure 8. Carte10, échantillon WS-45469, forage WS-11-69, Zone 1. Présentation d'une photographie en microscopie optique en lumière réfléchie, puis d'une représentation schématique des caractéristiques principales puis les cartographies de plusieurs éléments. Echelles en log(10) ppm.

Carte 1 : Les cartographies permettent de mettre en avant 3 phases de pyritisation tant dans la texture que dans les associations chimiques de chaque. On distingue :

- Une pyrite précoce, xénomorphe et très poreuse. Cette pyrite contient de nombreuses inclusions de chalcopyrite et quelques autres plus rares d'hématite. La chimie de cette pyrite primaire comprend les éléments : As, Pb, Bi, Cu, Ag et est pauvre en Co et Ni. La minéralisation est associée en partie à cette phase.
- Une pyrite toujours xénomorphe à sub-automorphe, sans inclusions et à rares porosités cependant plus grossières. Cette phase est relativement plus riche en Co et Ni comparativement à la pyrite primaire, mais ne présente pas d'anomalie chimique caractéristique. Aucune minéralisation ne semble associée à cette phase.
- Une phase tardive automorphe, légèrement plus réfléchissante sans anomalie chimique à l'exception d'un léger excès en plomb et bismuth. Aucune minéralisation ne semble associée à cette phase.
- Une phase non sulfurée mais associée à la fracturation de la pyrite enrichie en Au, Ag, Te principalement, ainsi qu'en Pb et Bi.

→ La phase minéralisée semble ici seulement associée à la pyrite primaire poreuse puis à un phénomène tardif d'origine tectonique.

Carte 8 : Deux phases de pyritisation sont identifiables d'après la photo, cependant 3 phases semblent se distinguer sur les cartes LA-ICP-MS.

- Une pyrite poreuse, primaire, identifiable sur la photo est premièrement enrichie en métaux de base (Pb, Bi, Zn, Cu) ainsi qu'en argent. Aucune concentration anormale en Au, Te, Mo ou As n'y est identifiée.

- Une deuxième pyrite entourant la première présente un pic en cobalt est associé à une faible concentration en Ni. L'or semble lié à cette phase, cependant il paraît associé à une porosité où des pics en Mo et Ag +/- Te sont observés. Les anomalies en or de cette phase peuvent également être interprétées comme associées à la couronne extérieure de cette pyrite.
- Une troisième phase pyriteuse sans particularité chimique notoire peut être sous entendue, à l'exception d'un léger enrichissement en Mo. Aucune minéralisation ne semble liée à cette phase.

→ La phase minéralisée semble ici associée à la pyrite 2, riche en Co mais sans anomalies particulières.

Carte 12 : Cartographie d'une pyrite fracturée, où les analyses MEB ont montré des concentrations locales importantes en Au, Ag et Au.

- La pyrite ne présente pas d'anomalie élémentaire particulière, et aucune minéralisation. On note que les zones riches en Ni sont pauvres en Co et inversement.
- Les fracturations sont quant à elles très riches en Au, Te et Ag. Les passes plus larges de fracturation présentent de l'anatase (Ti) associé à une anomalie en Vanadium. Les fractures présentent également des anomalies en Pb, Bi, Zn, Cu, Sb, Pt et Hg. Ces caractéristiques ont également été identifiées sur la carte 11.

→ La phase minéralisée semble ici seulement associée à un phénomène tardif d'origine tectonique. Le détail de l'organisation de la minéralisation dans la fracture est détaillée sur la cartographie en éléments Figure 9.

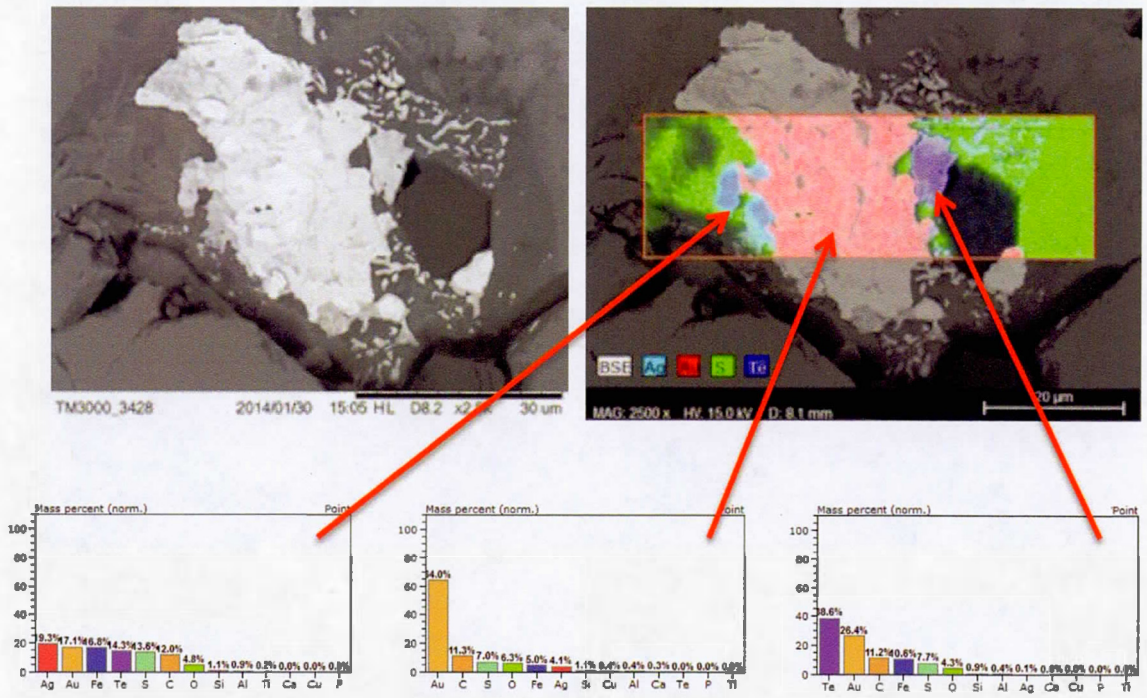

Figure 9. Photoghraphie MEB et cartographie qualitative des éléments de minéralisation. Valeurs semi-quantitatives de chaque zone représentée par les diagrammes figurant plusieurs éléments en %.

Carte 13 : Pyrite sub-automorphe de taille plus grossière que les précédentes. Ici plusieurs zonations semblent apparaître sur la photographie, principalement par l'organisation et par la concentration des porosités.

- Pyrite primaire peu poreuse, xénomorphe seulement riche en Ti et Pb. Ne semble pas minéralisée.
- Pyrite secondaire très poreuse enrichie en Te, As, Pb, Bi, Zn, Ba, Ti et paraissant anomalique en Au, Ag. Cette pyrite est automorphe. Cette phase semble minéralisée.

- Une troisième pyrite appauvrie en Co et Ni semblant présenter une couronne arséniée. Localement poreuse et présentant des anomalies supposées en Au, Ag et Te. Phase minéralisée ?
- Une quatrième pyrite peut être sous entendue mais reste similaire à la troisième, sans anomalie particulière à l'exception d'une couronne externe riche en Pb, Bi, Zn, +/- Te.

→ La phase minéralisée paraît être associée à la pyrite poreuse primaire, les anomalies en or non associées à cette phase lui sont contiguës donc associées à une seule phase primaire.

Remarquer sur la figure 10 les textures des phases successives de pyrite : une pyrite primaire peu poreuse et xénomorphe, une pyrite secondaire poreuse et automorphe, une deux ou trois phases de pyritisation à rextures similaires sub-automorphes à automorphes. Noter sur la photo 3 le grain de calavérite localisé sur le bord d'une inclusion de chalcopyrite au sein de l'une des pyrites de 3^{e} phase.

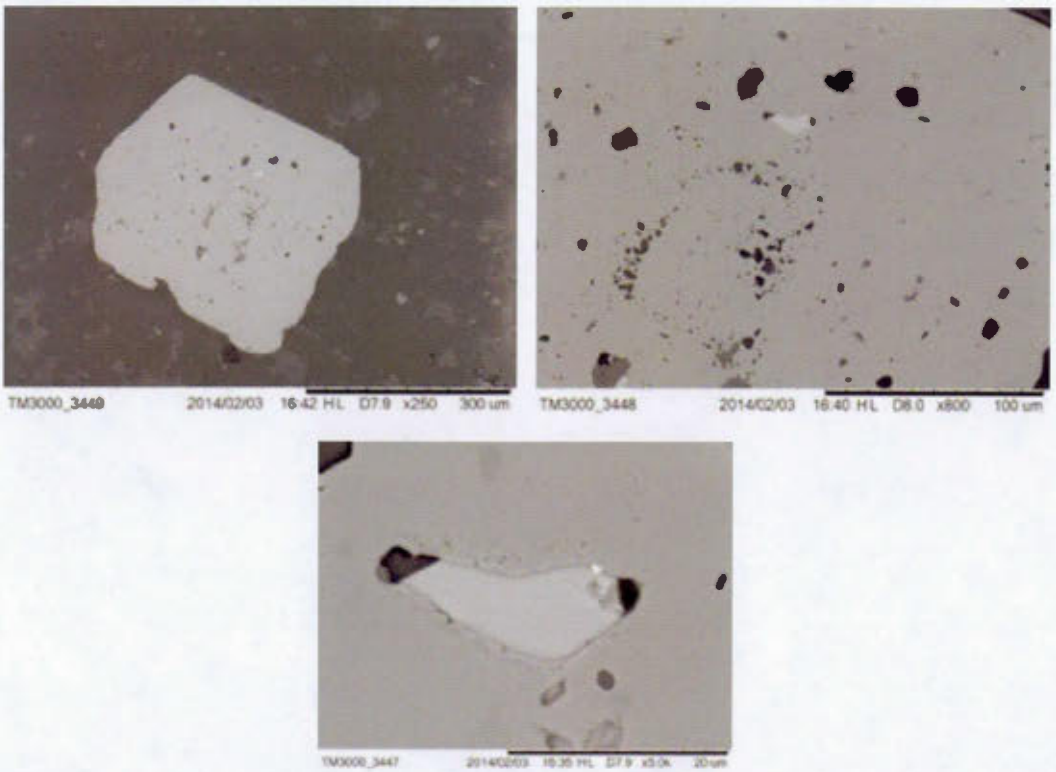

Figure 10. Photographies MEB de la carte 13, détails des textures et des inclusions des différentes phases. Zoom sur un remplissage de porosité en chalcopyrite et calavérite.

Carte 2 : La photographie présente une pyrite en partie poreuse et principalement « fraîche ». Les cartographies ne semblent cependant pas suivre la tendance de ces deux groupes :

- Une pyrite primaire formée de deux ou trois petites pyrites agglomérées peut être sous-entendue selon l'organisation du tellure principalement. L'or et l'argent suivent l'organisation spatiale du tellure, ce qui laisse penser à de la petzite vraisemblablement infra-micrométrique, ou invisble. En effet la texture poreuse de la pyrite ne suit pas l'organisation en couronne des inclusions de petzite.
- Une pyrite secondaire pauvre en éléments et non minéralisée.

- Une couronne externe est riche en Pb et Bi.

→ L'ensemble de la pyrite est généralement riche en Cu, mais la minéralisation se concentre à deux ou trois auréoles au sein de la pyrite, représentant possiblement la trace externe de pyrites primaires minéralisées.

Carte 10 : La pyrite analysée est généralement très poreuse, et présente des inclusions de près de 10µm de sphène. Un noyau pyriteux peu poreux semble être entouré d'une pyrite poreuse secondaire puis d'une troisième pyrite peu poreuse.

- La pyrite primaire peu poreuse semble présenter un point très riche en or au contact avec la pyrite poreuse secondaire, il s'agit d'une inclusion. Elle est enrichie en As, Se, Bi et Cu.
- La pyrite secondaire poreuse, est possiblement enrichie en Au, Ag et Te. Elle présente des anomalies en Ti, Bi, Pb et ainsi que des anomalies non communes à Wasamac en W et Sb.

→ La troisième phase pyriteuse peu poreuse est pauvre en éléments, mais présente une auréole tardive riche en Bi et Pb.

Discussion

Seules de petites pyrites ont été analysées, on peut alors supposer que plus de zonations existent, cependant une phase pyriteuse aurifère a été identifiée validant l'apport d'or via un fluide sulfuré, piégeant l'or par cristallisation des pyrites.
La variabilité des textures des pyrites en général et leur très petite taille rend la distinction des phases aurifères et la description de chaque difficile. Cependant l'outil LA-ICP-MS s'est révélé de grande aide pour la caractérisation de chaque phase de pyritisation.

Conclusion

Les pyrites des zones Principale et 2 présentent des zonations similaires associées à 2 à 4 phases de sulfuration dont une précocre aurifère.

Deux phases de minéralisation sont identifiés : une première d'origine chimique dans les pyrites, une deuxième d'origine tectonique. L'absence d'apport en éléments chimiques typique des contextes sédimentaires (As +/- Sb) décrite dans Large et al. (2009) va dans le sens de l'hypothèse d'un métasomatisme d'origine magmatique ou métamorphique. Le peu de teneur des pyrites en éléments mafiques tel que Cr ou Ni corroborent l'absence d'un métasomatisme d'origine mafique ou ultramafique tel que celui du groupe de Piché observé le long de la Faille Cadillac, l'absence de fuschite corrobore également cette interprétation. La richesse en Ag et Te des pyrites aurifères ainsi que l'apport en Co, Ni, Cu, Pb et Bi associé va dans le sens d'une origine syénitique du métasomatisme. En effet, l'article de Cook et al. 2009, montre un contexte chimique et textural des pyrites aurifères identique à Wasamac ainsi qu'un contexte métasomatique similaire. L'absence de Mo dans les pyrites est relevé dans les deux contextes, cependant il apparaît très anomalique dans l'assemblage des minéraux d'altérations.

Le contrôle de la minéralisation à Wasamac semble donc être double et diachrone. La mise en place ou la réactivation de la structure profonde Francoeur-Wasa permet un maintient de la porosité et le passage de fluides. Ces fluides ont participé à la cristallisation de minéraux métasomatiques différentiés en deux types (potassique et albitique), ainsi qu'à la cristallisation de plusieurs phases de pyrite dont une précoce minéralisée. Un premier contrôle d'ordre chimique est donc à prévaloir. Le deuxième type de cristallisation de l'or, natif, est très fréquent au sein de fractures larges dans les pyrites et libre dans la gangue. Ce type de minéralisation comprenant la libération de l'or du système cristallin de la pyrite et sa purification est de contrôle

tectonique, dans un contexte cassant où la pyrite est fracturée ou localement cataclasée. La pyrite poreuse peut localement ne pas contenir d'or mais en présenter proche: en inclusions dans la pyrite en surcroissance, au niveau de fractures ou natif dans la gangue métasomatique. En majorité l'or est associé à cette phase précoce de pyritisation où l'or semble principalement invisible. Aucune autre anomalie chimique ne suit précisément les anomalies Au, Ag et Te. L'or associé aux fractures est quant à lui accompagné d'anomalies en Te, Ag, Bi, Pb, Ti, Zn, et Cu. Les associations métalliques montrent également de forts liens entre Bi et Pb, Ti et V +/- Sb. Aussi, Co et Ni sont souvent inversement relatifs dans les phases pyriteuses peuvres en éléments. Un tableau et un schéma résument les observations Figure 11.

	Temps ---------->				
	Pyrite 1	**Pyrite 2**	**Pyrite 3**	**Pyrite 4**	**Fracturation**
Texture	Pyrite peu poreuse, généralement xénomorphe	Très poreuse et finement incluse de minéraux à Ti, Fe et/ou Cu.	Peu poreuse, incluse de minéraux de Ti, Fe et/ou Cu en inclusions plus grossières que la pyrite 1 en général, Au rare mais possible	Idem pyrite 3, souvent non discernables. Phase tardive de "plaquage" en Pb, Bi, +/- Ni, Te, Co, Ti	Fines à largement ouvertes. La chimie varie de strictement Au, Ag, Te, Pb, Bi pour les fines fractures à addition de Ti, Zn, Pt et Hg pour les larges fractures.
Forme	xénomorphe	Sub-automorphe à auromorphe	Sub-automorphe à automorphe	Sub-automorphe	Irrégulier
Éléments enrichis	Pauvre en éléments, peut contenir des traces de As, Se, Bi, Ba, Ti, V. **Au supposé mais observé rarement.**	Cu, Zn, Pb, Bi, Co, Ag, Au +/- As **Phase minéralisée et riche en éléments**	**Pas d'anomalie chimique particulière**, les pyrites sont parfois localement plus ou moins riches en Co et Ni, parfois présentant des **inclusions d'Au, Ag et Te locales**, vraisemblablement suite à un "recyclage" en ces éléments de la pyrite 2. Leur coronnes respectives sont parfois enrichies en Pb, Bi, As, Ni, Zn.		Cu, Zn, Pb, Bi, Au, Ag, Te +/- Ti

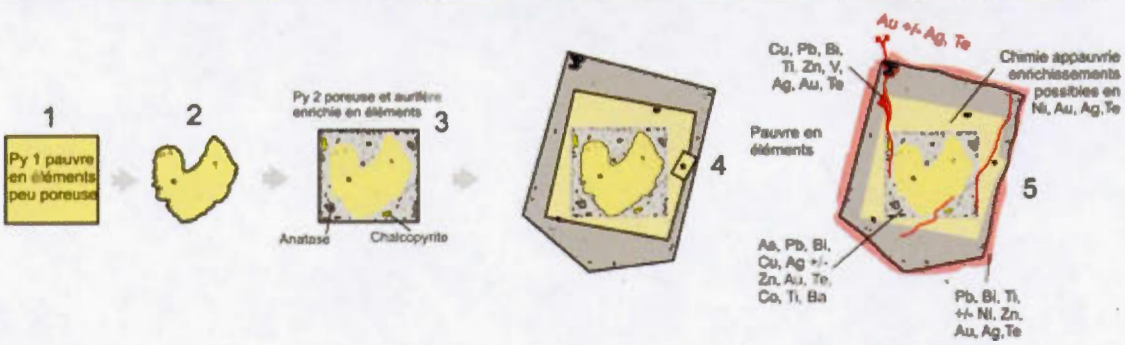

Figure 11. Tableau résumé des phases pyriteuses observées et modèle paragénétique associé.

BIBLIOGRAPHIE GÉNÉRALE

Ayer, J.A., Thurston, P.C., Bateman, R., Dubé, B., Gibson, H.L., Hamilton, M.A., Hathway, B., Hocker, S.M., Houlé, M.G., Hudak, G., Ispolatov, V.O., Lafrance, B., Lesher, C.M., MacDonald, P.J., Péloquin, A.S., Piercey, S.J., Reed, L.E. & Thompson, P.H., 2005. Overview of results from the Greenstone Architecture Project : Discover Abitibi Initiative. Ontario Geological Survey ; Open File Report 6154, 146p.

Beakhouse, G.P., 2011. The Abitibi Subprovince plutonic record : Tectonic and metallogenic implications. Ontario Geological Survey ; Open File Report 6268, 161p.

Bigot, L., & Jébrak, M., 2015. Gold Mineralization at the Syenite-Hosted Beattie Gold Deposit, Duparquet, Neoarchean Abitibi Belt, Canada. Economic Geology, v.110 (2), p.315-335.

Bonnemaison, M., & Marcoux, E., 1990. Auriferous mineralization in some shear-zones: A three-stage model of metallogenesis. Mineralium Deposita, v.25 (2), p.96-104.

Cabri, L.J., Chryssoulis, S.L., de Villiers, J.P., Laflamme, J.G., & Buseck, P.R., 1989. The nature of "invisible" gold in arsenopyrite. The Canadian Mineralogist, v.27 (3), p.353-362.

Cameron, E.M., & K. Hattori, (1987). Archean gold mineralization and oxidized hydrothermal fluids. Economic Geology and the Bulletin of the Society of Economic Geologists, v.82 (5), p.1177-1191.

Colvine, A.C., Fyon, J.A., Heather, K.B., Marmont, S., Smith, P.M., & Troop, D.G., 1988. Archean Lode Gold Deposits in Ontario; Ontario Geological Survey ; Miscellaneous Paper v.139, 136p.

Cook, N.J., & Chryssoulis, S.L., 1990. Concentrations of invisible gold in the common sulfides. The Canadian Mineralogist, v.28 (1), p.1-16.

Cook, N.J., Ciobanu, C.L., & Mao, J., 2009. Textural control on gold distribution in As-free pyrite from the Dongping, Huangtuliang and Hougou gold deposits,

North China craton (Hebei Province, China): Chemical Geology, v.264, p.101-121.

Corfu, F., Krogh, T.E., Kwok, Y.Y., & Jensen, L.S., 1989. U-Pb zircon geochronology in the SouthWestern Abitibi greenstone belt, Superior Province. Canadian Journal of Earth Sciences, v.26 (9), p.1747-1763.

Couture, J.F., & Pilote, P., 1993. The geology and alteration patterns of a disseminated, shear zone-hosted mesothermal gold deposit ; the Francoeur 3 Deposit, Rouyn-Noranda, Quebec. Economic Geology, v.88 (6), p.1664-1684.

Couture, J.F., & Pilote, P., 1994. Gîtologie des gisements d'or du district de Rouyn-Noranda : études récentes. Ministère de l'Énergie et des Ressources, Québec ; DV 92-07, 143p.

Daigneault, R., & Mueller, W.U., & Chown, E.H., 2002. Oblique Archean subduction: accretion and exhumation of an oceanic arc during dextral transpression, Southern Volcanic Zone, Abitibi Subprovince Canada. Precambrian Research, v.115 (1), p.261-290.

Daigneault, R., Mueller, W.U., & Chown, E.H., 2004. Abitibi greenstone belt plate tectonics: the diachronous history of arc development, accretion and collision. Developments in Precambrian Geology, The Precambrian Earth : Tempos and events. v.12, p.88-103.

Dube, B., & Gosselin, P., 2007. Greenstone-hosted quartz-carbonate vein deposits. Mineral Deposits of Canada: A synthesis of major deposit-types, district metallogeny, the evolution of geological provinces, and exploration methods: Geological Association of Canada, Mineral Deposits Division, Special Publication, v.5, p.49-73.

Eilu, P., & Groves, D.I., 2001. Primary alteration and geochemical dispersion haloes of Archaean orogenic gold deposits in the Yilgarn Craton: the pre-weathering scenario. Geochemistry: Exploration, Environment, Analysis, v.1(3), p.183-200.

Fairbairn, H.W., Hurley, P.M., Card, K.D., & Knight, C.J., 1969. Correlation of radiometric ages of Nipissing diabase and Huronian metasediments with Proterozoic orogenic events in Ontario. Canadian Journal of Earth Sciences, v.6, p.489-497.

Gélinas, L., Trudel, P., & Hubert, C., 1984. Chemostratigraphic division of the Blake

River Group, Rouyn-Noranda area, Abitibi, Quebec. Canadian Journal of Earth Sciences, v.21 (2), p.220-231.

Genkin, A.D., Bortnikov, N.S., Cabri, L.J., Wagner, F.E., Stanley, C.J., Safonov, Y.G., McMahon, G., Friedl, J., Kerzin, A.L., & Gamyanin, G.N., 1998. A multidisciplinary study of invisible gold in arsenopyrite from four mesothermal gold deposits in Siberia, Russian Federation. Economic Geology, v.93, p.463-487.

Goldfarb, R.J., Groves, D.I., & Gardoll, S., 2001. Orogenic gold and geologic time: a global synthesis. Ore Geology Reviews, v.18 (1), p.1-75.

Goldfarb, R.J., Baker, T., Dube, B., Groves, D.I., Hart, C.J., & Gosselin, P., 2005. Distribution, character, and genesis of gold deposits in metamorphic terranes. Economic Geology 100th anniversary volume, v.40, p.407-450.

Groves, D.I., Goldfarb, R.J., Robert, F., & Hart, C.J.R., 2003. Gold deposits in metamorphic belts: Overview of current understanding, outstanding problems, future research, and exploration significance: Economic Geology, v.98 (1), p.1-29.

Hart, C.J.R., & Goldfarb, R.J., 2005. Distinguishing intrusion-related from orogenic gold systems. New Zealand Minerals Conference Proceedings, p.125-133.

Helt, K.M., Williams-Jones, A.E., Clark, J.R., Wing, B.A., & Wares, R.P., 2014. Constraints on the Genesis of the Archean Oxidized, Intrusion-Related Canadian Malartic Gold Deposit, Quebec, Canada. Economic Geology, v.109 (3), p.713-735.

Ispolatov, V., Lafrance, B., Dubé, B., Creaser, R., & Hamilton, M., 2008. Geologic and structural setting of gold mineralization in the Kirkland Lake-Larder Lake gold belt, Ontario. Economic Geology, v.103 (6), p.1309-1340.

Jolly, W.T., 1978. Metamorphic history of the Archean Abitibi belt. Metamorphism in the Canadian Shield. Geological Survey of Canada, Paper, p.78-10.

Kishida, A., & Kerrich, R., 1987. Hydrothermal alteration zoning and gold concentration at the Kerr-Addison Archean lode gold deposit, Kirkland Lake, Ontario. Economic Geology, v.82 (3), p.649-690.

Kretschmar, U., & Scott, S.D., 1976. Phase relations involving arsenopyrite in the system Fe-As-S and their application, v.14, p.364-386.

Lang, J.R., & Baker, T., 2001. Intrusion-related gold systems: the present level of understanding. Mineralium Deposita. v.36 (6), p.477-489.

Large, R.R., Maslennikov, V.V., Robert, F., Danyushevsky, L.V., & Chang, Z., 2007, Multistage sedimentary and metamorphic origin of pyrite and gold in the giant Sukhoi Log deposit, Lena gold province, Russia, Economic Geology, v.102, p.1233-1267.

Large, R.R., Danyushevsky, L., Hollit, C., Maslennikov, V., Meffre, S., Gilbert, S., Bull, S., Scott, R., Emsbo, P., Thomas, H., Singh, B., & Foster, J., 2009. Gold and trace element zonation in pyrite using a laser imaging technique: implications for the timing of gold in orogenic and Carlin-style sediment-hosted deposits, Economic Geology, v.104 (5), p.635-668.

Legault, M., & Rabeau, O., 2006. Étude métallogénique et modélisation 3D de la Faille de Cadillac dans le secteur de Rouyn-Noranda. Ministère des Ressources Naturelles et de la Faune, Québec ; RP2006-03, 8p.

Legault, M., & Rabeau, O., 2007. Étude métallogénique et modélisation 3D de la Faille de Cadillac dans le secteur de Rouyn-Noranda (Phase 2). Ministère des Ressources Naturelles et de la Faune, Québec ; RP2007-03, 11p.

MacLean, W., and Barrett, T., 1993, Lithogeochemical techniques using immobile elements: Journal of geochemical exploration, v. 48, p. 109-133.

MacLean, W., and Kranidiotis, P., 1987, Immobile elements as monitors of mass transfer in hydrothermal alteration; Phelps Dodge massive sulfide deposit, Matagami, Quebec: Economic Geology, v. 82, p. 951-962.

Mair, J.L., Farmer, G.L., Groves, D.I., Hart, C.J., & Goldfarb, R. J., 2011. Petrogenesis of postcollisional magmatism at Scheelite Dome, Yukon, Canada: Evidence for a lithospheric mantle source for magmas associated with intrusion-related gold systems. Economic Geology, v.106 (3), p.451-480.

McCuaig, T.C., & Kerrich, R., 1998. P-T-t deformation fluid characteristics of lode gold deposits: evidence from alteration systematics. Ore Geology Reviews, v.12 (6), p.381-453.

Mikucki, E.J., 1998. Hydrothermal transport and depositional processes in Archean lode-gold systems: a review. Ore Geology Reviews, v.13 (1), p.307-321.

Monecke, T., Gibson, H., Dubé, B., Laurin, J., Hannington, M.D., & Martin, L., 2008. Geology and Volcanic Setting of the Horne Deposit, Rouyn-Noranda, Quebec, Initial Results of a New Research Project. Geological Survey of Canada.

Morey, A.A., Tomkins, A.G., Bierlein, F.P., Weinberg, R.F., & Davidson, G.J., 2008. Bimodal distribution of gold in pyrite and arsenopyrite: Examples from the Archean Boorara and Bardoc shear systems, Yilgarn craton, Western Australia, Economic Geology, v.103, p.599-614.

Mueller, W. U., Daigneault, R., Mortensen, J. K., & Chown, E.H., 1996. Archean terrane docking : upper crust collision tectonics, Abitibi greenstone belt, Quebec, Canada, Tectonophysics, v.265 (1), p.127-150.

Mueller, W.U., Friedman, R., Daigneault, R., Moore, L., & Mortensen, J., 2012. Timing and characteristics of the Archean subaqueous Blake River Megacaldera Complex, Abitibi greenstone belt, Canada. Precambrian Research v.214-215, p.1-27.

Mumin, A.H., Fleet, M.E., & Chryssoulis, S., 1994, Gold mineralization in As-rich mesothermal gold ores of the Bogosu-Prestea mining district of the Ashanti Gold Belt, Ghana: Remobilization of "invisible" gold. Mineralium Deposita, v.29 (6), p.445-460.

Neumayr, P., Walshe, J., Hagemann, S., Petersen, K., Roache, A., Frikken, P., Horn, L., & Halley, S., 2008. Oxidized and reduced mineral assemblages in greenstone belt rocks of the St. Ives gold camp, Western Australia: vectors to high-grade ore bodies in Archaean gold deposits ? Mineralium Deposita, v.43 (3), p.363-371.

Pearson, V., & Daigneault, R., 2009. An Archean megacaldera complex: the Blake River Group, Abitibi greenstone belt. Precambrian Research, v.168 (1), p.66-82.

Pilote, P., & Couture, J.F., 1989. Gisements aurifères. Rouyn-Noranda. Ministère de l'Énergie et des Ressources du Québec, DV 89-05, 95-96.

Poulsen, K.H., Robert, F., & Dubé, B., 2000. Geological classification of Canadian gold deposits v.540. Geological Survey of Canada.

Putnis, A., 2002. Mineral replacement reactions; from macroscopic observations to

microscopic mechanisms, Mineralogical Magazine, v.66, p.689-708.

Rabeau, O., Royer, J.J., Jébrak, M., & Cheilletz, A., 2013. Log-uniform distribution of gold deposits along major Archean fault zones. Mineralum Deposita, v.48, p.817-824.

Rafini, S., 2014. Typologie des minéralisations aurifères associées à la Faille de Cadillac. Rapport du projet CONSOREM 2011-01 et 2012-01, 45p.

Robert, F., 2001. Syenite-associated disseminated gold deposits in the Abitibi greenstone belt, Canada. Mineralium Deposita. v.36 (6), p.505-516.

Sharp, Z.D., Essene, E.J., & Kelly, W.C., 1985. A re-examination of the arsenopyrite geothermometer: Pressure condiserations and applications to natural assemblages. Canadian Mineralogist, v.23, p.517-534.

Simard, M., Gaboury, D., Daigneault, R., & Mercier-Langevin, P., 2013. Multistage gold mineralization at the Lapa mine, Abitibi Subprovince: insights into auriferous hydrothermal and metasomatic processes in the Cadillac-Larder Lake Fault Zone. Mineralium Deposita, v.48 (7), p.883-905.

Smith, J.R., Spooner, E.T.C., Broughton, D.W., & Ploeger, F.R., 1993. Archean Au-Ag-(W) Quartz Vein/Disseminated mineralisation within the Larder Lake - Cadillac Break, Kerr Addison - Chesterville System, North East Ontario, Canada, Ontario Geoscience Research Grant Program, Grant No. 364; Ontario Geological Survey, Open File Report 5831, 310p.

Sillitoe, R.H., 1991. Intrusion-related gold deposits. In : Gold metallogeny and exploration. Springer US, p.165-209.

Sillitoe, R.H., 2002. Some metallogenic features of gold and copper deposits related to alkaline rocks and consequences for exploration. Mineralium Deposita. v.37 (1), p.4-13.

Sillitoe, R.H., 2008. Special paper: major gold deposits and belts of the North and South American Cordillera: distribution, tectonomagmatic settings, and metallogenic considerations. Economic Geology, v.103 (4), p.663-687.

Thompson, J.F.H., Sillitoe, R.H., Baker, T., Lang, J.R., & Mortensen, J.K., 1999. Intrusion-related gold deposits associated with tungsten-tin provinces. Mineralium Deposita. v.34 (4), p.323-334.

Trépanier, S., 2013. Norme Lithomodeleur. Rapport du projet CONSOREM 2011-04, 91p.

Witt, W.K., 1992. Porphyry intrusions and albitites in the Bardoc-Kalgoorlie area, Western Australia, and their role in Archean epigenetic gold mineralization. Canadian Journal of Earth Sciences, v.29 (8), p.1609-1622.

Zhang, J., Lin, S., Linnen, R., & Martin, R., 2014. Structural setting of the Young-Davidson syenite-hosted gold deposit in the Western Cadillac-Larder Lake Deformation Zone, Abitibi Greenstone Belt, Superior Province, Ontario. Precambrian Research, v.248, p.39-59.